

Sensor and Simulation Notes

Note 252

March 1979

Equivalent Electromagnetic Properties
of a Concentric Wire Cage
as Compared to a Circular Cylinder

Korada R. Umashankar
Carl E. Baum

Air Force Weapons Laboratory

CLEARED
FOR PUBLIC RELEASE

PL/PA 5/14/97

Abstract

The electromagnetic equivalence of an infinitely long loaded wire-cage structure and loaded hollow cylindrical geometry is established based on the same radiated fields under identical conditions. Analysis of the canonical infinitely long loaded wire geometries are given by treatment as boundary-value antenna problems. An expression for the equivalent radius of the wire cage and an equivalent impedance-loading function are obtained, including frequency dependence.

PL 96-1259

I. INTRODUCTION

The electromagnetic equivalence of radiating objects has been a subject of study for a long time by many investigators.¹⁻³ This yields a simple equivalence corresponding to a complex radiating structure based on a predefined electromagnetic equivalence criterion. The question of equivalence criterion may be defined according to the same total radiated fields, or the same total current induced, or even the same effective impedance(s) of the geometries under equivalence study. There does not appear as yet to be a unique equivalence criterion one may establish; it entirely depends on the specific need and its application. In this paper, the field radiated by the structure is taken as the basis for comparison and for establishing electromagnetic equivalence.

Even though the question of electromagnetic equivalence is basic in nature, the motivation for the present investigation is to come up with suitable modeling for hybrid EMP simulators.⁴ In figures 1.1 and 1.2 are shown examples of wire cage hybrid simulators with complex bicone feed structures.^{5,6} A straightforward analysis in a given frequency spectrum is quite complicated. Hence a systematic modeling of the conical feed and generator, wire cage hybrid simulator, and the transition region between the conical feed and the simulator is required.⁷

This note is primarily concerned with the development of a theory for equivalent electromagnetic properties of a wire cage as compared to a hollow conducting cylinder. Wire cage structures have been extensively used in the design of hybrid simulators^{5,6} from the practical standpoint of lower structural weight, lower wind resistance, ease of construction and erection at the experimental sites. The exact analysis of the wire cage hybrid simulator is very complicated; one has to suitably model it to simplify the analysis. The reader should note that the wire cage by itself is inadequate to model a hybrid simulator since certain parts of it involve conducting conical, cylindrical, and other transition sections which are physically quite different from a wire cage (and desirably so, for improved performance).

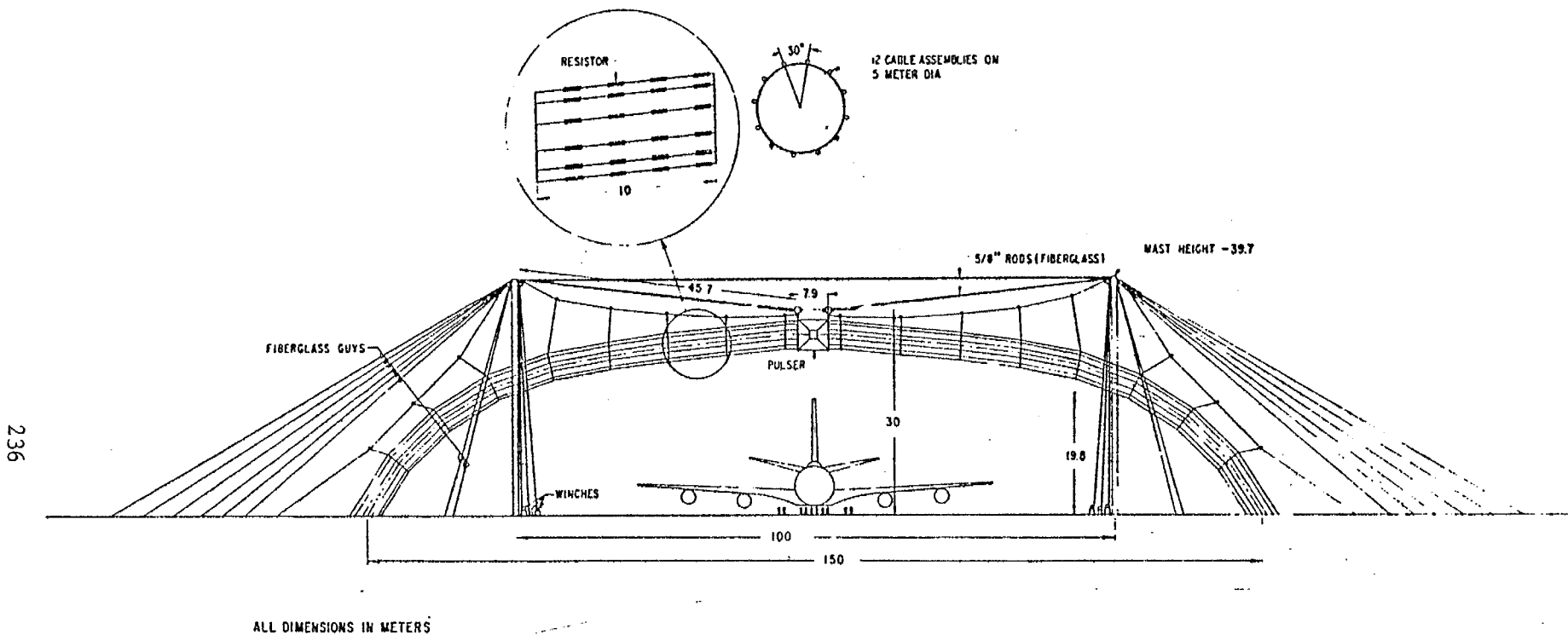


Figure 1.1. Sketch of the ATHAMAS I Simulator Facility at Kirtland AFB, New Mexico

237

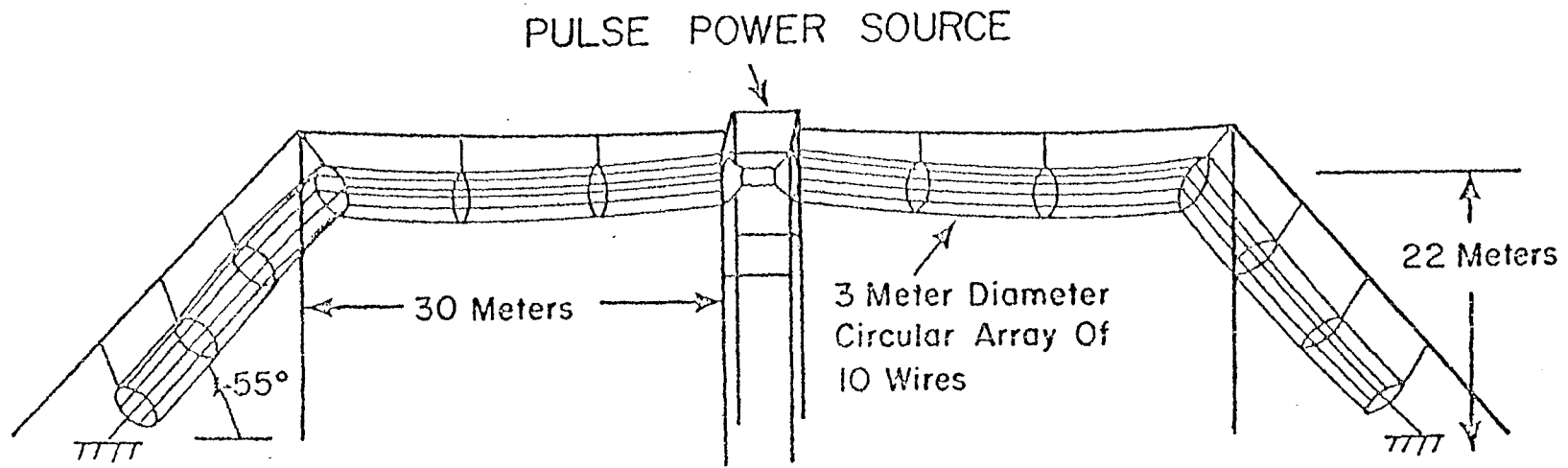


Figure 1.2. Illustration of the Achilles II EMP Simulator Facility, Kirtland AFB, New Mexico

The subject of electromagnetic equivalences as applied to wire cage models is previously studied by Schelkunoff,¹ King,² and also recently by Baum,³ to obtain an equivalent radius. The results obtained¹⁻³ are in principle applicable to only perfectly conducting wire cages in the limit as frequency approaches zero. In one study¹ a cage consisting of conical wires equally spaced over the surface of a bicone is studied, and compared with respect to a solid cone of same characteristic impedance so that there is only a transmission line mode excited. In the limit as the cone angle becomes small, the result of the effective radius of the cage is the same as the one obtained in reference 3 which is based on conformal transformation; an equivalence between a single charged conductor and a number of equally spaced concentric charged conductors is thereby derived in the static case. A different approach is studied in reference 2 wherein a cage antenna consisting of closely spaced parallel and identical conductors placed around a circle is compared with respect to a single conductor antenna, so that the total axial assumed current distribution is approximately the same in both cases.

This note considers various, but comparatively more accurate, alternative analyses of the impedance loaded, infinitely long cylindrical models which can be used as substitutes to the complex wire cage structure having the same electromagnetic field properties. The question of electromagnetic equivalence of wire cages (both circular cylindrical and circular conical) used in hybrid (and other) simulators as compared to a cylindrical solid wire, a cylindrical cage of strips, or a hollow circular cylinder with complex impedance loading functions is investigated in a larger perspective, based on the detailed analysis of the infinitely long canonical geometries with uniformly loaded impedance functions, treated as boundary value problems. These in general fit into the category of boundary connection supermatrices⁸ for the radiated fields.

II. ANALYSIS OF INFINITELY LONG CANONICAL THIN WIRE ANTENNA GEOMETRIES

An analysis for electromagnetic radiation by two-dimensional uniformly loaded structures is treated as a boundary value problem. The following antenna geometries are considered below:

1. Infinitely long loaded wire antenna (thin)
2. Infinitely long loaded wire cage antenna and its special case of an infinitely long loaded circular cylindrical wire cage antenna
3. Infinitely long loaded hollow circular cylindrical antenna

Integral expressions are derived for the current induced and the corresponding fields radiated for the above canonical problems. Using saddle point integration, the electric and the magnetic far fields and the asymptotic solution for the induced current are evaluated.

A. Infinitely Long Loaded Wire Antenna

An infinitely long thin wire is oriented along the z axis in a free space isotropic homogeneous medium. The radius of the cross section of the wire is b and it is excited by a source generator of voltage $\tilde{V}(s)$ across a gap of width $2d$ centered at $z = 0$ as shown in figure 2.1. The electric and the magnetic fields radiated into the surrounding medium are calculated from the induced electric current $\tilde{I}(z,s)$ on the wire, which can be obtained by solving the boundary value problem⁹ and enforcing the impedance boundary condition on the surface of the wire. Due to the symmetry of the problem and nature of excitation, the radiated electric field $\tilde{E}(\psi, z, s)$ and magnetic field $\tilde{H}(\psi, z, s)$ are obtained by

$$\begin{bmatrix} \tilde{E}(\psi, z, s) \\ \tilde{H}(\psi, z, s) \end{bmatrix} = \frac{1}{2\pi j} \int_{C_\zeta} \begin{bmatrix} \tilde{E}(\psi, \zeta, s) \\ \tilde{H}(\psi, \zeta, s) \end{bmatrix} \cdot e^{\zeta z} d\zeta \quad (2.1)$$

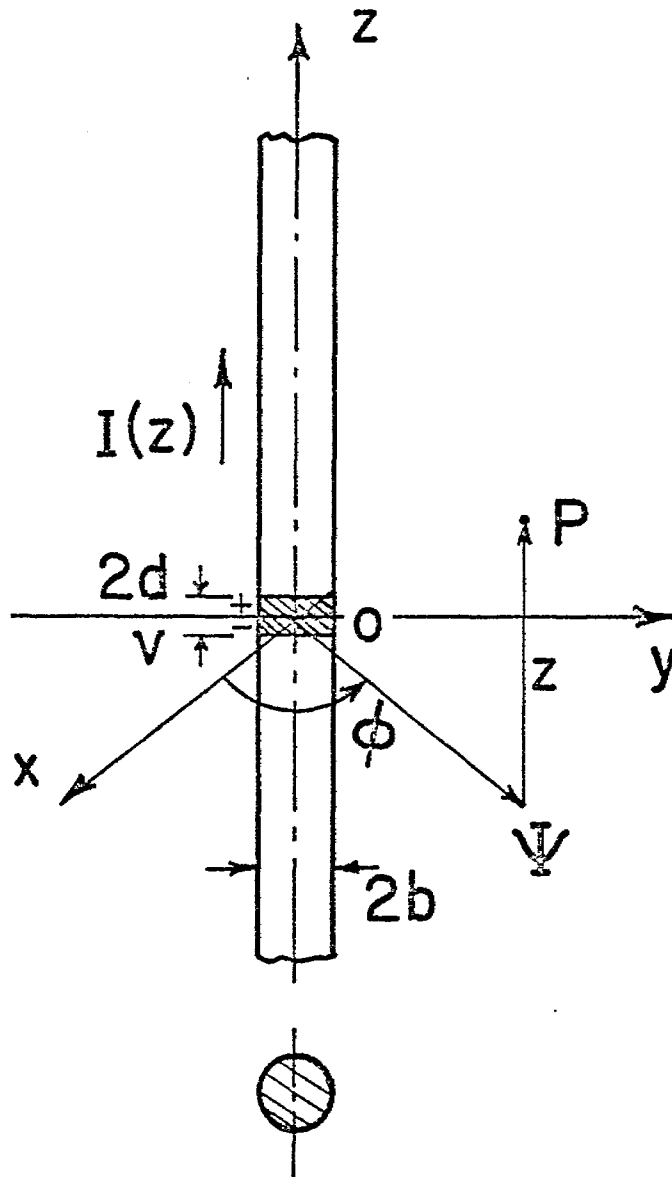


Figure 2.1. Infinitely Long Thin Solid Wire Antenna

where $\tilde{\tilde{E}}(\Psi, \zeta, s)$ and $\tilde{\tilde{H}}(\Psi, \zeta, s)$ are the spectral distributions of the corresponding electric and magnetic fields.

In the present analysis, the following Laplace-transform definitions (two-sided) are followed for the time variable t and the space coordinate variable z ,

$$\begin{array}{ccc} (t, z) & \xleftrightarrow{\text{Laplace}} & (s, \zeta) \\ & \text{Transform} & \\ F_1(t) & & \tilde{\tilde{F}}_1(s) \\ F_2(z) & & \tilde{\tilde{F}}_2(\zeta) \\ F_3(t, z) & & \tilde{\tilde{F}}_3(s, \zeta) \end{array}$$

$$\tilde{\tilde{F}}_1(s) = \int_{-\infty}^{\infty} F_1(t) e^{-st} dt \quad (2.2a)$$

$$\tilde{\tilde{F}}_2(\zeta) = \int_{-\infty}^{\infty} F_2(z) e^{-\zeta z} dz \quad (2.2b)$$

which have the corresponding inverse Laplace transforms

$$F_1(t) = \frac{1}{2\pi j} \int_{C_\gamma} \tilde{\tilde{F}}_1(s) e^{st} ds \quad (2.2c)$$

$$F_2(z) = \frac{1}{2\pi j} \int_{C_\zeta} \tilde{\tilde{F}}_2(\zeta) e^{\zeta z} d\zeta \quad (2.2d)$$

where C_γ and C_ζ are the contours of integration in the s - and ζ -complex planes as shown in figure 2.2.

At any point P , there exists only the z -component of the magnetic vector potential,^{9,11}

$$\tilde{\tilde{A}}_z(\Psi, z, s) = \frac{1}{2\pi j} \int_{C_\zeta} \tilde{\tilde{F}}(b, \zeta, s) K_0(u\Psi) e^{\zeta z} d\zeta \quad (2.3)$$

from which the radiated electric and the magnetic fields can be obtained as

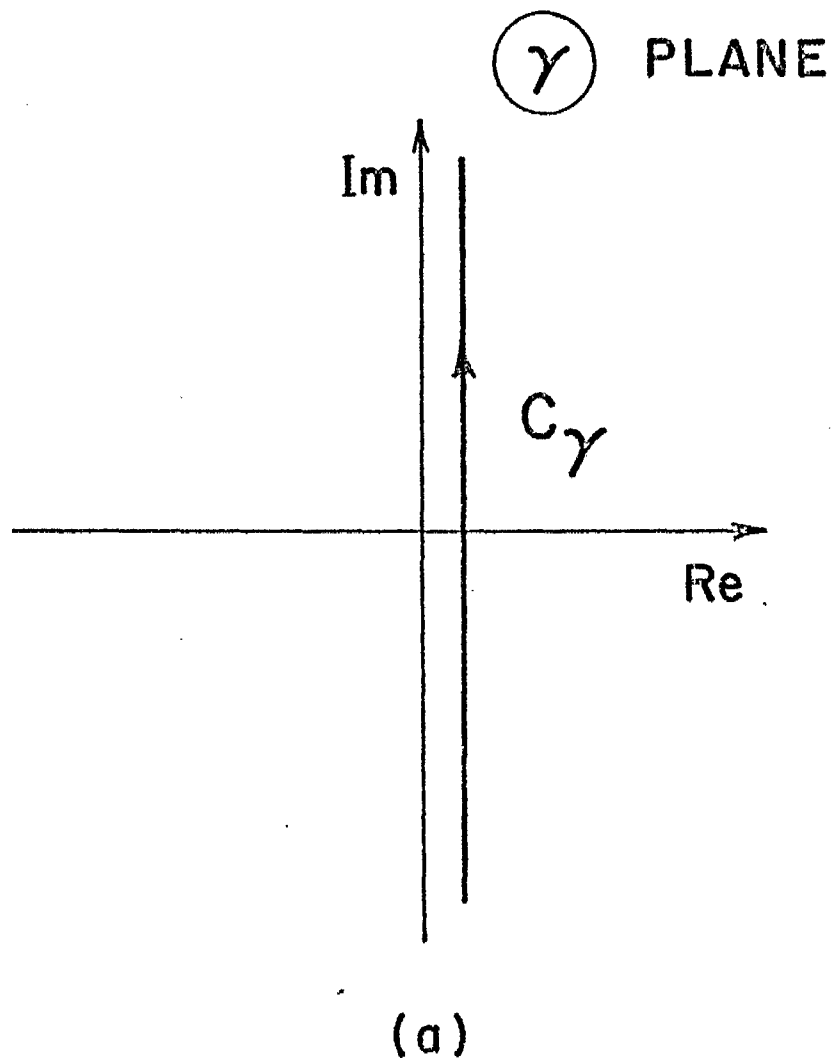


Figure 2.2(a). Integration Contour C_γ in the Complex γ Plane

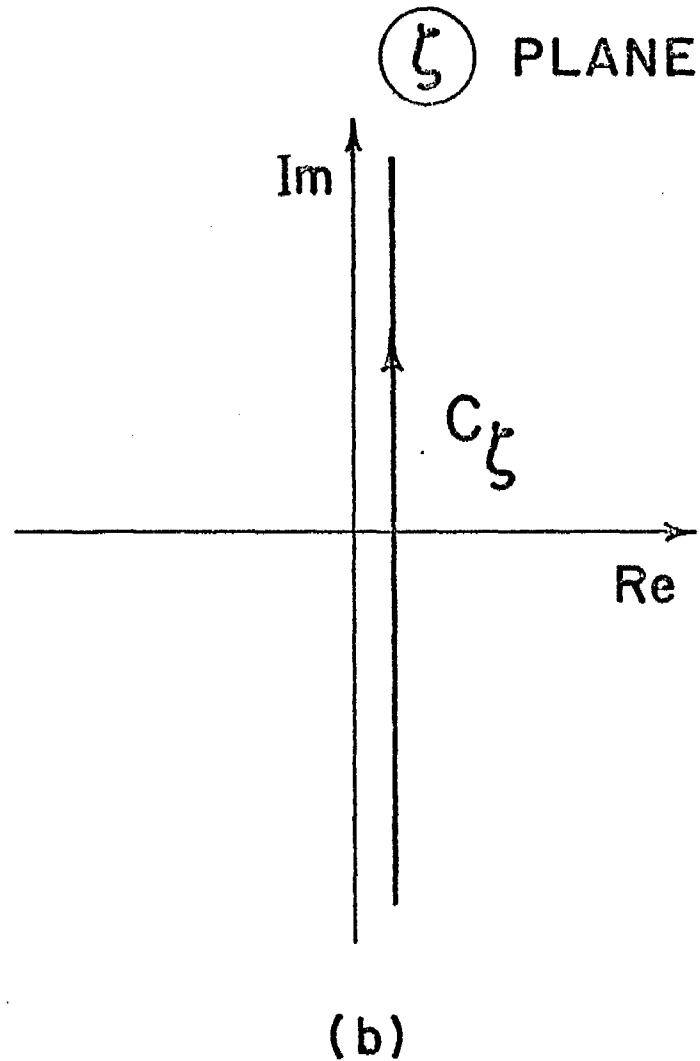


Figure 2.2(b). Integration Contour C_ζ in the Complex ζ Plane

$$\tilde{H}(\Psi, z, s) = \left[\frac{s}{\gamma^2} \left(\frac{\partial^2}{\partial z^2} - \gamma^2 \right) \tilde{I}_z + \frac{s}{\gamma^2} \frac{\partial^2}{\partial \Psi \partial z} \tilde{I}_\Psi \right] \tilde{A}_z(\Psi, z, s) \quad (2.4a)$$

$$\tilde{H}(\Psi, z, s) = - \frac{1}{\mu} \frac{\partial}{\partial \Psi} \tilde{A}_z(\Psi, z, s) \tilde{I}_\phi \quad (2.4b)$$

In the expression (2.3),

$$u = [\gamma^2 - \zeta^2]^{\frac{1}{2}} \quad (2.5a)$$

and the cylindrical radial coordinate

$$\Psi = [x^2 + y^2]^{\frac{1}{2}} \quad (2.5b)$$

K_0 is the modified Bessel function of the second kind, zero order, and the propagation constant is

$$\gamma = [s\mu(\sigma + s\varepsilon)]^{\frac{1}{2}} \quad (2.5c)$$

$$= jK \quad (2.5d)$$

where μ , ε , and σ are the permeability, permittivity, and the conductivity of the homogeneous medium. The spectral term $\tilde{F}(b, \zeta, s)$ in the expression (2.3), is the term proportional to the Laplace transform of the induced electric current $\tilde{I}(z, s)$ on the infinitely long wire. In the above spectral representation, an $e^{st+\zeta z}$ field variation is assumed, s being the two-sided Laplace transform variable. The infinitely long wire is sufficiently thin to satisfy

$$|\gamma b| \ll 1 \quad (2.6)$$

so that no internal modes are excited.

The spectral term $\tilde{F}(b, \zeta, s)$ is to be determined based on enforcing the following impedance boundary relationship for the tangential total electric field on the surface of the wire. The infinitely long wire is excited by an ideal source generator of

voltage $\tilde{V}(s)$ across a gap of width $2d$. Within the gap the z component of the electric field is specified to have the variation $-\tilde{V}(s)/2d$. Hence, on the surface of the infinitely long thin wire, the induced electric current $\tilde{I}(b,z,s)$ and the electric field $\tilde{E}_z(b,z,s)$ should satisfy,⁹

$$\tilde{E}_z(b,z,s) = \left(-\frac{\tilde{V}(s)}{2d}\right) p_d(z) + \tilde{Z}'_w(s) \tilde{I}(b,z,s) \quad (2.7)$$

where

$$p_d(z) = 1, \quad |z| < d$$

$$= 0, \quad |z| > d$$

In the above expression, $\tilde{Z}'_w(s)$ is the series axial impedance per unit length of the infinitely long loaded wire. In this analysis, the impedance function $\tilde{Z}'_w(s)$ has the definition of impedance per unit length which is the ratio of the tangential electric field to the total current along the axial direction. This impedance function includes a contribution due to the lossy characteristics of the wire in addition to the externally introduced loading terms. Depending on the cross section of the wire geometry, complex s dependence may arise at very high frequencies. In Appendix A, the series impedance $\tilde{Z}'_w(s)$ per unit length is discussed for certain geometries. However, with large external loading, the contribution due to lossy material of the wire can be ignored for all practical purposes.

In terms of the transformed spectral quantities, the boundary relationship (2.7) becomes, with the following source function expansion,⁹

$$\left(\frac{\tilde{V}(s)}{2d}\right) p_d(z) = \frac{\tilde{V}(s)}{2\pi j} \int_{C_\zeta} \tilde{G}(\zeta) e^{\zeta z} d\zeta \quad (2.8a)$$

$$\tilde{G}(\zeta) = \frac{\sinh(\zeta d)}{(\zeta d)} \quad (2.8b)$$

$$\rightarrow 1, \quad \text{as } |\zeta d| \rightarrow 0$$

and hence,

$$\tilde{E}_z(b, \zeta, s) = -\tilde{V}(s) G(\zeta) + \tilde{Z}'_w(s) \tilde{I}(b, \zeta, s) \quad (2.9)$$

According to the expressions (2.1), (2.2d), (2.3), and (2.4a), the z component of the spectral electric field is

$$\tilde{E}_z(\Psi, \zeta, s) = -\frac{s}{\gamma^2} u^2 K_0(u\Psi) \tilde{F}(b, \zeta, s) \quad (2.10)$$

The induced electric current along the infinitely long wire is obtained as a line integral of the ϕ component of the magnetic field (2.4b) evaluated just outside the surface of the infinitely long wire,

$$\tilde{I}(b, z, s) = -\frac{1}{\mu} \int_{\phi=0}^{2\pi} \left[\frac{\partial \tilde{A}_z(\Psi, z, s)}{\partial \Psi} \right]_{\Psi=b} d\phi \quad (2.11)$$

The electric current has no ϕ -angular variation, and using the expressions (2.1), (2.2d), (2.3), and (2.4b), the spectral distribution of the electric current is

$$\tilde{I}(b, \zeta, s) = \frac{1}{\mu} 2\pi b u K_1(ub) \tilde{F}(b, \zeta, s) \quad (2.12)$$

where K_1 is the modified Bessel function of second kind, first order. As pointed out earlier, the term $\tilde{F}(b, \zeta, s)$ is proportional to the transform of the electric current.

On substituting the expressions (2.10) and (2.12) into the impedance boundary relationship (2.9), the expression for the spectral term $\tilde{F}(b, \zeta, s)$ is obtained as,

$$\tilde{F}(b, \zeta, s) = \tilde{V}(s) \frac{\gamma^2}{s} \frac{G(\zeta)}{u \tilde{D}(\zeta, s)} \quad (2.13a)$$

where

$$\tilde{D}(\zeta, s) = u K_0(ub) + 2\pi b \gamma K_1(ub) \frac{\tilde{Z}'_w(s)}{Z_0} \quad (2.13b)$$

and the characteristic impedance of the medium is

$$Z_o = \left[\frac{s\mu}{\sigma + se} \right]^{\frac{1}{2}} \quad (2.13c)$$

Hence from the expressions (2.2d), (2.12), and (2.13a), the total induced electric current on the infinitely long loaded wire antenna has the distribution,

$$\tilde{I}(z,s) = \frac{\tilde{V}(s)\gamma b}{jZ_o} \int_{C_\zeta} G(\zeta) \frac{K_1(ub)}{\tilde{D}(\zeta,s)} e^{\zeta z} d\zeta \quad (2.14)$$

In fact one can verify the expression (2.14) for the special case of a perfectly conducting, $\tilde{Z}'_w(s) = 0$, solid cylindrical antenna. Assuming the source to be an ideal slice generator, the electric current on a thin solid perfectly conducting infinitely long antenna^{12,13} is given by,

$$\begin{aligned} \tilde{I}^{pc}(z,s) &= \tilde{I}(z,s) \Big|_{\tilde{Z}'_w(s)=0} \\ &= \frac{\tilde{V}(s)\gamma b}{jZ_o} \int_{C_\zeta} \frac{K_1(ub)}{uK_o(ub)} e^{\zeta z} d\zeta \end{aligned} \quad (2.15)$$

Since $\tilde{F}(b,\zeta,s)$ is known from the expression (2.13a), the z component of the magnetic vector potential defined in (1.3) takes the form

$$\tilde{A}_z(\Psi,z,s) = \frac{\tilde{V}(s)}{2\pi j} \frac{\gamma^2}{s} \int_{C_\zeta} G(\zeta) \frac{K_o(u\Psi)}{\tilde{u}\tilde{D}(\zeta,s)} e^{\zeta z} d\zeta \quad (2.16)$$

It is now possible to calculate the electric and the magnetic fields as defined in the expressions (2.1) and (2.4), and using the expression (2.13a), we have the spectral fields

$$\begin{bmatrix} \tilde{E}_z(\Psi, \zeta, s) \\ Z_0 \tilde{H}_\phi(\Psi, \zeta, s) \end{bmatrix} = \begin{bmatrix} \tilde{M}_1 \\ \tilde{M}_2 \end{bmatrix} \quad (2.17a)$$

where $[\tilde{M}]$ is a vector for the infinitely long thin wire antenna and represents the spectral distribution of the radiated fields,

$$\begin{bmatrix} \tilde{M} \\ \tilde{M} \end{bmatrix} = \begin{bmatrix} \tilde{M}_1 \\ \tilde{M}_2 \end{bmatrix} \quad (2.17b)$$

where the elements of the above vector are,

$$\tilde{M}_1 = -\tilde{V}(s) \tilde{G}(\zeta) \frac{uK_0(u\Psi)}{\tilde{D}(\zeta, s)} \quad (2.17c)$$

and

$$\tilde{M}_2 = \tilde{V}(s) \tilde{G}(\zeta) \frac{\gamma K_1(u\Psi)}{\tilde{D}(\zeta, s)} \quad (2.17d)$$

Due to the symmetry of the structure and its excitation, the fields are independent of ϕ -angular variations. The general solution to the radiated fields (2.1) is difficult by direct analytical methods, where the integration is to be performed along the contour C_ζ in the complex ζ -plane, figure 2.2.

If the far-field distribution is the quantity of interest, it is possible to obtain explicit expressions for the various field components defined in (2.1). A classical approach is based on the saddle point integration,¹³ and using this technique, the radiated far fields of the infinitely long perfectly conducting wire antenna are obtain in reference 14, and are extended to infinitely long loaded wire antenna structures conveniently; a summary of the procedure of the saddle point integration method to obtain far field distribution of the $\tilde{H}_\phi(\Psi, z, s)$ as $\Psi \rightarrow \infty$ is given in Appendix B. Hence asymptotically as $\Psi \rightarrow \infty$, the integral expression (2.1) reduces to the following forms:

$$\tilde{E}_z(r, \alpha, s) \sim - \frac{\tilde{V}(s)}{2} \frac{\cos \alpha}{\tilde{L}_1(\gamma, \alpha)} \frac{e^{-\gamma r}}{r} \quad (2.18a)$$

$$Z_0 \tilde{H}_\phi(r, \alpha, s) \sim \frac{\tilde{V}(s)}{2} \frac{1}{\tilde{L}_1(\gamma, \alpha)} \frac{e^{-\gamma r}}{r} \quad (2.18b)$$

where $\alpha = 90 - \theta$ and $\gamma \tilde{L}_1(\gamma, \alpha)$ is defined in Appendix B and repeated below for future usage

$$\tilde{L}_1(\gamma, \alpha) = \cos(\alpha) K_0(\gamma b \cos \alpha) + \tilde{h}_1(s) K_1(\gamma b \cos \alpha) \quad (2.18c)$$

$$\tilde{h}_1(s) = 2\pi b \frac{\tilde{Z}'_w(s)}{Z_0} \quad (2.18d)$$

In the expressions (2.18), r and $\theta = 90 - \alpha$ are the spherical coordinate variables, while α is the angle measured from $z = 0$ plane, figure B-1.

In a similar way, it is possible to obtain an asymptotic solution for the total axial current $\tilde{I}(z, s)$ as given in the expression (2.14) or one can evaluate $\tilde{H}_\phi(\Psi, z, s)$ on the surface of the infinitely long wire in the limit as $z \rightarrow \infty$,¹⁴

$$\tilde{I}(s) \sim 2\pi b \tilde{H}_\phi(\Psi, z, s) \Big|_{\Psi=b^+} \quad \text{as } z \rightarrow \infty \quad (2.19a)$$

To evaluate $\tilde{H}_\phi(\Psi, z, s)$ on the surface of the wire structure $\Psi = b$ for large values of z , it is necessary to restrict the radial distance r and angle α so that $b = r \cos(\alpha)$, and we have $z = r \sin(\alpha)$. For $\alpha \approx \pi/2$, $z \approx r$ so that in (2.18c) the arguments of the Bessel function can be replaced by $\gamma b \cos(\alpha) = \gamma b^2/z$. Hence the expression (2.19a) yields

$$\tilde{I}(s) \sim \frac{\pi \tilde{V}(s)}{Z_0} \frac{e^{-\gamma z}}{K_0(\gamma b^2/z) + [\tilde{h}_1(s)z/b] K_1(\gamma b^2/z)} \quad \text{as } z \rightarrow \infty \quad (2.19b)$$

As z takes on larger values, $\gamma b^2/z$ is very small. The modified Bessel functions can be replaced by their small argument approximation,¹⁵

$$K_0(z) \approx -\ln \frac{\Gamma z}{2} \quad (2.19c)$$

$$K_1(z) \approx \frac{1}{z} \quad (2.19d)$$

$$\Gamma = 0.5772\dots \quad (2.19e)$$

and (2.19b) simplifies to

$$\begin{aligned} \tilde{I}(s) &\sim \frac{\pi \tilde{V}(s)}{Z_0} \frac{e^{-\gamma z}}{-\ln(\Gamma \gamma b^2/2z) + [\tilde{h}_1(s)\gamma/b](z/\gamma b)^2} \\ &= \frac{\pi \tilde{V}(s)}{Z_0} \frac{e^{-\gamma z}}{-\ln(\Gamma \gamma b^2/2z) + 2\pi[\tilde{Z}'_w(s)/Z_0](z/\gamma b)^2} \end{aligned} \quad (2.19f)$$

as $z \rightarrow \infty$

B. Numerical Results: Far Field

The infinitely long thin-wire loaded antenna has been analyzed in the previous section, and the integral expressions for the induced electric current, and the radiated electric and magnetic fields have been derived. The reader may refer to references 16 and 17 for further discussion and solution of the integral expression (2.15) for the induced electric current. As stated earlier, direct analytical solutions for the radiated fields, expressions (2.1) and (2.17), are complex unless one resorts to numerical techniques.¹⁸ Further, based on the saddle point method, explicit expressions (2.18a, b) have been obtained in the far-field region for the radiated fields.

In figures 2.3 through 2.6 are shown the numerical results of the distribution of the radiated far fields. These are appropriately normalized with respect to $(e^{-\gamma r}/r)$ and $\tilde{V}(s) = 1$ is

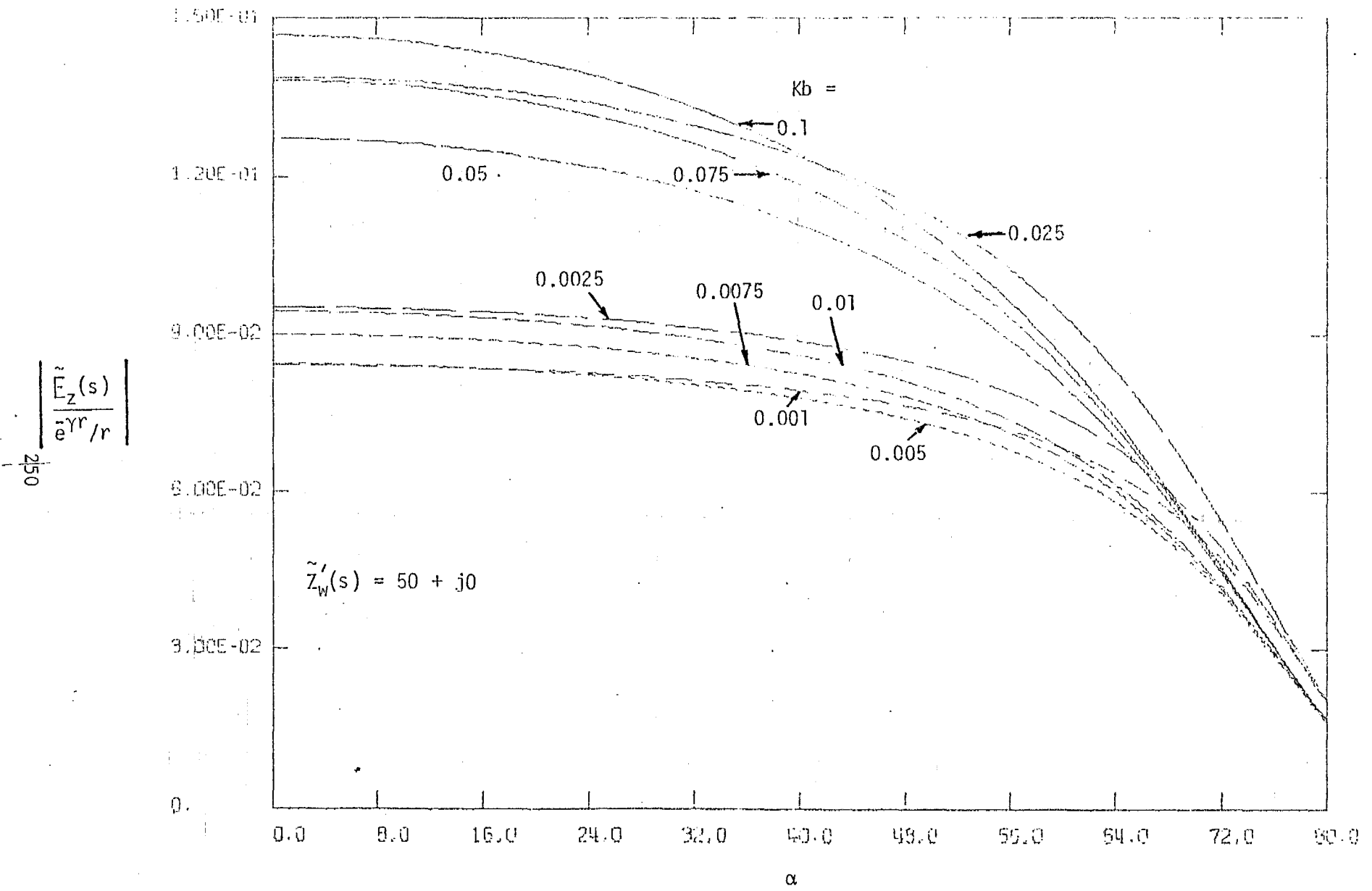


Figure 2.3(a). Magnitude of the Far-Field Distribution, Infinitely Long Thin Wire Loaded Antenna, \tilde{E}_z

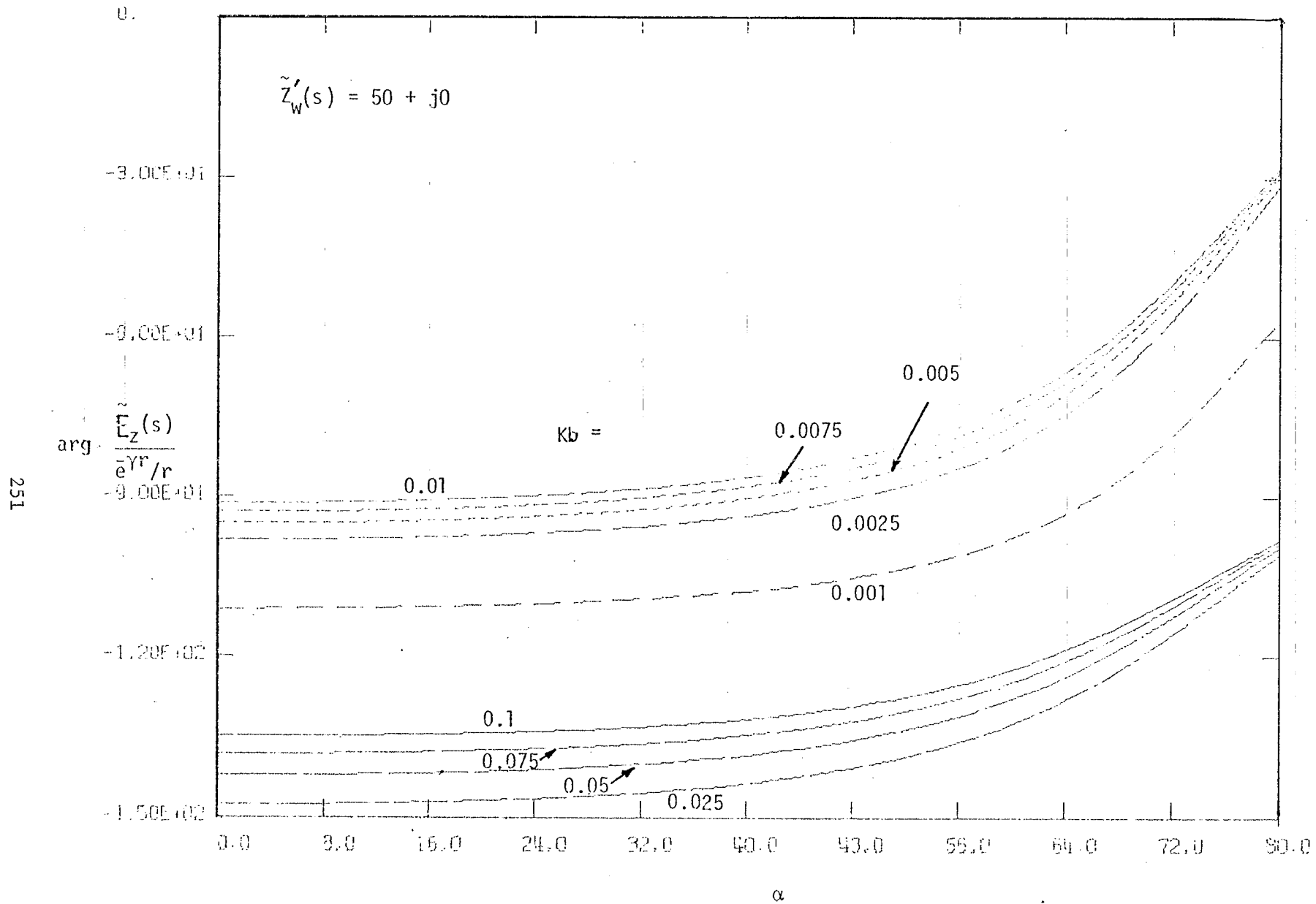


Figure 2.3(b). Phase of the Far-Field Distribution, Infinitely Long Thin Wire Loaded Antenna, \tilde{E}_z

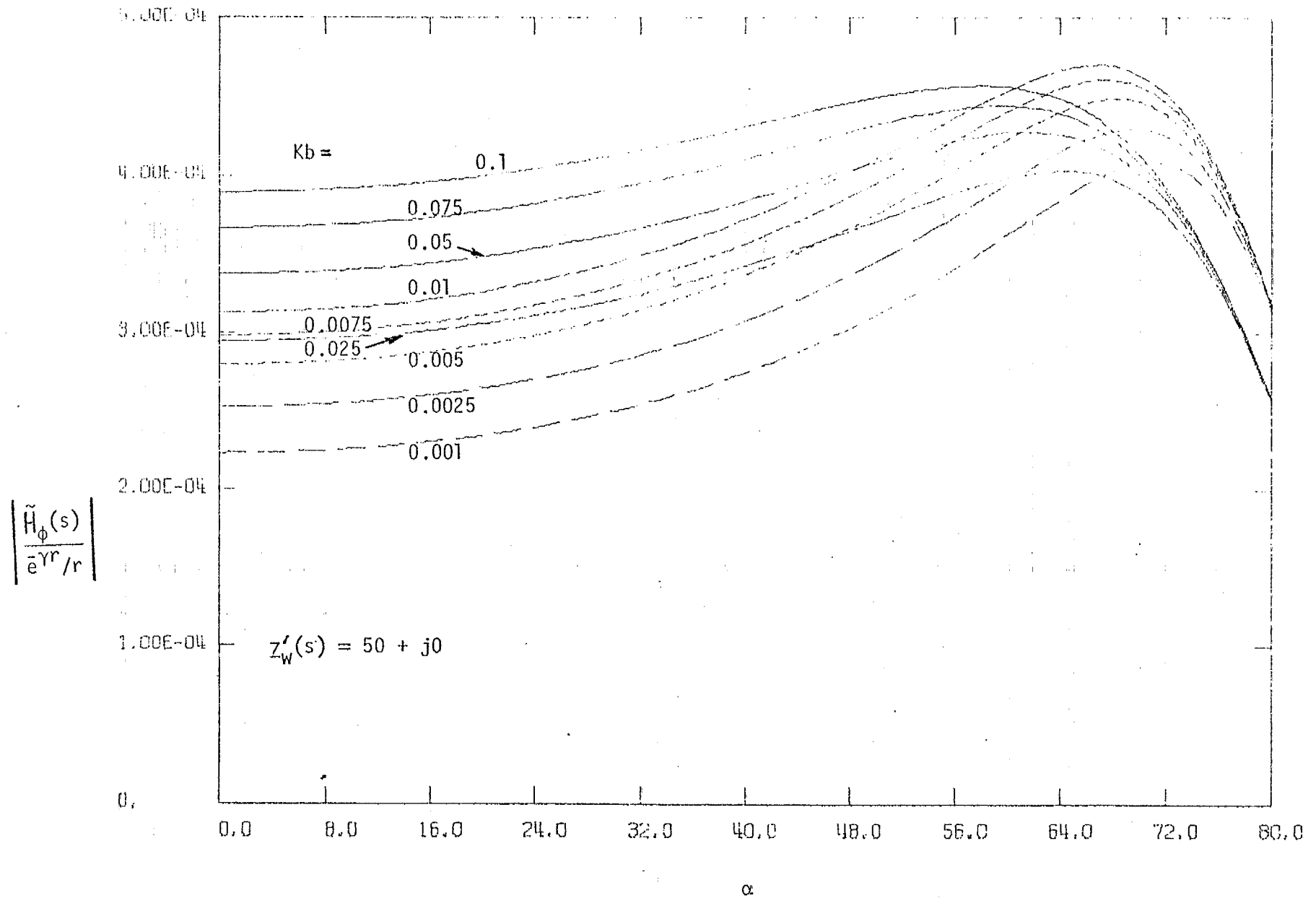


Figure 2.4(a). Magnitude of the Far-Field Distribution, Infinitely Long Thin Wire Loaded Antenna, \tilde{H}_ϕ

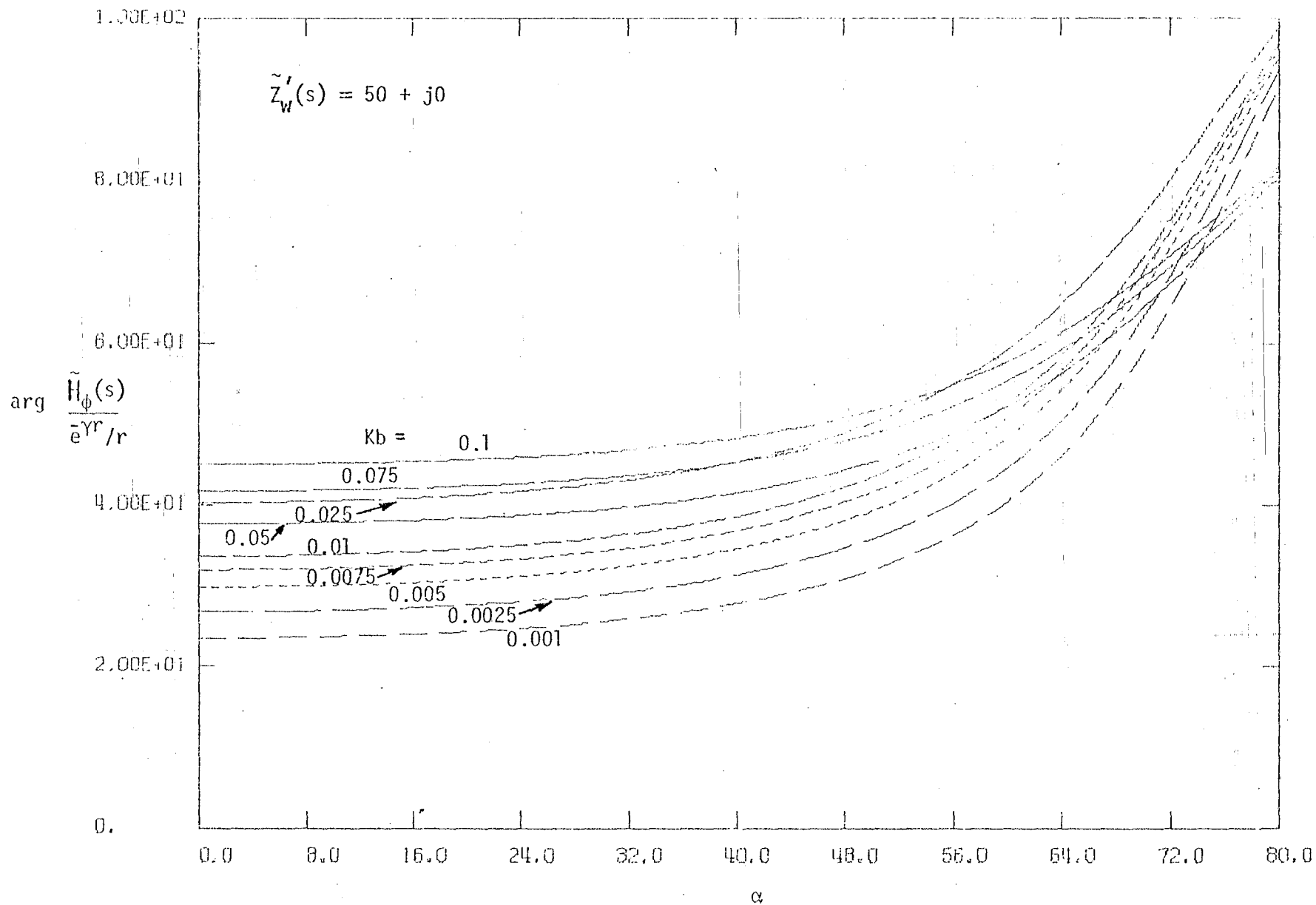


Figure 2.4(b), Phase of the Far-Field Distribution, Infinitely Long Thin Wire Loaded Antenna, \tilde{H}_ϕ

$$\left| \frac{\tilde{E}_z(s)}{e^{-\gamma r}/r} \right|$$

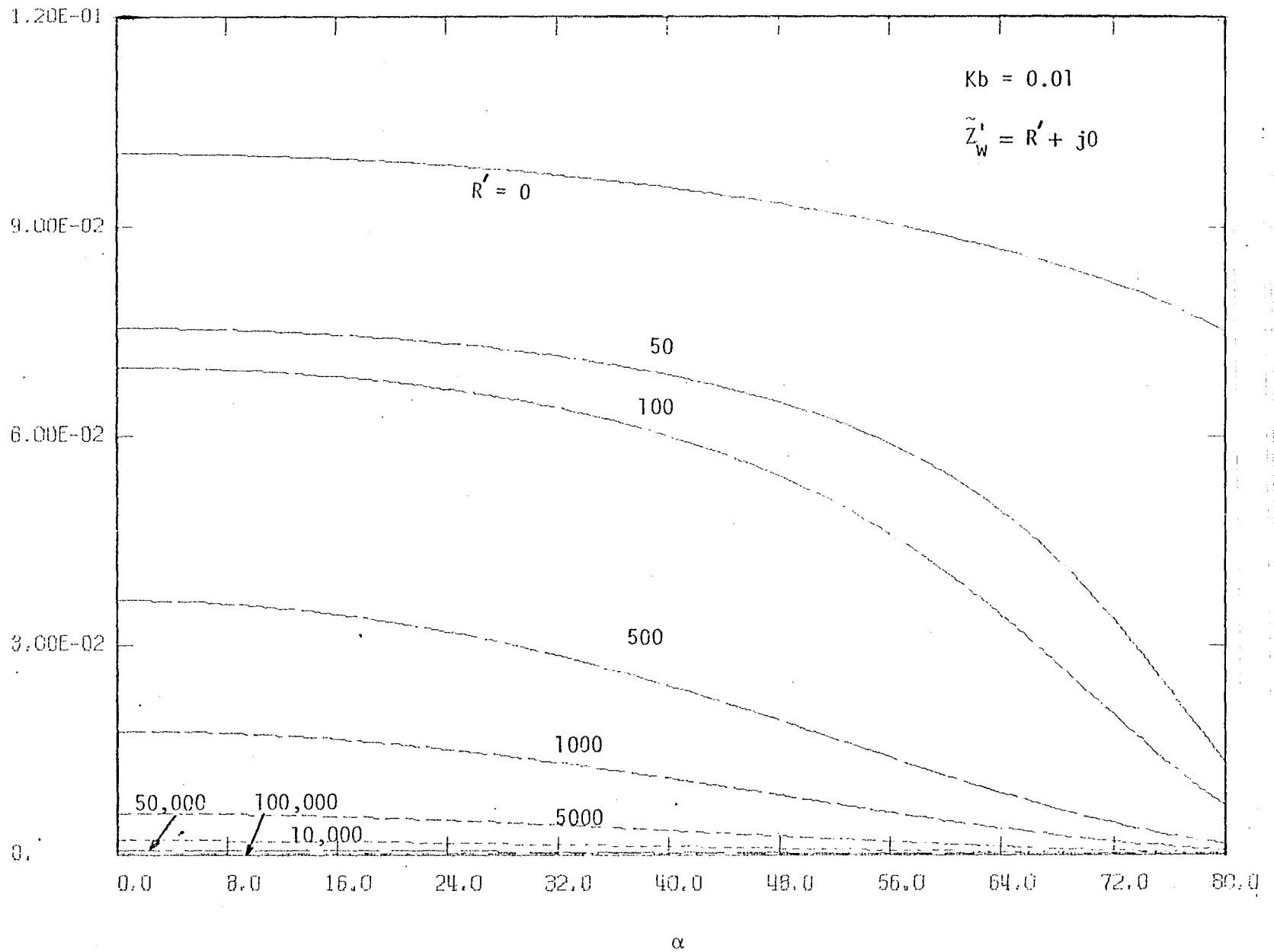


Figure 2.5(a). Magnitude of the Far-Field Distribution, Infinitely Long Thin Wire Loaded Antenna, \tilde{E}_z

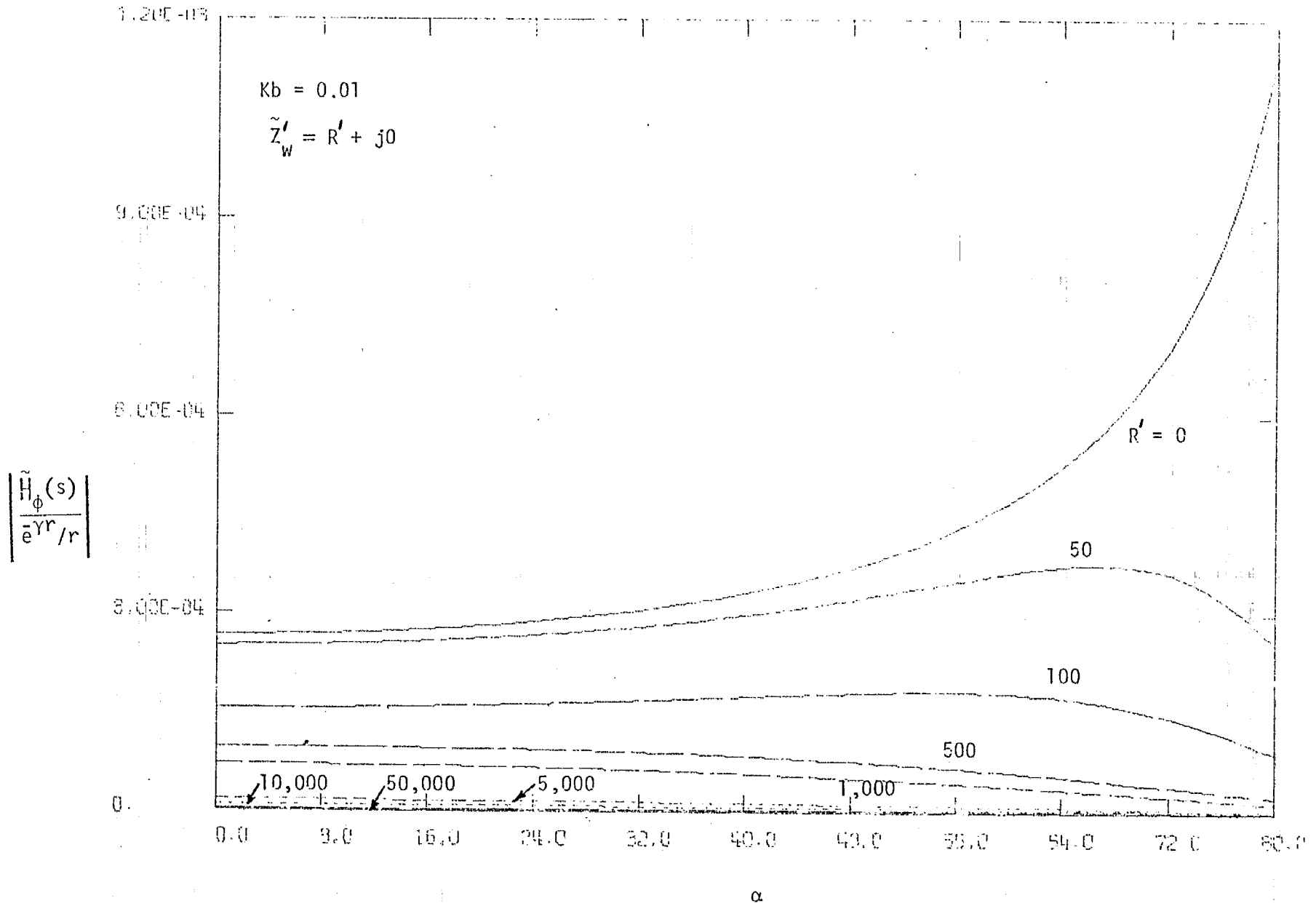


Figure 2.6(a). Magnitude of the Far-Field Distribution, Infinitely Long Thin Wire Loaded Antenna, \tilde{H}_ϕ

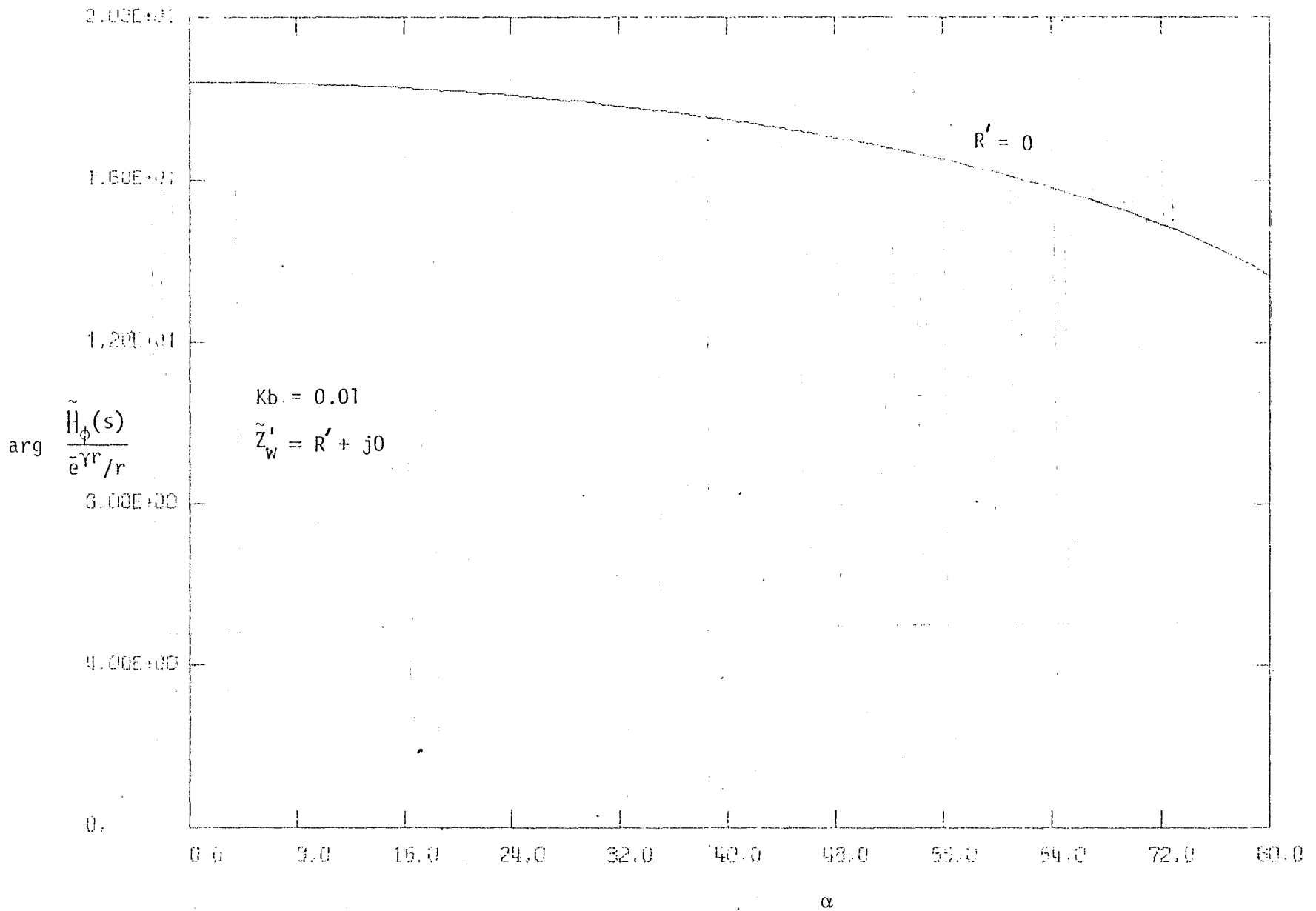


Figure 2.6(b). Phase of the Far-Field Distribution, Infinitely Long Thin Wire Loaded Antenna, \tilde{H}_ϕ

assumed. In figures 2.3a and b are shown the magnitude and phase of \tilde{E}_z far field distribution as a function of observation angle α for different values of $|\gamma b| = \frac{\omega b}{c}$ ($\gamma = jK$) and for a fixed value of loading $\tilde{Z}'_w(s) = 50 + j0$. The same results are obtained in figures 2.4a and b for \tilde{H}_ϕ . Figures 2.5a and b indicate the magnitude and phase of \tilde{E}_z far field distribution as a function of α for different values of the impedance loading \tilde{Z}'_w for a fixed value of $|\gamma b| = 0.01$. The same variations are given in figures 2.6a and b for \tilde{H}_ϕ . The results thus far obtained are useful to analyze infinitely long parallel cage wires.

C. Infinitely Long Loaded Wire Cage

The analysis of the infinitely long loaded wire antenna as discussed in section II-A, can be similarly extended to infinitely long multiple parallel loaded cage wires. We shall first discuss the general problem and later specialize to a circular cylindrical wire cage.

A set of infinitely long loaded thin wires are all oriented parallel to the z axis in an isotropic homogeneous medium as shown in figure 2.7. There are N parallel wires of radius a_n , $n = 1, 2, 3, \dots, N$ which are located at (Ψ_n, ϕ_n) with their axes displaced at least a few radii apart. The respective parallel wires are excited by source generators of voltage $\tilde{V}_n(s)$ across a gap of width $2d_n$, all centered at $z = 0$. If $\tilde{I}_n(z, s)$ is the induced axial current on the nth infinitely long thin cage wire, at any point P in the medium the z component of the magnetic vector potential is given by the superposition of the individual wire contributions,²

$$\tilde{A}_z^{(c)}(\Psi, z, s) = \sum_{n=1}^N \tilde{A}_{z_n}(\Psi, z, s) \quad (2.20a)$$

where the superscript c refers to the cage wires and referring to expression (2.3),

$$\tilde{A}_{z_n}(\Psi, z, s) = \frac{1}{2\pi j} \int_{C_\zeta} \tilde{F}_n(a_n, \zeta, s) K_0(u|\Psi - \Psi_n|) e^{\zeta z} d\zeta \quad (2.20b)$$

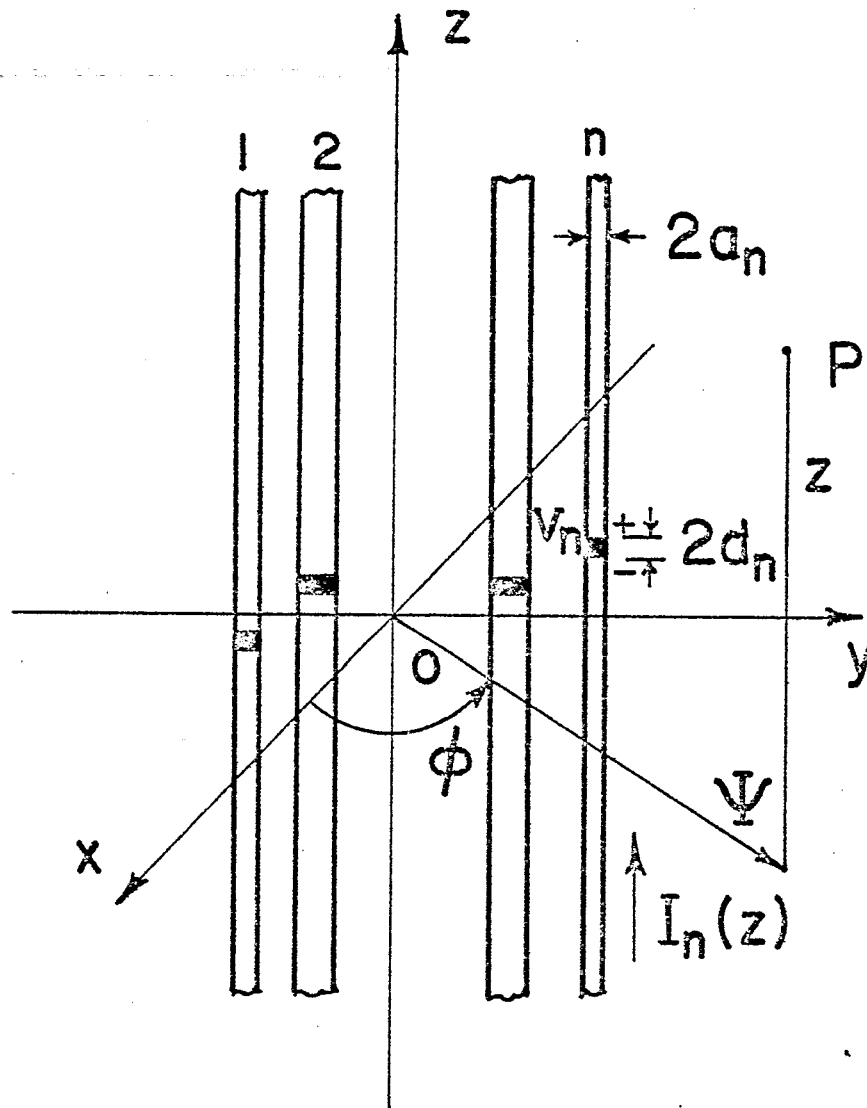


Figure 2.7. Infinitely Long Parallel Loaded Thin Cage Wires

in which

$$|\tilde{\Psi} - \tilde{\Psi}_n| = [(x - x_n)^2 + (y - y_n)^2]^{\frac{1}{2}} \quad (2.20c)$$

and the term $\tilde{F}_n(a_n, \zeta, s)$ is proportional to the Laplace-transform of the corresponding induced electric current on the n th wire. Again it is assumed $\tilde{I}_n(z, s)$ has no angular variations and for each of the n wires

$$|\gamma a_n| \ll 1, \quad n = 1, 2, \dots, N \quad (2.21)$$

so that no modes internal to a wire are excited. The electric and the magnetic fields for the wire cage structure are obtained by the expressions (2.4a,b) with \tilde{A}_z replaced by $\tilde{A}_z^{(c)}$. Since each of the cage wires is excited by an ideal gap of width $2d_n$, within each gap the electric field varies approximately as $-\tilde{V}_n(s)/2d_n$; similar to the expression (2.7), the electric current $\tilde{I}_n(a_n, z, s)$ and the scattered electric field $\tilde{E}_z^{(c)}(\psi, z, s)$ should satisfy the following impedance boundary relationship,

$$\begin{aligned} \tilde{E}_z^{(c)}(\psi, z, s) &= \left(-\frac{\tilde{V}_n(s)}{2d_n} \right) p_{d_n}(z) + \tilde{Z}'_{w,n}(s) \tilde{I}_n(a_n, z, s) \\ &\text{at } \tilde{\Psi} = \tilde{\Psi}_n \\ &n = 1, 2, 3, \dots, N \end{aligned} \quad (2.22)$$

where

$$\begin{aligned} p_{d_n}(z) &= 1, & |z| < d_n \\ &= 0, & |z| > d_n \end{aligned}$$

and $\tilde{Z}'_{w,n}(s)$ is the series axial impedance per unit length on the n th cage wire (Appendix A). In terms of the transformed quantities, the impedance boundary relationship (2.22) becomes

$$\tilde{E}_Z^{(c)}(\Psi_n, \zeta, s) = -\tilde{V}_n(s) G_n(\zeta) + \tilde{Z}'_{w,n}(s) \tilde{I}_n(a_n, \zeta, s) \quad (2.23)$$

$$n = 1, 2, 3, \dots, N$$

According to the expressions (2.1), (2.2d), (2.4a), and (2.20), the z component of the spectral electric field is

$$\tilde{E}_Z(\Psi_n, \zeta, s) = \sum_{m=1}^N -\frac{s}{\gamma^2} u^2 K_0(u|\tilde{\Psi}_n - \tilde{\Psi}_m|) \tilde{F}_m(a_m, \zeta, s) \quad (2.24)$$

Similarly, the induced electric current along the nth infinitely long cage wire is obtained from, referring to expression (2.11),

$$\tilde{I}(a_n, z, s) = -\frac{1}{u} \int_{\phi'=0}^{2\pi} \Psi' \left. \frac{\partial \tilde{A}_z(\Psi', z, s)}{\partial \Psi'} \right|_{\Psi'=a_n} \partial \phi' \quad (2.25)$$

where Ψ' and ϕ' are the local cylindrical coordinates about the axis of the nth wire. Assuming $\tilde{I}_n(a_n, z, s)$ has no ϕ' angular variations and the cage wires are placed at least a few radii apart, the expressions (2.1), (2.2d), (2.4b), and (2.20) yield,

$$\tilde{I}(a_n, \zeta, s) = \frac{1}{u} 2\pi a_n u K_1(u a_n) \tilde{F}_n(a_n, \zeta, s) \quad (2.26)$$

On substituting the expressions (2.24) and (2.26) into the impedance boundary relationship (2.23), the following expression is obtained for determining $\tilde{F}_n(a_n, \zeta, s)$,

$$\sum_{m=1}^N -\frac{s}{\gamma^2} u^2 K_0(u|\tilde{\Psi}_n - \tilde{\Psi}_m|) \tilde{F}_m(a_m, \zeta, s) = -\tilde{V}_n(s) G_n(\zeta) + \tilde{Z}'_{w,n}(s) \left[\frac{1}{u} 2\pi a_n u K_1(u a_n) \tilde{F}_n(a_n, \zeta, s) \right] \quad (2.27)$$

$$n = 1, 2, 3, \dots, N$$

This forms a set of linear simultaneous equations and the spectral term $F_n(a_n, \zeta, s)$, $n = 1, 2, 3, \dots, N$ can be determined as the solution to the following matrix equation

$$\begin{bmatrix} \tilde{S}_{nm} \end{bmatrix} \begin{bmatrix} \tilde{F}_m \end{bmatrix} = \begin{bmatrix} \tilde{E}_n \end{bmatrix} \tag{2.28a}$$

where the matrix elements are

$$\tilde{S}_{nm} = u^2 K_0(u|\tilde{\Psi}_n - \tilde{\Psi}_m|) , \quad n \neq m \tag{2.28b}$$

$$\tilde{S}_{nm} = u^2 K_0(ua_n) + 2\pi a_n u \gamma K_1(ua_n) \frac{\tilde{Z}'_{w,n}(s)}{Z_0} , \quad n = m \tag{2.28c}$$

and

$$\tilde{E}_n = \tilde{V}_n(s) \frac{\sinh(\zeta d_n)}{(\zeta d_n)} \frac{\gamma^2}{s} \tag{2.28d}$$

The matrix equation (2.28a) yields the solution

$$\begin{bmatrix} \tilde{F}_m \end{bmatrix} = \begin{bmatrix} \tilde{S}_{nm} \end{bmatrix}^{-1} \begin{bmatrix} \tilde{E}_n \end{bmatrix} \tag{2.29}$$

The current on each cage wire is obtained from (2.2d) and (2.26), and the magnetic vector potential obtained by substituting the result of (2.28) into the expression (2.20). Thus the radiated fields are obtained from the expressions (2.4) and (2.20).

D. Infinitely Long Loaded Circular Cylindrical Wire Cage

The general problem discussed in the previous section is specialized to a circular cylindrical wire cage. Suppose all the N wires are placed along the circumference of a large circle of diameter $2A$ and distributed uniformly around the circumference. If the circular wire cage consists of identical wire geometries, figure 2.8, which are fed from identical source generators, the matrix equation (2.9a) simplifies into a diagonal form.

Referring to figures 2.7 and 2.8, let

$$\tilde{V}(s) = \tilde{V}_n(s) \quad \text{source voltage across each gap}$$

$$2d = 2d_n \quad \text{width of each gap}$$

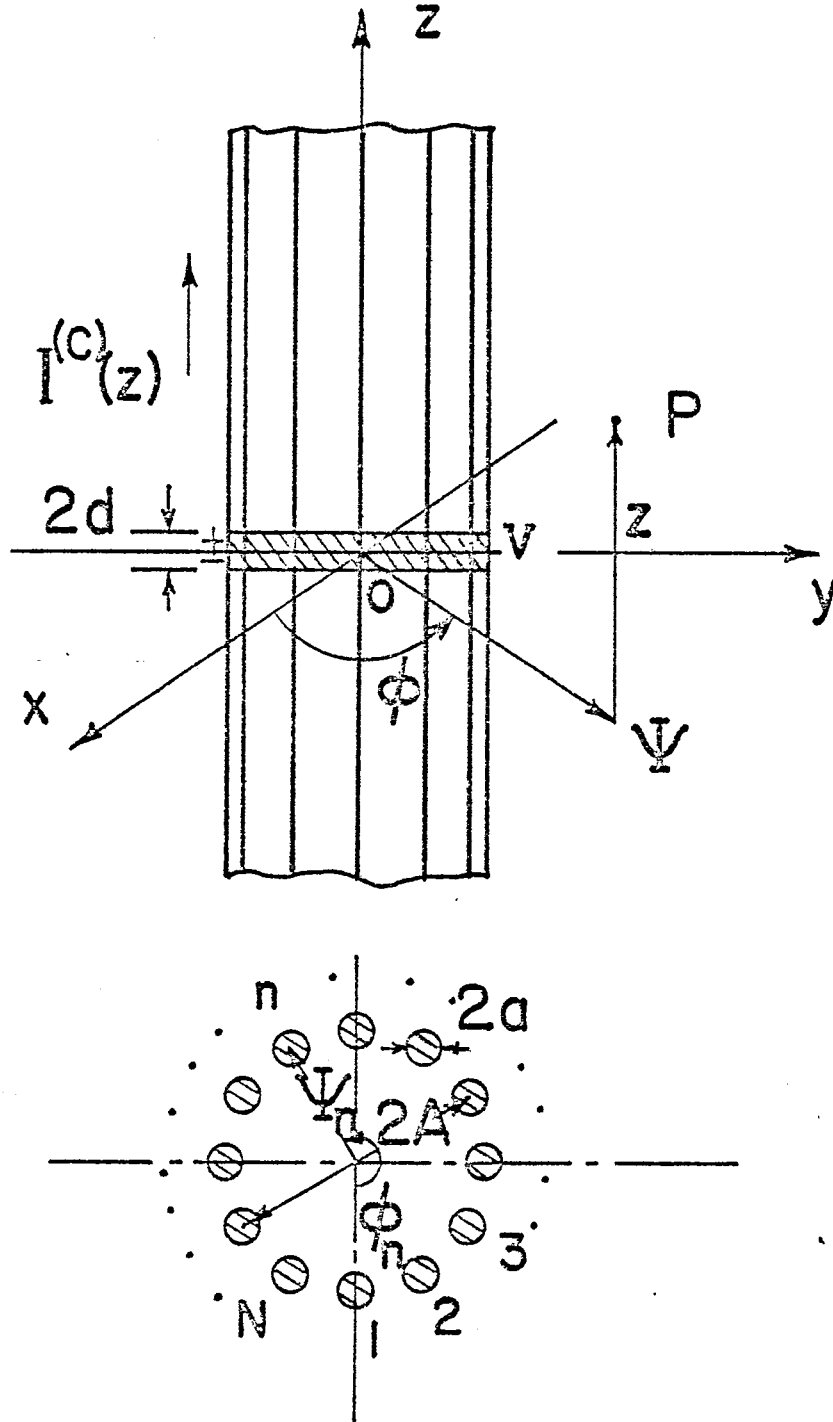


Figure 2.8. Infinitely Long Circular Cylindrical Wire Cage Antenna

$a = a_n$ radius of each cage wire

$\tilde{Z}_w^{(c)'}(s) = \tilde{Z}'_{w,n}(s)/N$ axial series impedance loading of each cage wire per unit length

for $n = 1, 2, 3, \dots, N$

Under these symmetrical conditions, the spectral functions $\tilde{F}_n(a_n, \zeta, s)$ are all the same, i.e., $\tilde{F}_1 = \tilde{F}_2 = \tilde{F}_3 = \dots = \tilde{F}_N$ ($= \tilde{F}^{(c)}(a, \zeta, s)$). Hence the induced electric current on each of the cage wires is the same, $\tilde{I}_1(z, s) = \tilde{I}_2(z, s) = \tilde{I}_3(z, s) = \dots = \tilde{I}_N(z, s)$ ($= \tilde{I}^{(c)}(z, s)/N$). Applying these relationships for the concentric wire cage, the expression (2.28) yields the solution,

$$\tilde{F}^{(c)}(a, \zeta, s) = \tilde{V}(s) \frac{\gamma^2}{s} \frac{G(\zeta)}{u\tilde{B}(\zeta, s)} \quad (2.30a)$$

where

$$\tilde{B}(\zeta, s) = \left\{ u \sum_{n=1}^N K_0(uA_{1,n}) \right\} + 2\pi a \gamma K_1(ua) \frac{\tilde{Z}_w^{(c)'}(s)}{Z_0} \quad (2.30b)$$

comparing the expressions (2.13b) and (2.30b), the summation in (2.30b) accounts for various mutual interactions and the factor $A_{1,n}$ is the inter-chord distance from wire 1 to wire n given by,

$$A_{1,n} = a, \quad n = 1 \quad (2.30c)$$

$$A_{1,n} = |\tilde{\Psi}_1 - \tilde{\Psi}_n|, \quad n = 2, 3, \dots, N \quad (2.30d)$$

Since the angle between any two consecutive wires is $2\pi/N$, the inter-chord distances (2.30d) can be written as

$$A_{1,n} = 2a \sin\left[\frac{\pi}{N}(n-1)\right], \quad n = 2, 3, \dots, N \quad (2.30e)$$

Hence the current on each cage wire is obtained from the expressions (2.2d), (2.26), and (2.30a),

$$\frac{1}{N} \tilde{I}^{(c)}(a, z, s) = \frac{\tilde{V}(s)\gamma a}{jZ_0} \int_{C_\zeta} \tilde{G}(\zeta) \frac{K_1(ua)}{\tilde{B}(\zeta, s)} e^{\zeta z} d\zeta \quad (2.31)$$

and the corresponding magnetic vector potential is obtained by substituting (2.30a) into the expression (2.20),

$$\tilde{A}_Z^{(c)}(\psi, z, s) = \frac{\tilde{V}(s)}{2\pi j} \frac{\gamma^2}{s} \int_{C_\zeta} \tilde{G}(\zeta) \left[\frac{\sum_{m=1}^N K_0(u|\tilde{\Psi} - \tilde{\Psi}_m|)}{u\tilde{B}(\zeta, s)} \right] e^{\zeta z} d\zeta \quad (2.32)$$

The electric and the magnetic fields can now be written using the expressions (2.1), (2.4), and (2.32) in spectral form as

$$\begin{bmatrix} \tilde{E}_Z^{(c)}(\psi, \zeta, s) \\ Z_0 \tilde{H}_\phi^{(c)}(\psi, \zeta, s) \end{bmatrix} = \begin{bmatrix} \tilde{Q}_1 \\ \tilde{Q}_2 \end{bmatrix} \quad (2.33a)$$

where $[\tilde{Q}]$ is a vector for the circular cylindrical wire cage antenna and is given by

$$\begin{bmatrix} \tilde{Q}_1 \\ \tilde{Q}_2 \end{bmatrix} = \begin{bmatrix} \tilde{Q}_1 \\ \tilde{Q}_2 \end{bmatrix} \quad (2.33b)$$

and the elements of the vector are,

$$\tilde{Q}_1 = -\tilde{V}(s) \tilde{G}(\zeta) \left\{ \frac{\sum_{m=1}^N u K_0(u|\tilde{\Psi} - \tilde{\Psi}_m|)}{\tilde{B}(\zeta, s)} \right\} \quad (2.33c)$$

$$\tilde{Q}_2 = \tilde{V}(s) \tilde{G}(\zeta) \left\{ \frac{\sum_{m=1}^N \gamma K_1(u|\tilde{\Psi} - \tilde{\Psi}_m|)}{\tilde{B}(\zeta, s)} \right\} \left[\frac{d}{d\tilde{\Psi}} (|\tilde{\Psi} - \tilde{\Psi}_m|) \right] \quad (2.33d)$$

Again we have difficulty obtaining general solutions for the fields (2.33a), since the integrations are to be performed along the C_ζ contour, figure 2.2. But in the far field region as $\Psi \rightarrow \infty$, the expressions (2.33) reduce to simpler forms (Appendix B) based on the saddle-point integration method. Hence for the infinitely long circular wire cage structure, in the far field region the electric and the magnetic field components are obtained as (figure B-1),

$$\tilde{E}_z^{(c)}(r, \alpha, s) \sim - \frac{\tilde{V}(s)}{2} \frac{\cos(\alpha)}{\tilde{L}_2(\gamma, \alpha)} \frac{e^{-\gamma r}}{r} \tilde{C}_f \quad (2.34a)$$

$$Z_0 \tilde{H}_\phi^{(c)}(r, \alpha, s) \sim \frac{\tilde{V}(s)}{2} \frac{1}{\tilde{L}_2(\gamma, \alpha)} \frac{e^{-\gamma r}}{r} \tilde{C}_f \quad (2.34b)$$

where the cage factor is

$$\tilde{C}_f = NI_0(\gamma A \cos(\alpha)) \quad (2.34c)$$

I_0 is the modified Bessel function of the first kind, zero order, r and $\theta = 90 - \alpha$ are the spherical coordinate variables. In the above expressions

$$\tilde{L}_2(\gamma, \alpha) = \cos \alpha \sum_{n=1}^N K_0(\gamma A_{1,n} \cos \alpha) + \tilde{h}_2(s) K_1(\gamma a \cos \alpha) \quad (2.34d)$$

$$\tilde{h}_2(s) = 2\pi a \frac{\tilde{Z}_w^{(c)'}(s)}{Z_0} \quad (2.34e)$$

E. Numerical Results: Far Field

In section II-C the infinitely long loaded wire cage is analyzed, while the specialization to the circular wire cage is given in section II-D along with the expressions for the induced electric current, radiated fields and far-field distributions.

In figures 2.9a and b are shown the magnitude and phase of the $E_Z^{(c)}$ far-field distribution as a function of observation angle α for different values of the loading $\tilde{Z}_W^{(c)}$ and for a fixed value of $KA = 1.0$, $Ka = 0.01$ and number of cage wires $N = 12$. The same variations are given in figures 2.10a and b, but for the far-field $\tilde{H}_\phi^{(c)}$. Similarly in figures 2.11a and b are shown the magnitude and phase of the $E_Z^{(c)}$ far-field distribution as a function of angle α for different number of cage wires N and fixed impedance loadings $\tilde{Z}_W^{(c)} = (50 + j0) \Omega/m$. Further, the figures 2.12a and b give the distribution of the corresponding $\tilde{H}_\phi^{(c)}$ of the far field.

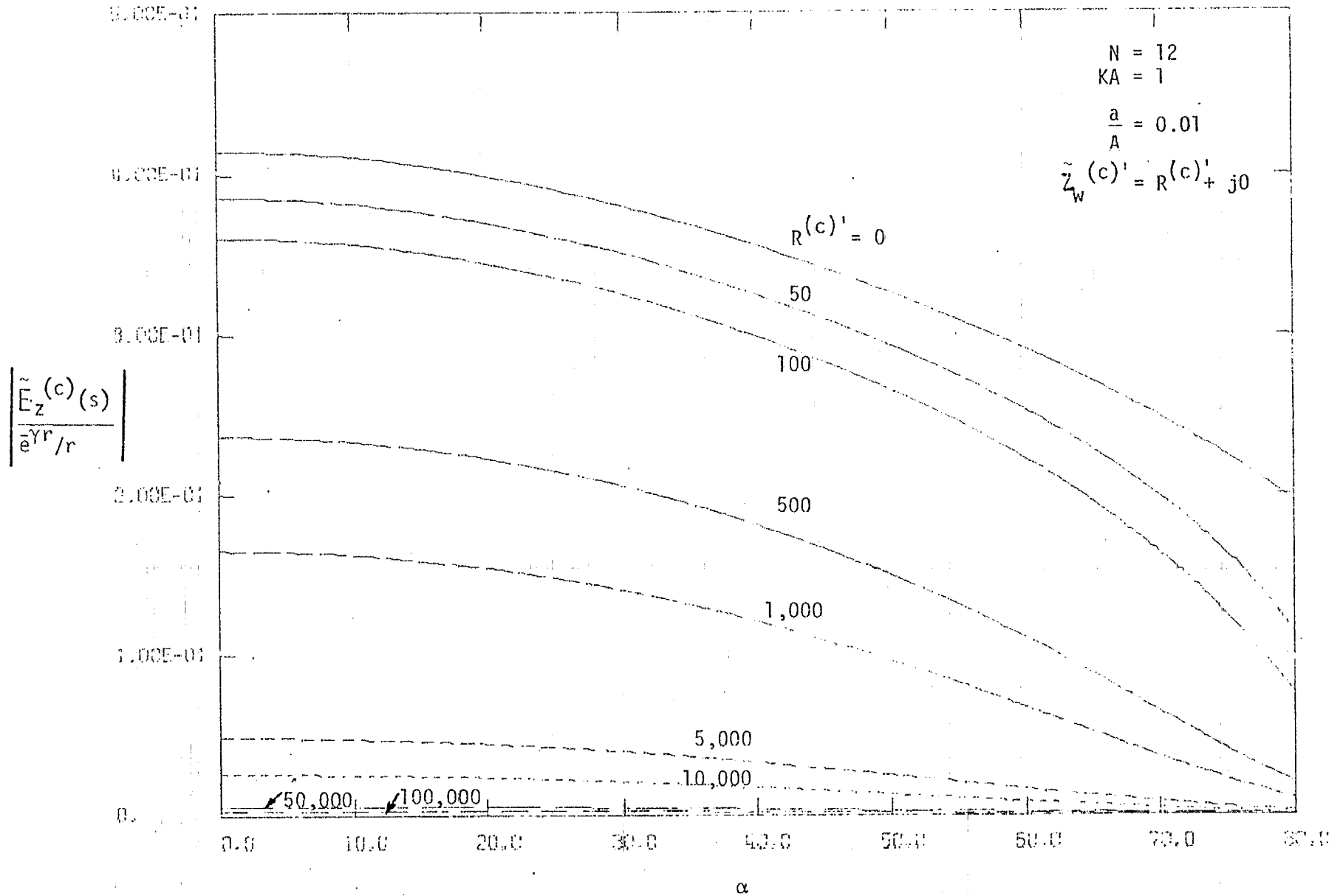


Figure 2.9(a). Magnitude of the Far-Field Distribution, Infinitely Long Loaded Circular Wire Cage Antenna, $\tilde{E}_z(c)$

III. INFINITELY LONG LOADED HOLLOW CIRCULAR CYLINDRICAL ANTENNA

The analysis of the hollow cylindrical structure^{16,17} is slightly different from the previous cases discussed wherein the wire antenna structure is assumed as thin, so that the fields inside the wire can be completely neglected. This is particularly true with the case of solid thin-wire structures.¹³ But when the radius becomes large, one has to analyze both the external and the internal regions separately and enforce the relevant impedance boundary condition on the surface of the hollow cylinder. It is assumed the cylinder wall is very thin and for all the mathematical considerations, the thickness of the wall can be neglected. The material of the wall of the hollow cylinder is lossy and homogeneous and can be characterized in terms of a uniform sheet impedance (Appendix A). Even with an external impedance loading function introduced, the concept of the boundary condition is based on a uniform sheet impedance in contrast to the surface impedance concept utilized in the previous sections.

The infinitely long hollow cylinder is oriented along the z axis in an isotropic homogeneous medium. The radius of the cylinder is C and is excited by a source generator of voltage $\tilde{V}(s)$ across a gap of width $2d$ centered at $z = 0$, as shown in figure 3.1. The medium characteristics (μ, ϵ, σ) are the same both for the internal region 1 and the external region 2. The z component of the magnetic vector potential is given by, in region 1,

$$\tilde{A}_z^{(1)}(\psi, z, s) = \frac{1}{2\pi j} \int_{C_\zeta} \tilde{F}_1(C, \zeta, s) K_0(uC) I_0(u\psi) e^{\zeta z} d\zeta$$

$$\psi < C \quad (3.1a)$$

and in region 2,

$$\tilde{A}_z^{(2)}(\psi, z, s) = \frac{1}{2\pi j} \int_{C_\zeta} \tilde{F}_2(C, \zeta, s) I_0(uC) K_0(u\psi) e^{\zeta z} d\zeta$$

$$\psi > C \quad (3.1b)$$

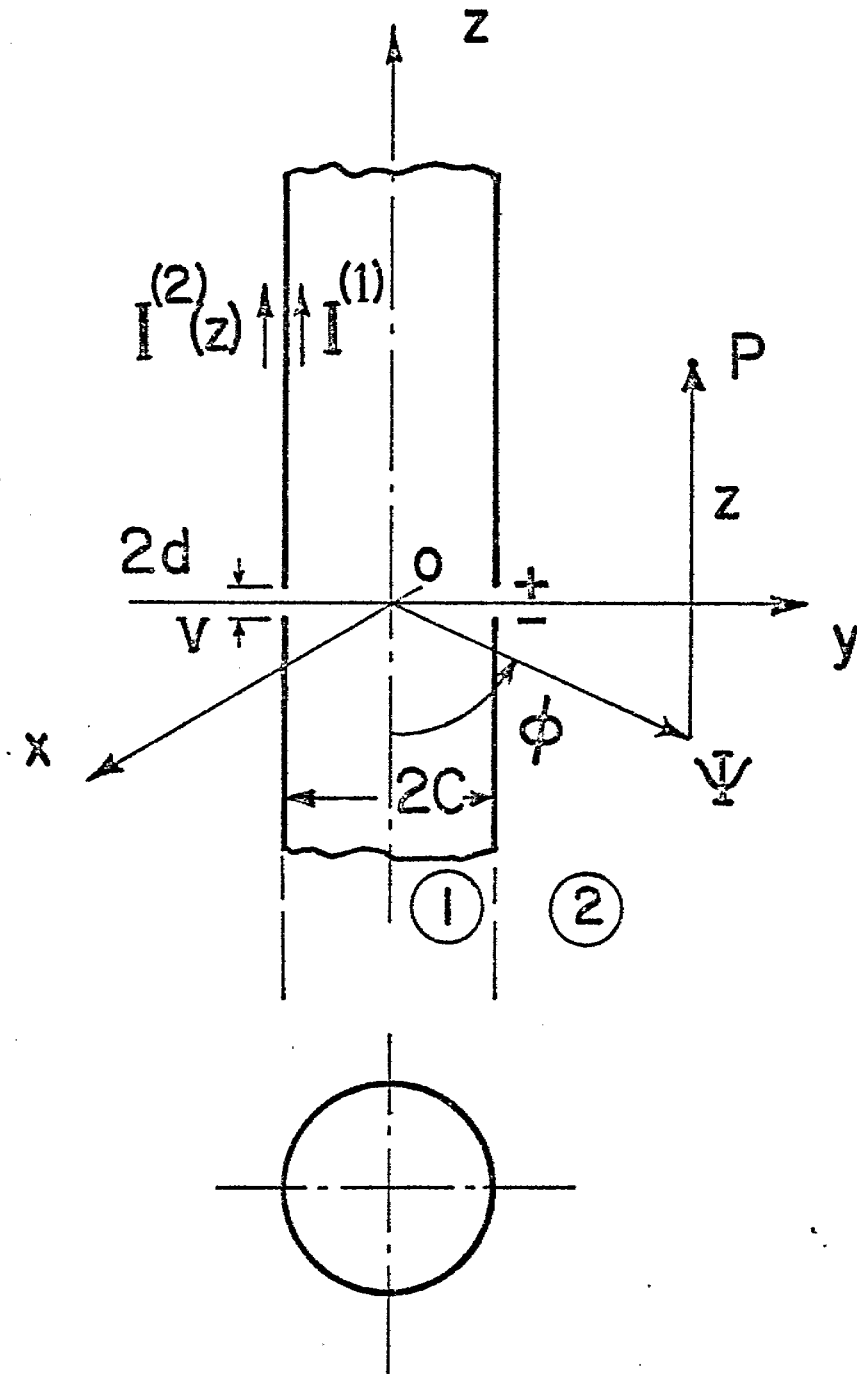


Figure 3.1. Infinitely Long Loaded Hollow Circular Cylindrical Antenna

where I_0 and K_0 are the modified Bessel functions of first and second kind, zero order. The spectral terms $\tilde{F}_1(C, \zeta, s)$ and $\tilde{F}_2(C, \zeta, s)$ are proportional to the Laplace transform of the net electric current $[\tilde{I}_2(C, \zeta, s) + \tilde{I}_1(C, \zeta, s)]$ of the external and internal surface of the hollow cylinder. Again electric and magnetic fields in the regions 1 and 2 are obtained by substituting (3.1) into the expressions (2.1) and (2.4). The tangential electric field $\tilde{E}_z(\Psi, z, s)$ at the wall surface is continuous, while the tangential magnetic field $\tilde{H}_\phi(\Psi, z, s)$ is discontinuous to the extent proportional to the difference of the external and the internal surface currents. Hence we have the following impedance boundary relationship

$$\begin{aligned} \tilde{E}_z^{(1)}(C^-, z, s) &= \tilde{E}_z^{(2)}(C^+, z, s) \\ &= -\frac{\tilde{V}(s)}{2d} p_d(z) + \tilde{Z}'(s) [\tilde{I}^{(2)}(C^+, z, s) + \tilde{I}^{(1)}(C^-, z, s)] \end{aligned} \quad (3.2)$$

where $\tilde{Z}'(s)$ is the impedance loading function per unit length of the infinitely long hollow cylinder,

$$\tilde{Z}'(s) = \frac{\tilde{Z}_s(s)}{2\pi C} \quad (3.3)$$

and $\tilde{Z}_s(s)$ is the sheet impedance in ohm of the hollow cylinder (Appendix A). In terms of transformed variables the boundary relationship (3.2) becomes,

$$\begin{aligned} \tilde{E}_z^{(1)}(C^-, \zeta, s) &= \tilde{E}_z^{(2)}(C^+, \zeta, s) \\ &= -\tilde{V}(s) G(\zeta) + \tilde{Z}'(s) [\tilde{I}^{(2)}(C^+, \zeta, s) + \tilde{I}^{(1)}(C^-, \zeta, s)] \end{aligned} \quad (3.4)$$

Referring to the expressions (2.1), (2.2d), (2.4a), and (3.1) the z component of the electric field is given by,

$$\tilde{E}_Z^{(1)}(\Psi, \zeta, s) = -\frac{s}{\gamma^2} u^2 K_0(uC) I_0(u\Psi) \tilde{F}_1(C, \zeta, s) \quad (3.5a)$$

$\Psi < C$

and

$$\tilde{E}_Z^{(2)}(\Psi, \zeta, s) = -\frac{s}{\gamma^2} u^2 I_0(uC) K_0(u\Psi) \tilde{F}_2(C, \zeta, s) \quad (3.5b)$$

$\Psi > C$

Further, the external and the internal currents on the hollow cylinder using the expressions (2.1), (2.2d), (2.4b), and (3.1) are obtained as

$$\tilde{I}^{(2)}(C^+, \zeta, s) = \frac{1}{u} 2\pi Cu I_0(uC) K_1(uC) \tilde{F}_2(C, \zeta, s) \quad (3.6a)$$

$$\tilde{I}^{(1)}(C^-, \zeta, s) = \frac{1}{u} 2\pi Cu K_0(uC) I_1(uC) \tilde{F}_1(C, \zeta, s) \quad (3.6b)$$

on substituting the expressions (3.5) and (3.6) into the boundary relationship (3.4), we have

$$\begin{aligned} \tilde{F}_1(C, \zeta, s) &= \tilde{F}_2(C, \zeta, s) \\ &= \tilde{V}(s) \frac{\gamma^2}{s} \frac{G(\zeta)}{u\tilde{P}(\zeta, s)} \end{aligned} \quad (3.7a)$$

where

$$\tilde{P}(\zeta, s) = uI_0(uC) K_0(uC) + 2\pi C\gamma \frac{\tilde{Z}'(s)}{Z_0} \left[\frac{1}{uC} \right] \quad (3.7b)$$

Hence the electric current on the internal and the external surface of the hollow cylinder is obtained from (2.2d), (3.6), and (3.7) as,

$$\tilde{I}^{(1)}(C, z, s) = \frac{\tilde{V}(s)\gamma C}{jZ_0} \int_{C_\zeta} G(\zeta) \frac{K_0(uC) I_1(uC)}{\tilde{P}(\zeta, s)} e^{\zeta z} d\zeta \quad (3.8a)$$

$$\tilde{I}^{(2)}(C, z, s) = \frac{\tilde{V}(s)\gamma C}{jZ_0} \int_{C_\zeta} \tilde{G}(\zeta) \frac{I_0(uC) K_1(uC)}{\tilde{P}(\zeta, s)} e^{\zeta z} d\zeta \quad (3.8b)$$

The net total current flowing on the hollow cylinder, with the assumption of current flowing in the z direction as positive, is $[\tilde{I}^{(2)}(C, z, s) + \tilde{I}^{(1)}(C, z, s)]$,

$$\tilde{I}^{(t)}(C, z, s) = \frac{\tilde{V}(s)\gamma}{jZ_0} \int_{C_\zeta} \tilde{G}(\zeta) \frac{1}{u\tilde{P}(\zeta, s)} e^{\zeta z} d\zeta \quad (3.8c)$$

Since the surface current density is independent of ϕ , it is obtained by dividing the expression (3.8c) by the circumferential length $2\pi C$. The z component of the magnetic vector potential in the regions 1 and 2 is obtained by substituting the spectral term (3.7a) in the expressions (3.1a, b),

$$\tilde{A}_z^{(1)}(\Psi, z, s) = \frac{\tilde{V}(s)}{2\pi j} \frac{\gamma}{s} \int_{C_\zeta} \tilde{G}(\zeta) \frac{K_0(uC) I_0(u\Psi)}{u\tilde{P}(\zeta, s)} e^{\zeta z} d\zeta \quad (3.9a)$$

$\Psi < C$

$$\tilde{A}_z^{(2)}(\Psi, z, s) = \frac{\tilde{V}(s)}{2\pi j} \frac{\gamma}{s} \int_{C_\zeta} \tilde{G}(\zeta) \frac{I_0(uC) K_0(u\Psi)}{u\tilde{P}(\zeta, s)} e^{\zeta z} d\zeta \quad (3.9b)$$

$\Psi > C$

The electric and the magnetic fields radiated are obtained using the expressions (2.1), (2.4), and (3.9b) in the regions 1 and 2 in the spectral form as,

$$\begin{bmatrix} \tilde{E}_z^{(1,2)}(\Psi, \zeta, s) \\ Z_0 \tilde{H}_\phi^{(1,2)}(\Psi, \zeta, s) \end{bmatrix} = \begin{bmatrix} \tilde{W}^{(1,2)} \end{bmatrix} \quad (3.10a)$$

where $[\tilde{W}^{(1,2)}]$ is the vector for the infinitely long hollow cylindrical antenna,

$$\begin{bmatrix} \tilde{W}(1,2) \\ \tilde{W} \end{bmatrix} = \begin{bmatrix} \tilde{W}_1(1,2) \\ \tilde{W}_2(1,2) \end{bmatrix} \quad (3.10b)$$

and the elements of the vector have the form

$$\tilde{W}_1(1,2) = \tilde{V}(s) \tilde{G}(\zeta) \frac{\begin{Bmatrix} uK_0(uC) & I_0(u\Psi) \\ uI_0(uC) & K_0(u\Psi) \end{Bmatrix}}{\tilde{P}(\zeta, s)} \quad (3.10c)$$

$$\tilde{W}_2(1,2) = \tilde{V}(s) \tilde{G}(\zeta) \frac{\begin{Bmatrix} -\gamma K_0(uC) & I_1(u\Psi) \\ \gamma I_0(uC) & K_1(u\Psi) \end{Bmatrix}}{\tilde{P}(\zeta, s)} \quad (3.10d)$$

As $\Psi \rightarrow \infty$, the field expressions can be reduced to simpler forms in the far field region using the saddle point method¹⁴ discussed in Appendix B,

$$\tilde{E}_z^{(2)}(r, \alpha, s) \sim -\frac{\tilde{V}(s)}{2} \frac{\cos \alpha}{\tilde{L}_3(\gamma, \alpha)} \frac{e^{-\gamma r}}{r} \tilde{P}_f \quad (3.11a)$$

$$Z_0 \tilde{H}_\phi^{(2)}(r, \alpha, s) \sim \frac{\tilde{V}(s)}{2} \frac{1}{\tilde{L}_3(\gamma, \alpha)} \frac{e^{-\gamma r}}{r} \tilde{P}_f \quad (3.11b)$$

where the hollow cylinder factors are

$$\tilde{P}_f = I_0(\gamma C \cos \alpha) \quad (3.11c)$$

$$\tilde{L}_3(\gamma, \alpha) = \cos \alpha I_0(\gamma C \cos \alpha) K_0(\gamma C \cos \alpha) + \tilde{h}_3(s) \left[\frac{1}{\gamma C \cos \alpha} \right] \quad (3.11d)$$

$$\tilde{h}_3(s) = 2\pi C \frac{\tilde{Z}'(s)}{Z_0} \quad (3.11e)$$

A. Numerical Results: Far Fields

Based on the analytical expressions formulated in the previous section for the induced electric current, radiated fields, and far-field distribution for the case of infinitely long loaded hollow cylinder, numerical results are presented in figures 3.2 through 3.5 for the radiated far-field distribution.

In figures 3.2a and b are shown the magnitude and phase of $\tilde{E}_Z^{(2)}$ of the far-field distribution as a function of the observation angle α for different values of the radius C of the hollow cylinder, and for a fixed $\gamma = j1$ and loading function $\tilde{Z}' = 50 + j0$. Figures 3.3a and b indicate the same variations, but for the $\tilde{H}_\phi^{(2)}$ component. Similarly in figures 3.4a and b are shown the magnitude and phase of the $\tilde{E}_Z^{(2)}$ component far-field as a function of α for different values of the loading function \tilde{Z}' and for fixed value of $|\gamma C| = 1$. Further the figures 3.5a and b indicate the same variations, but for the $\tilde{H}_\phi^{(2)}$.

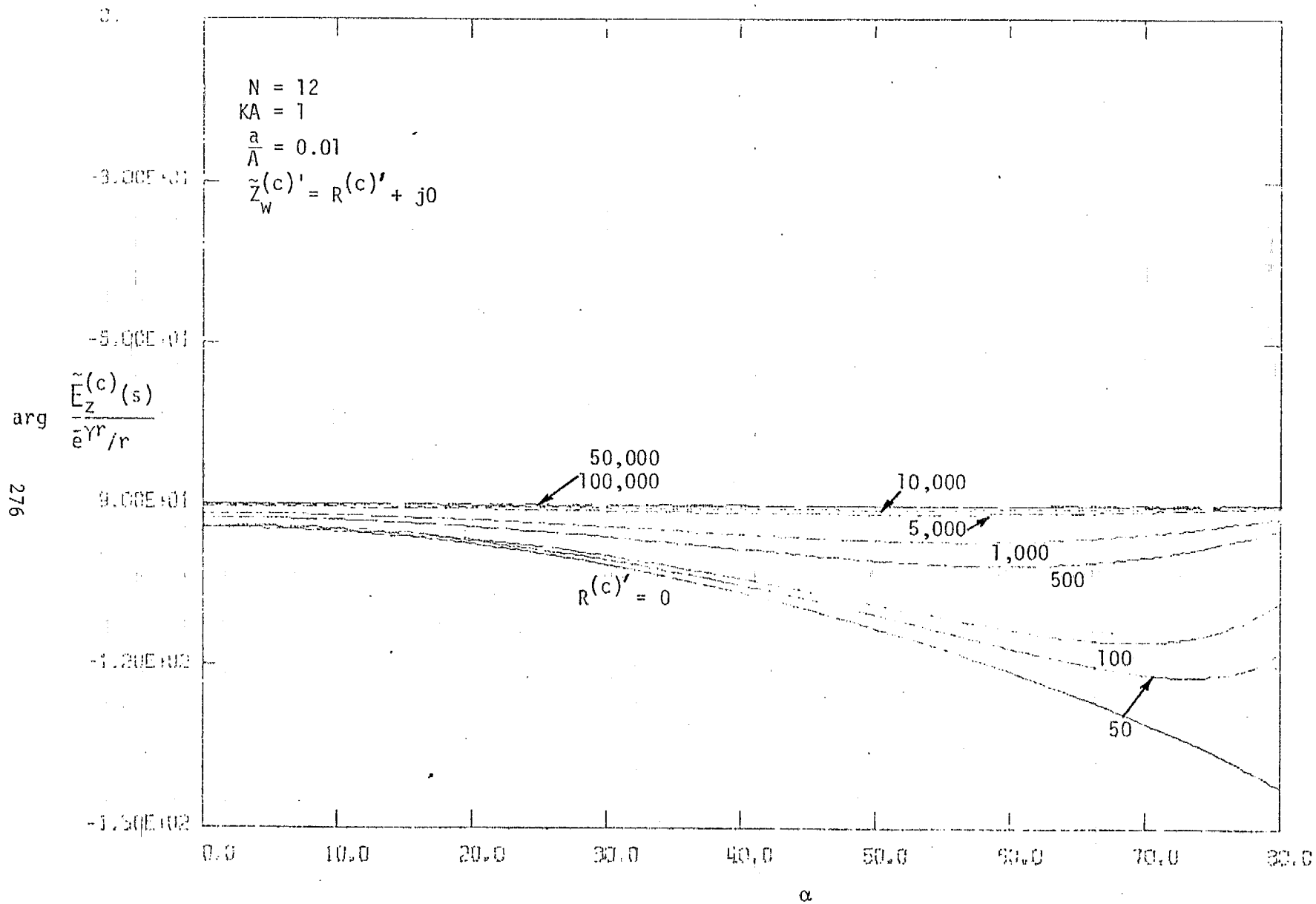


Figure 2.9(b). Phase of the Far-Field Distribution, Infinitely Long Loaded Circular Wire Cage Antenna, $\tilde{E}_Z^{(c)}$

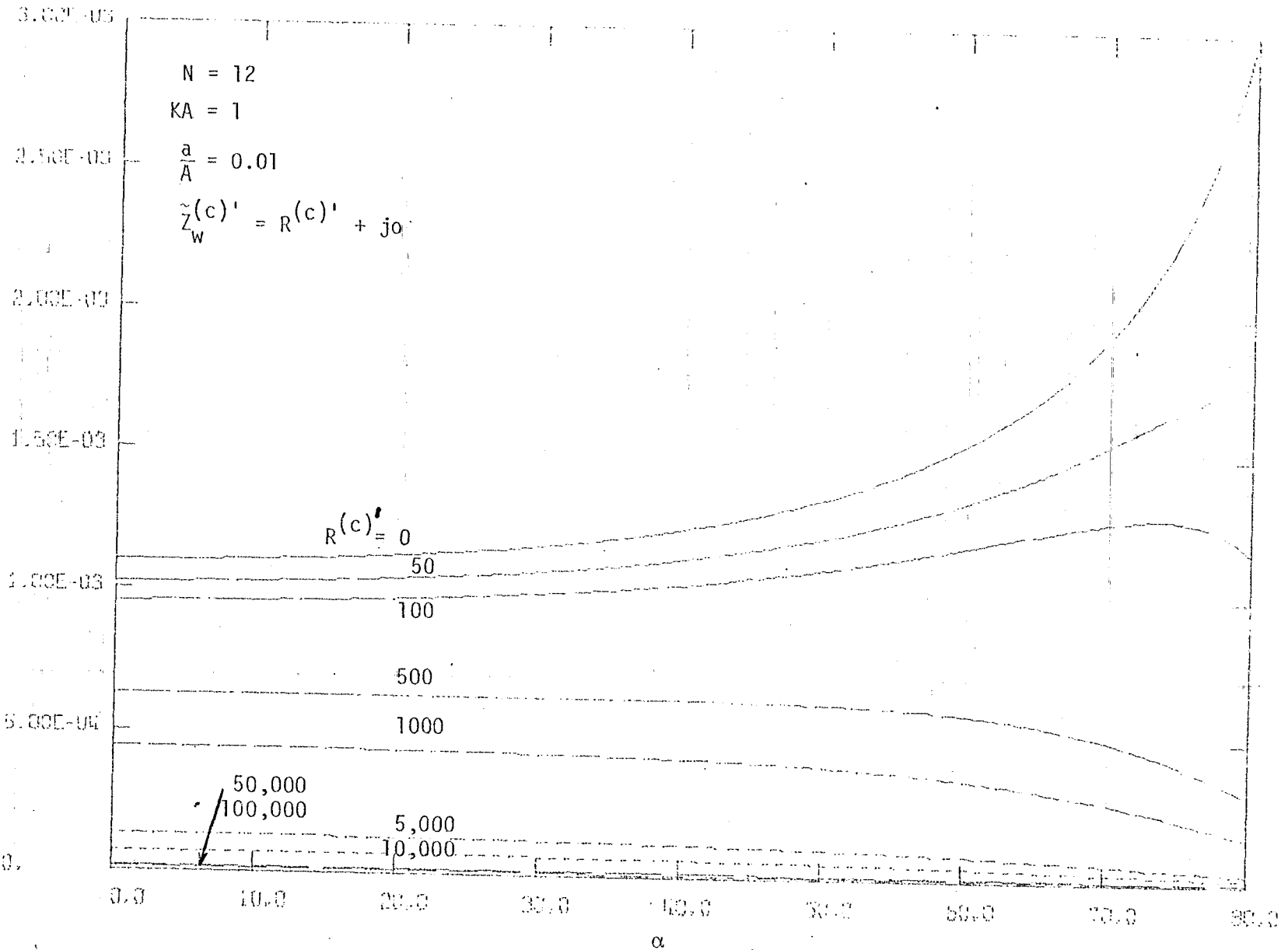


Figure 2.10(a). Magnitude of the Far-Field Distribution, Infinitely Long Loaded Circular Wire Cage Antenna, $H_\phi(c)$

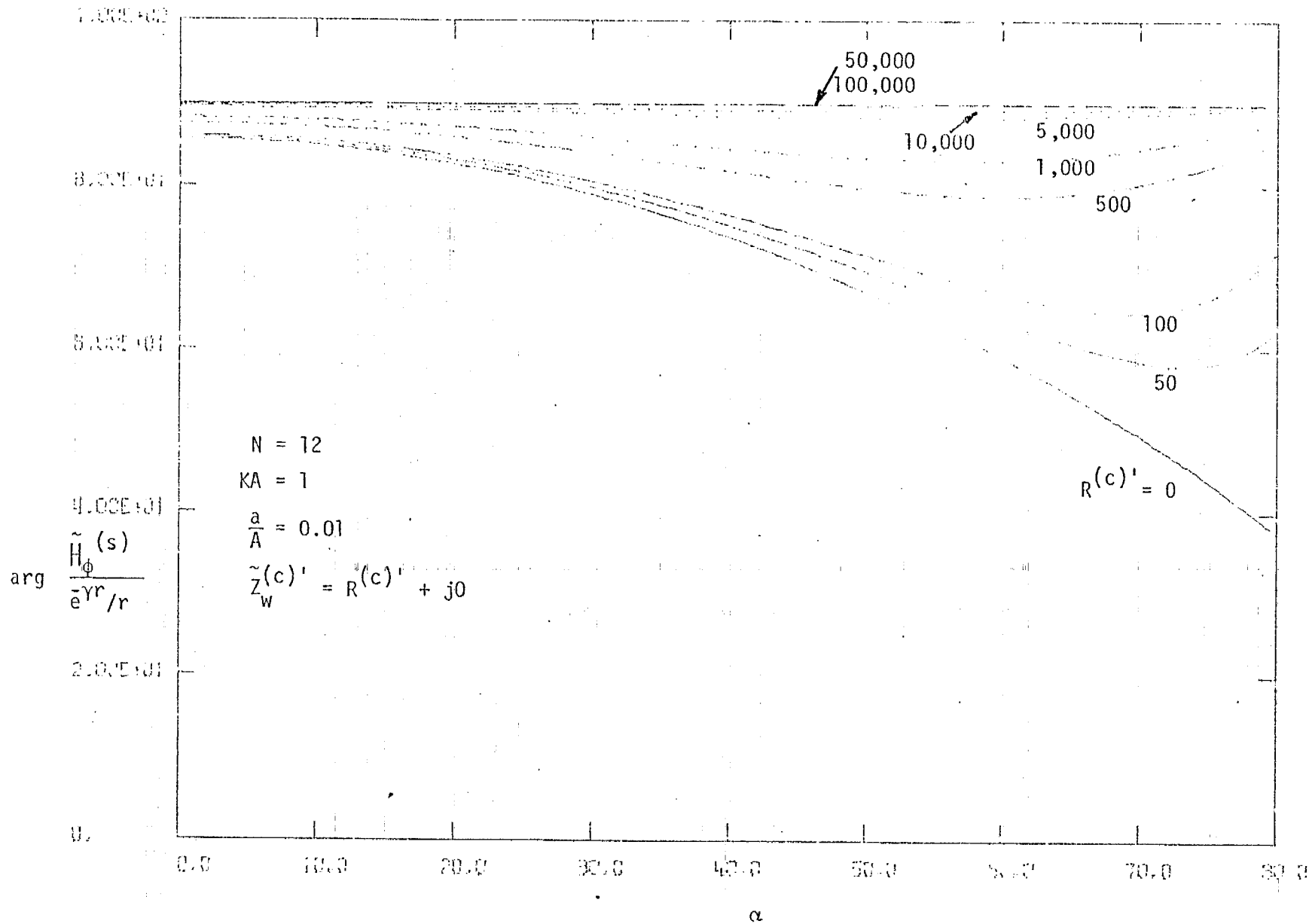


Figure 2.10(b). Phase of the Far-Field Distribution, Infinitely Long Loaded Circular Wire Cage Antenna, $\tilde{H}_\phi(c)$

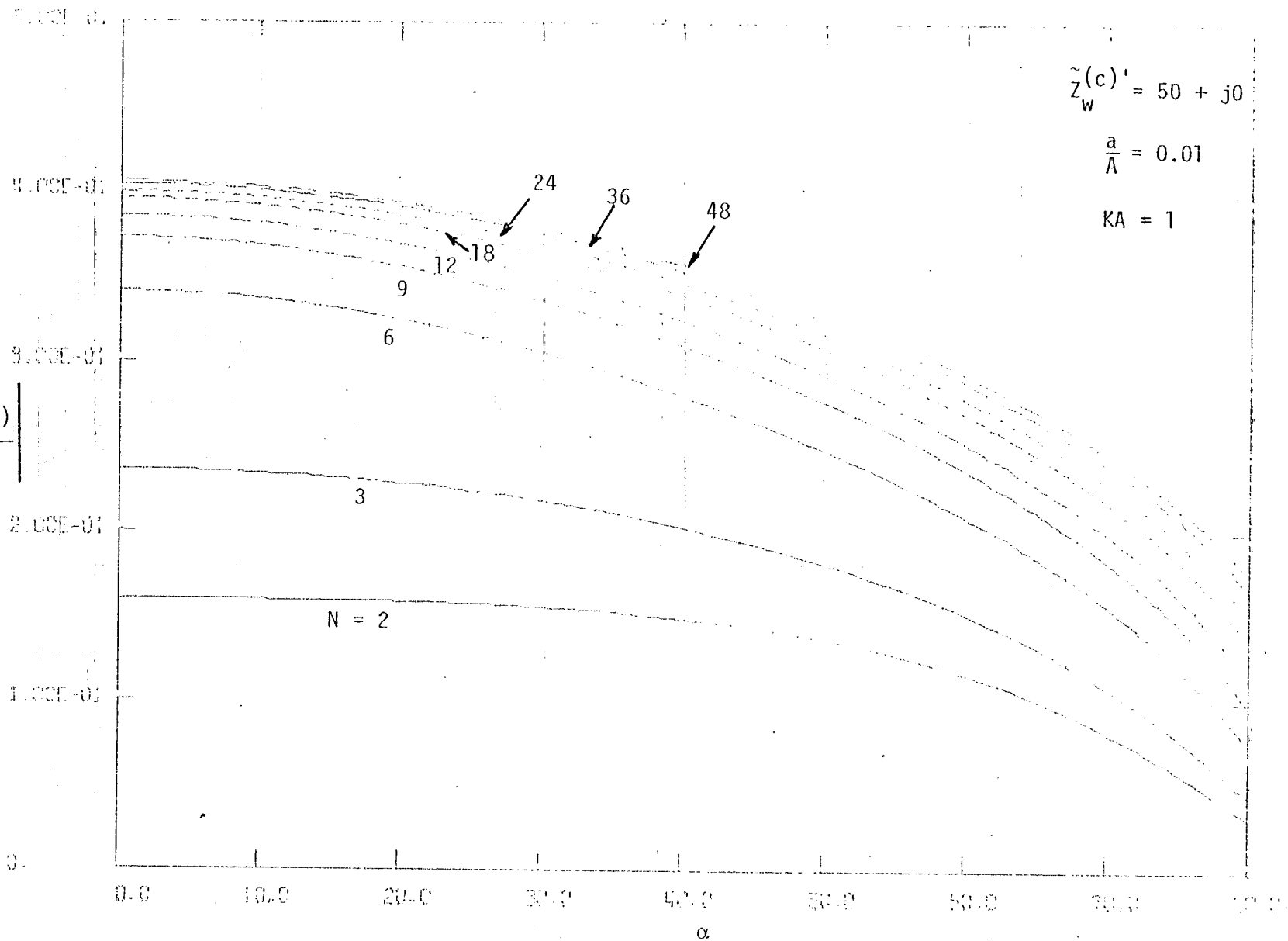


Figure 2.11(a). Magnitude of the Far-Field Distribution, Infinitely Long Loaded Circular Wire Cage Antenna, $\tilde{E}_z(c)$

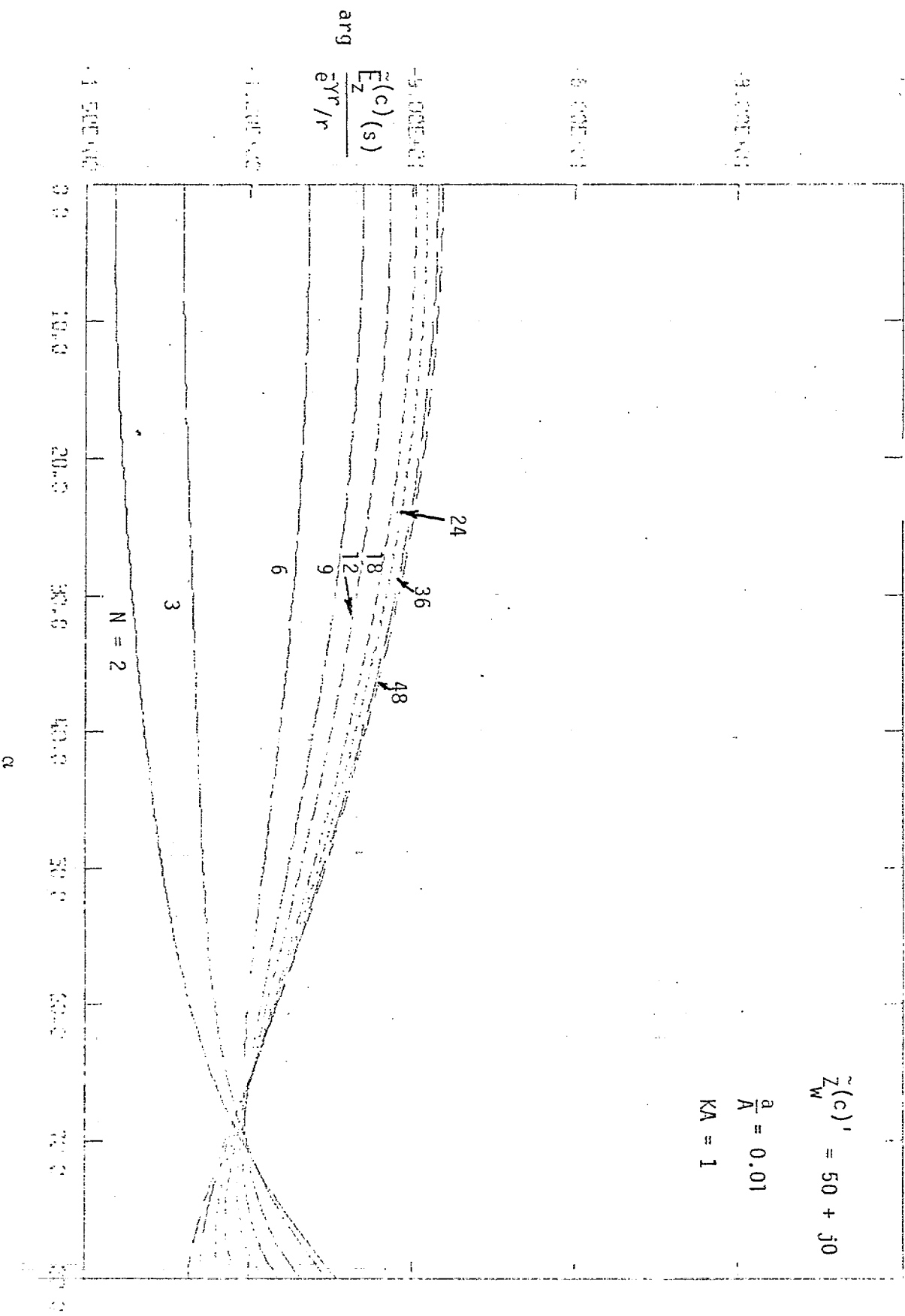


Figure 2.11(b). Phase of the Far-Field Distribution, Infinitely Long Loaded Circular Wire Cage Antenna, $\tilde{E}_z(c)$

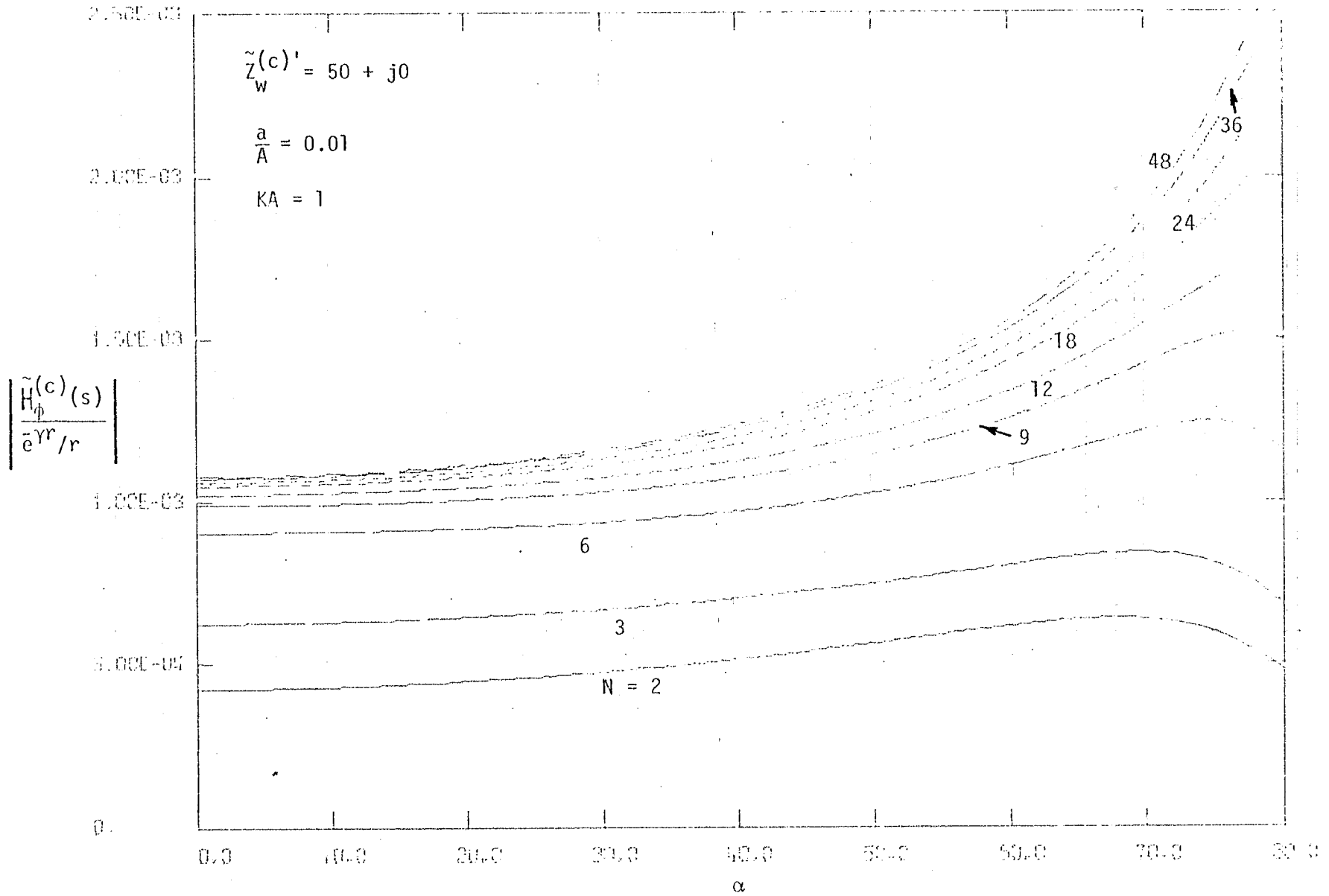


Figure 2.12(a). Magnitude of the Far-Field Distribution, Infinitely Long Loaded Circular Wire Cage Antenna, $\tilde{H}_\phi^{(c)}$

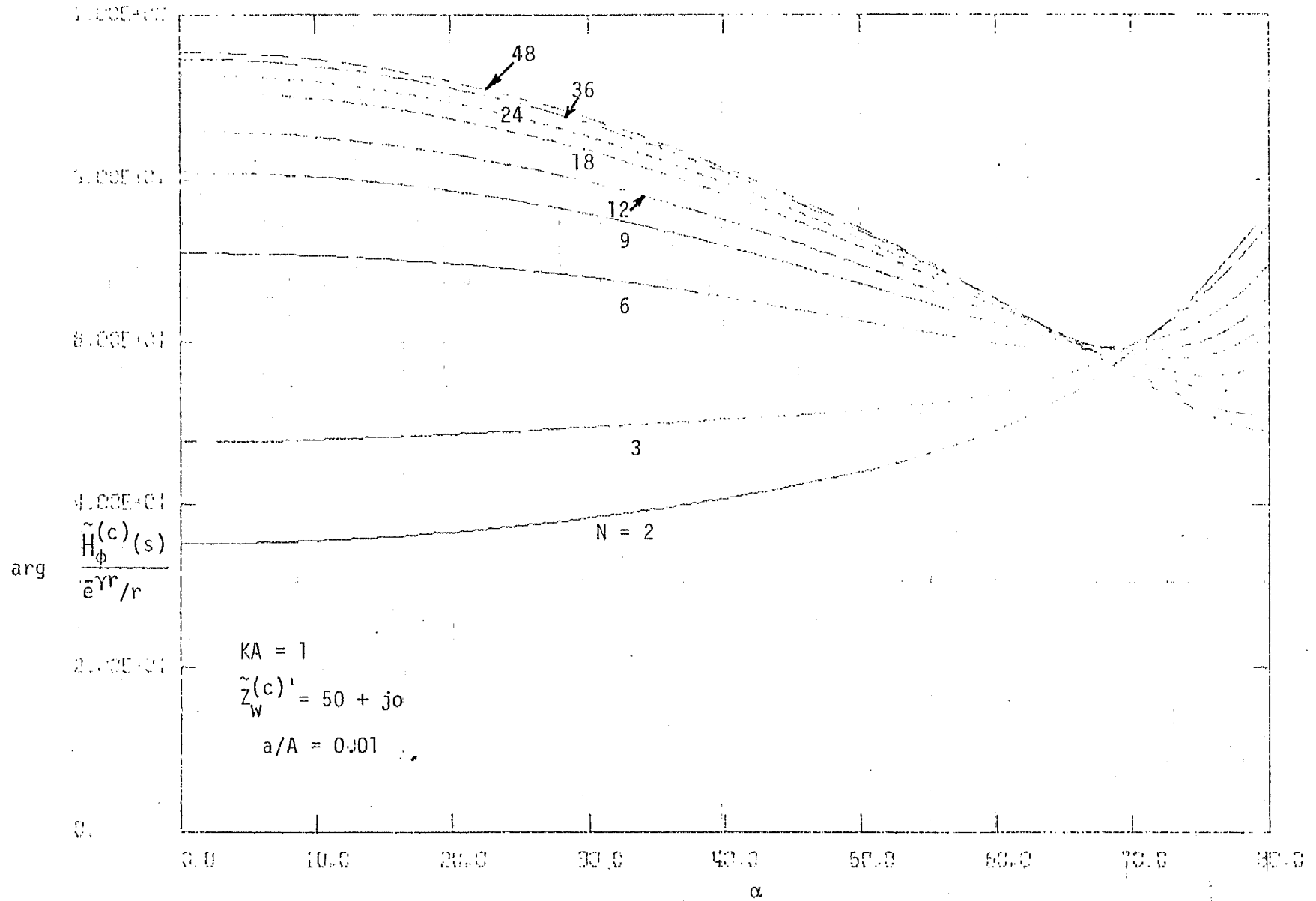


Figure 2.12(b). Phase of the Far-Field Distribution, Infinitely Long Loaded Circular Wire Cage Antenna, $\tilde{H}_\phi^{(c)}$

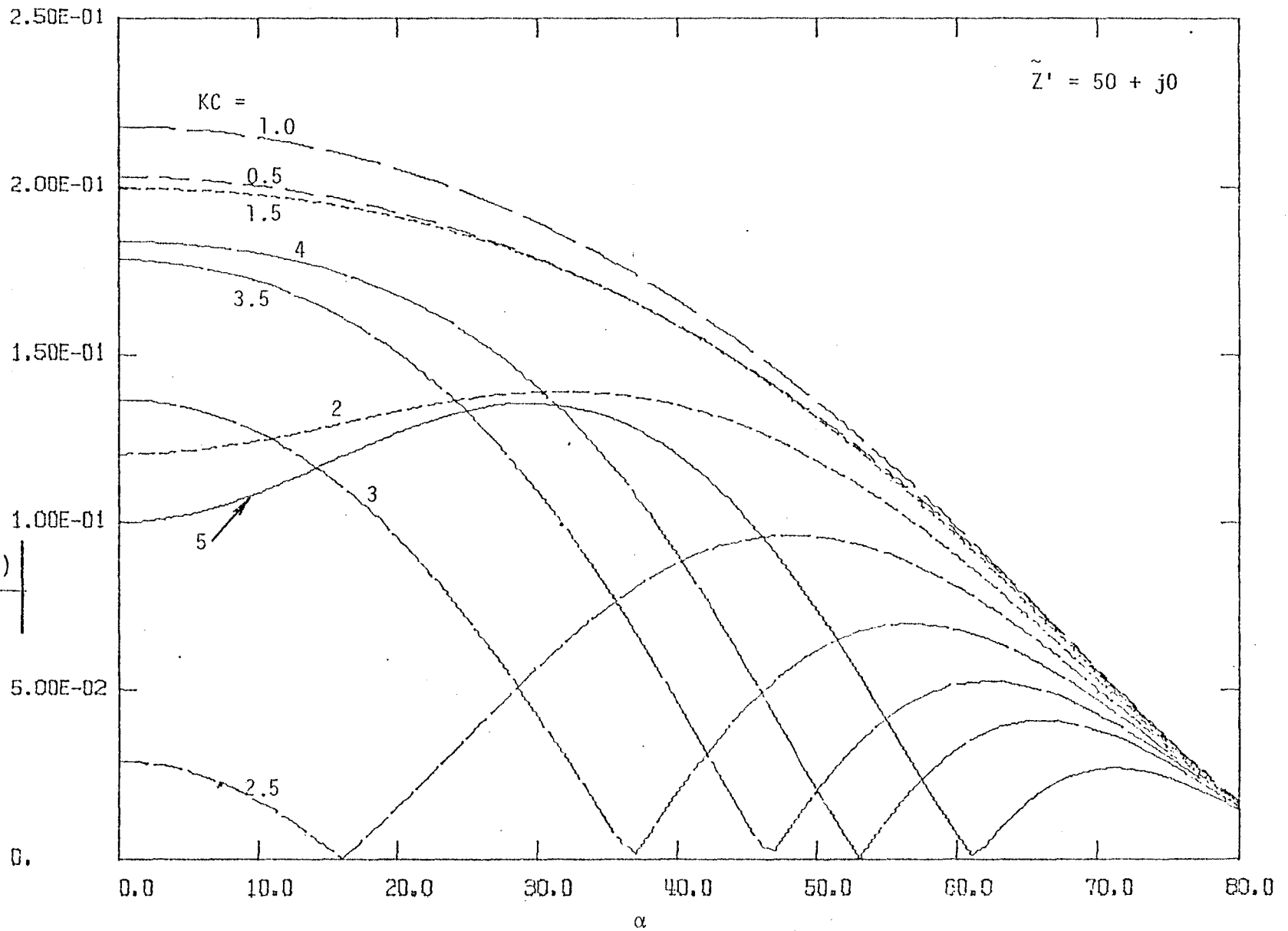


Figure 3.2(a). Magnitude of the Far-Field Distribution, Infinitely Long Loaded Hollow Cylindrical Antenna, $\tilde{E}_z^{(2)}$

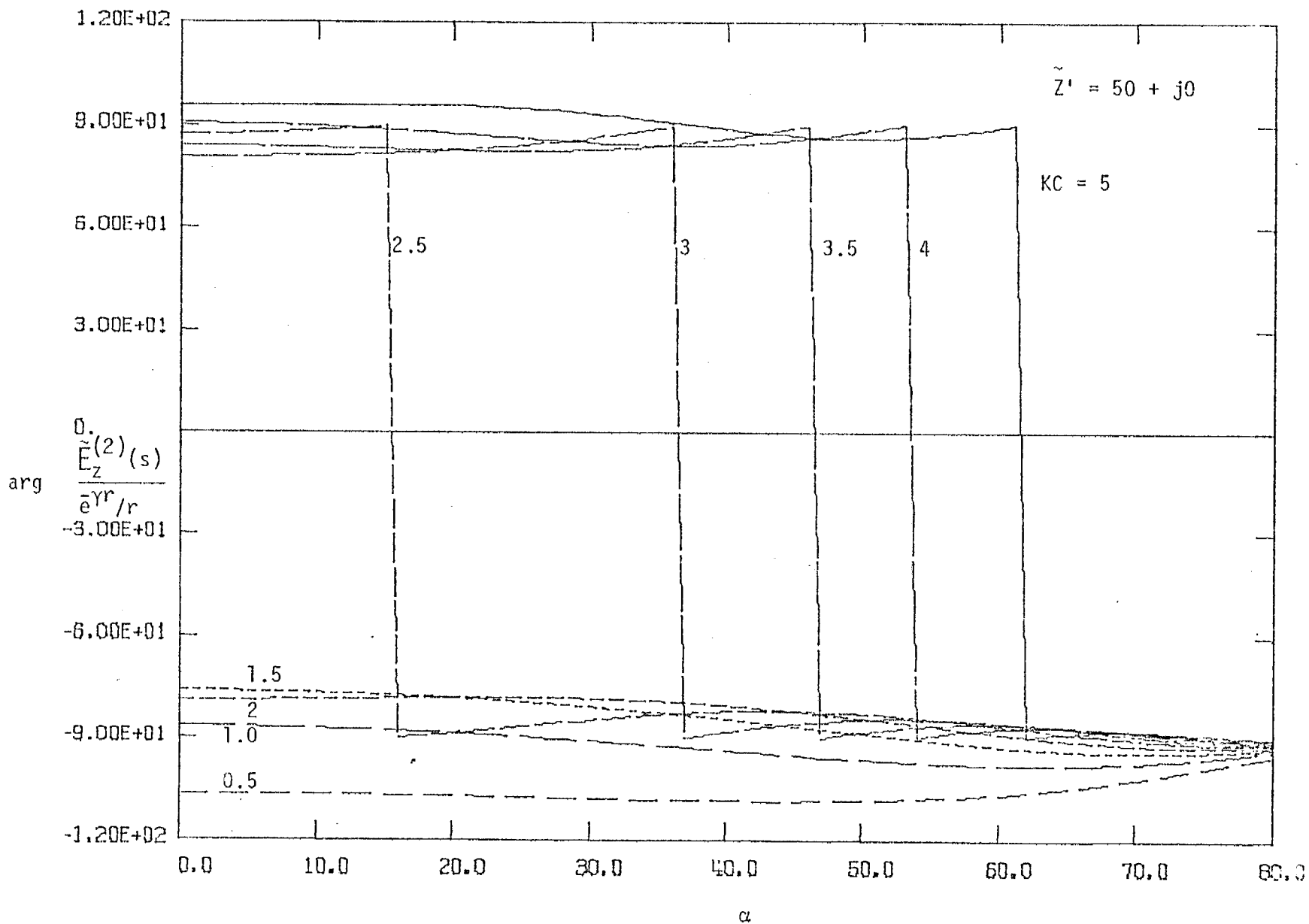


Figure 3.2(b). Phase of the Far-Field Distribution, Infinitely Long Loaded Hollow Cylindrical Antenna, $\tilde{E}_z^{(2)}$

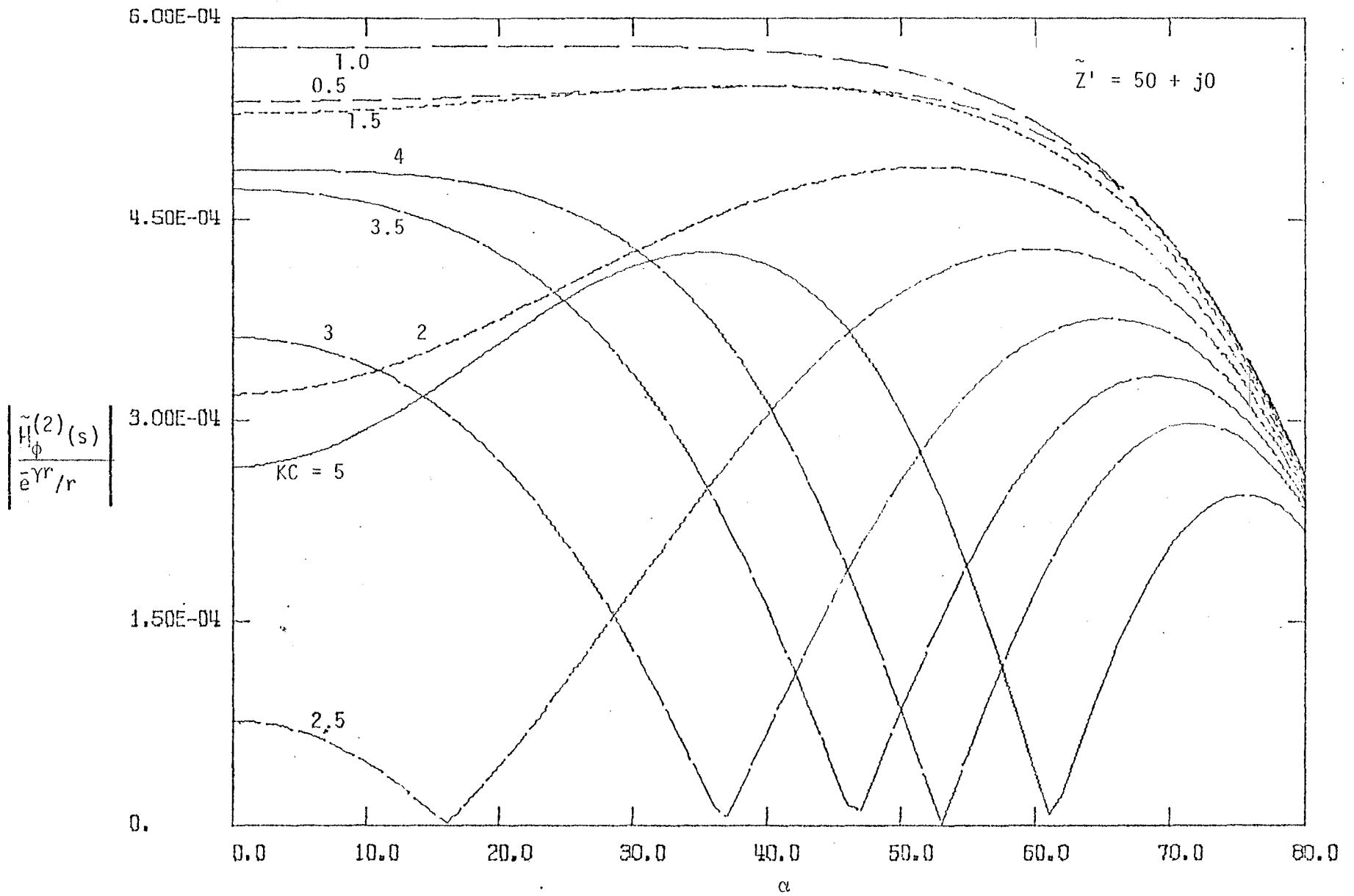


Figure 3.3(a). Magnitude of the Far-Field Distribution, Infinitely Long Loaded Hollow Cylindrical Antenna, $\tilde{H}_\phi^{(2)}$

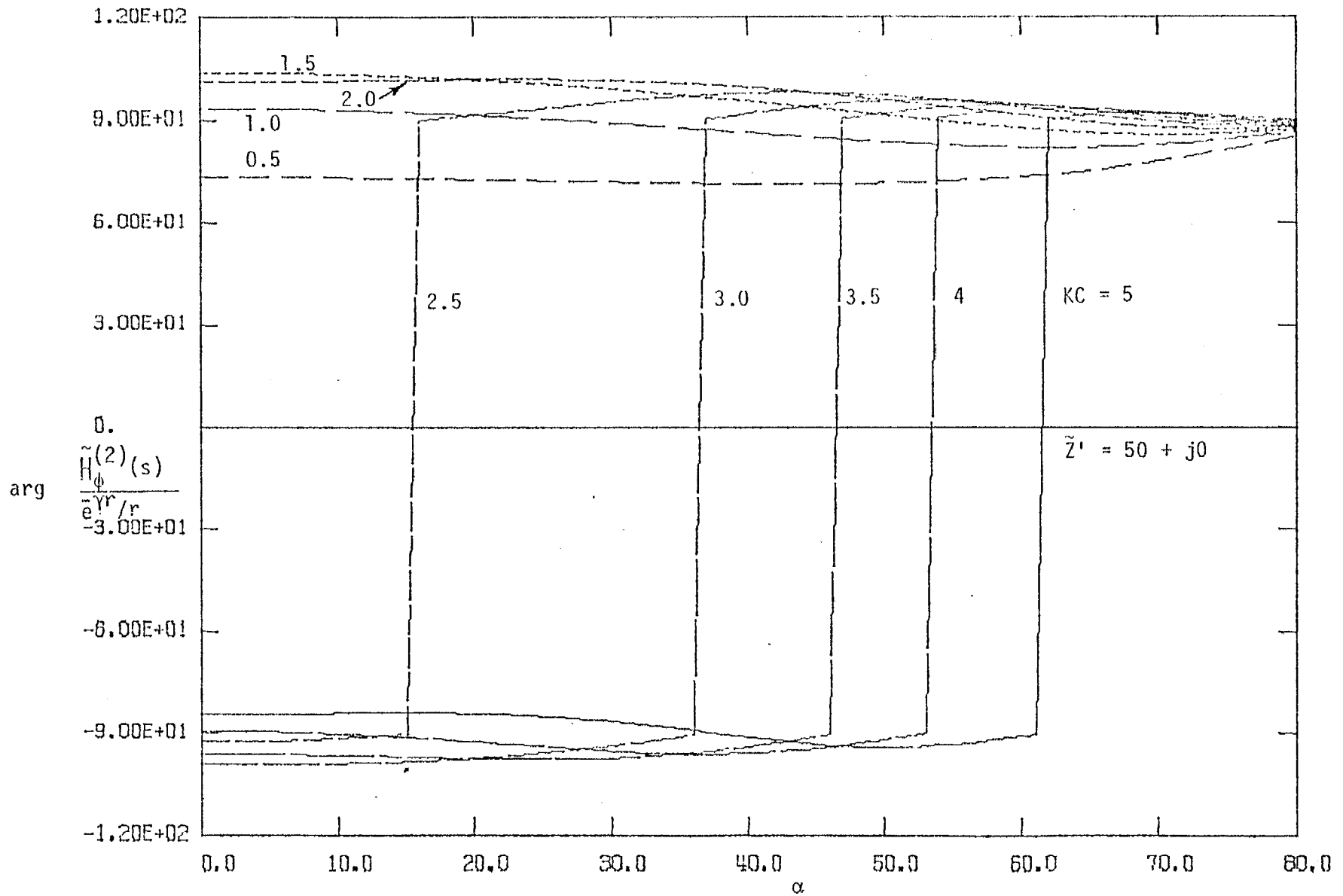


Figure 3.3(b). Phase of the Far-Field Distribution, Infinitely Long Loaded Hollow Cylindrical Antenna, $\tilde{H}_\phi^{(2)}$

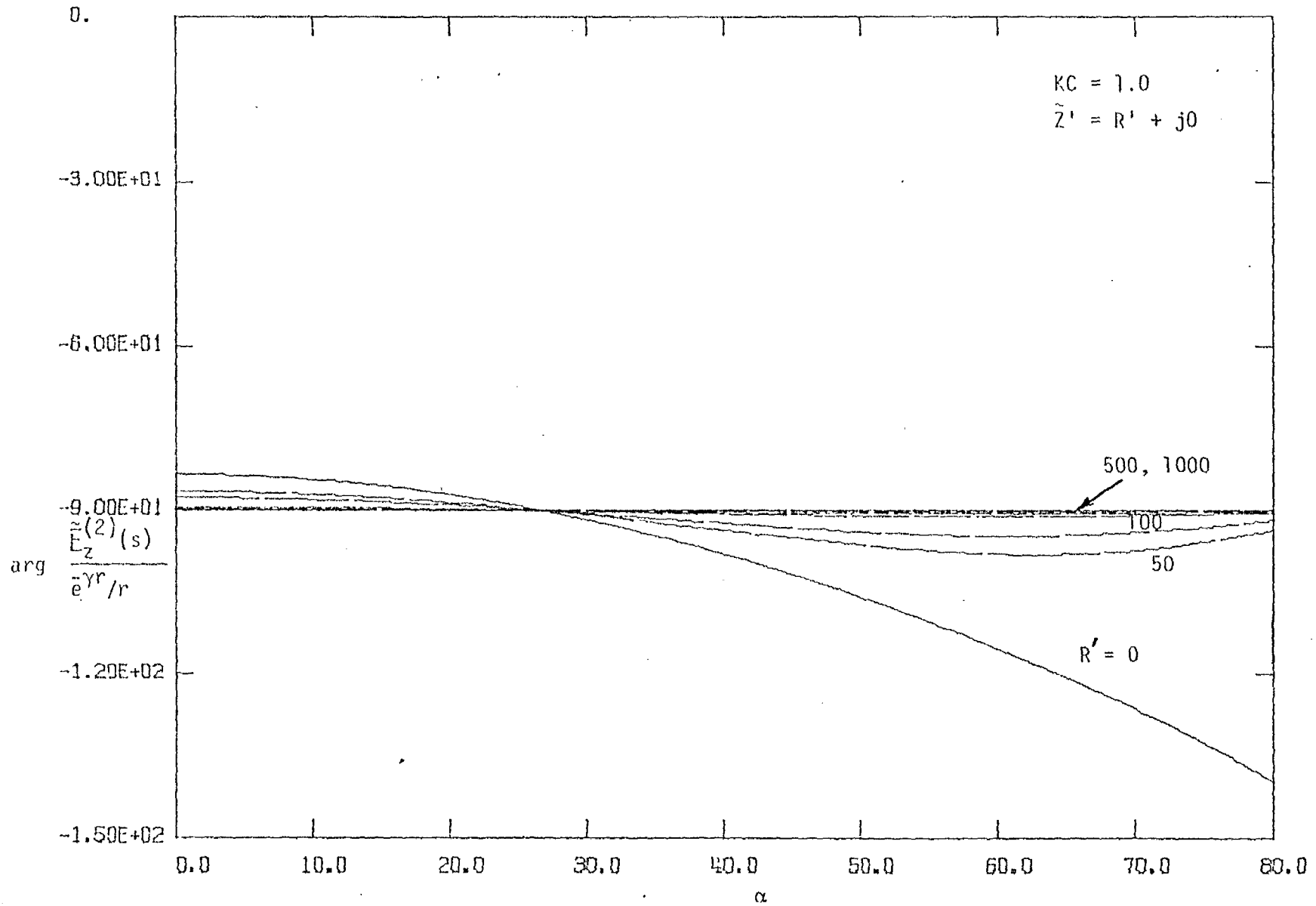


Figure 3.4(b). Phase of the Far-Field Distribution, Infinitely Long Loaded Hollow Cylindrical Antenna, $\tilde{E}_z^{(2)}$

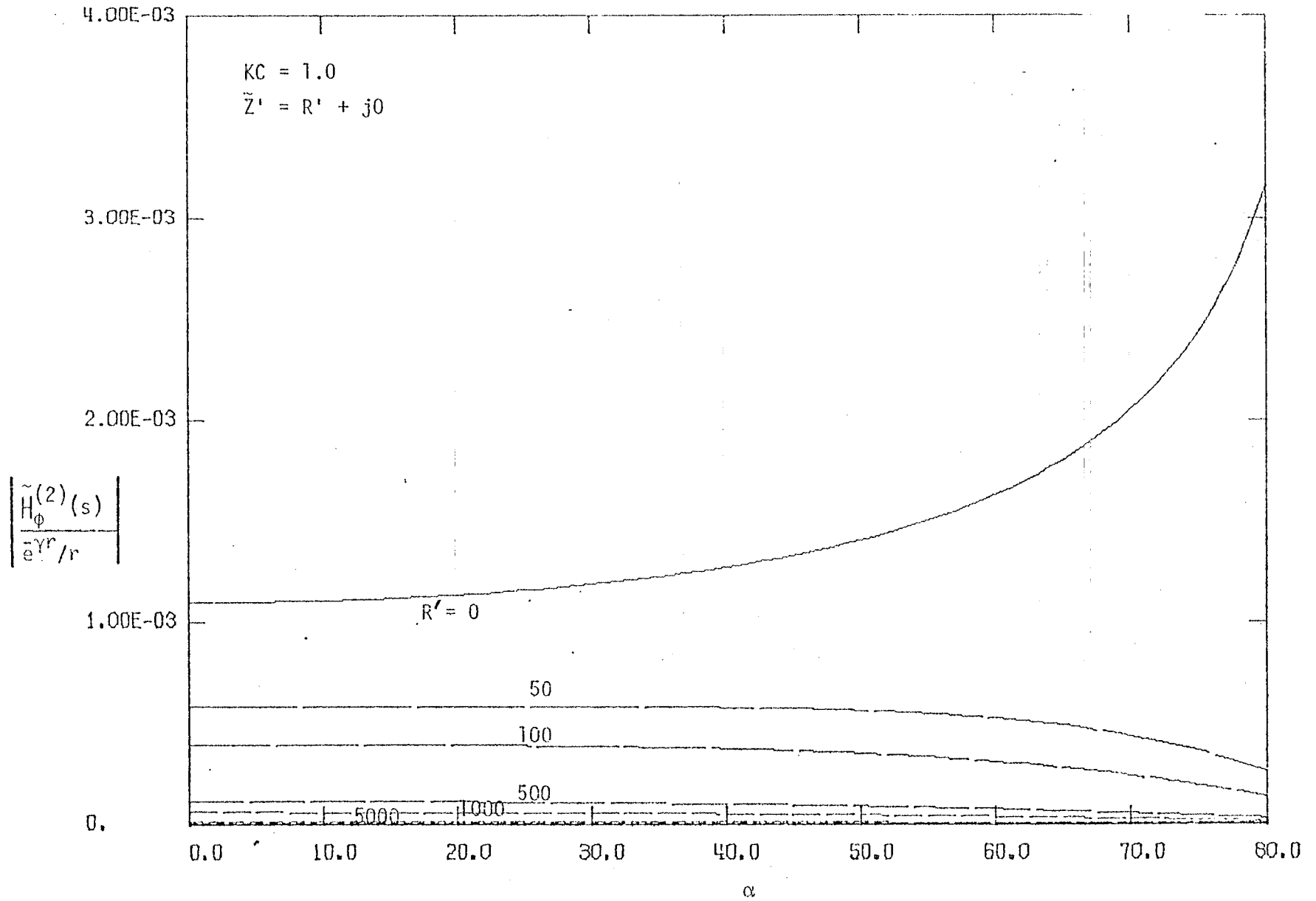


Figure 3.5(a). Magnitude of the Far-Field Distribution, Infinitely Long Loaded Hollow Cylindrical Antenna, $\tilde{\Pi}_\phi^{(2)}$

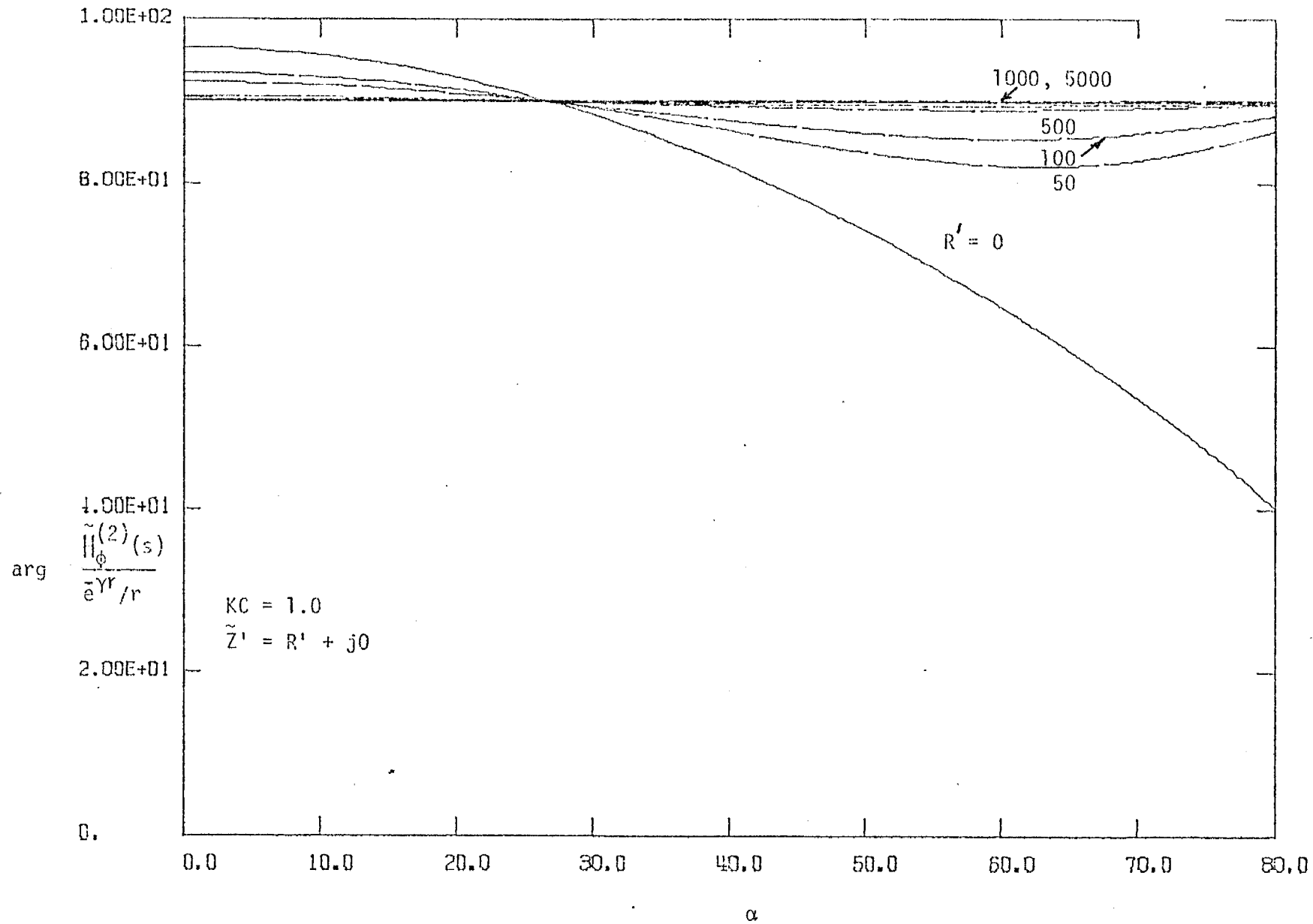


Figure 3.5(b). Phase of the Far-Field Distribution, Infinitely Long Loaded Hollow Cylindrical Antenna, $\tilde{H}_\phi^{(2)}$

IV. ELECTROMAGNETIC EQUIVALENCE BASED ON FAR FIELDS

In the previous sections, three different types of canonical infinitely long antenna geometries are studied viz., (i) the infinitely long loaded solid wire antenna of radius b and impedance loading function per unit length $\tilde{Z}'_w(s)$, (ii) the infinitely long loaded circular wire cage antenna of cage radius A , radius of each cage wire a , number of cage wires N and its corresponding impedance loading function per unit length along each of the cage wires $\tilde{Z}'_w^{(c)}(s)$, and (iii) the infinitely long loaded hollow cylindrical antenna of radius C and sheet impedance loading function $\tilde{Z}'(s)$.

For each of the above canonical antenna structures integral expressions for the induced current, and for the radiated electric and magnetic fields are derived. Based on the saddle-point technique, far-field electric and magnetic field components are obtained in a more simplified form. Table II summarizes the results thus far obtained for the far-field distribution.

It is now possible to compare (and thus approximately equate) the distribution of the far-field components of the circular wire cage antenna as against the far-field distribution of a hollow cylindrical antenna. Such a comparison would allow establishing electromagnetic equivalences based on the far-field distributions. Given the circular wire-cage parameters viz., number of cage wires N , cage radius A , wire radius a ; and its loading function $\tilde{Z}'_w^{(c)}(s)$, the electromagnetic equivalence allows one to pick equivalent radius $C = \Psi_{eq}$ and the corresponding loading function $\tilde{Z}'(s) = \tilde{Z}'_{eq}(s)$, so that both the structures radiate the same far-field distributions. The equivalent parameters are in fact a function of the complex frequency s , and the observation angle α . The dependence on α can be eliminated in some cases discussed further.

We shall now consider the electromagnetic equivalence between an infinitely long loaded circular wire cage structure and a loaded hollow circular cylinder based on the same radiated far fields. Columns 2 and 3 in table IIA for the far-field distributions are equated,

Table I

| | 1 | 2 | 3 |
|-------------------------|----------------------------------|----------------------------------|---|
| | Infinitely Long Loaded Thin Wire | Infinitely Long Loaded Wire Cage | Infinitely Long Loaded Hollow Circular Cylinder |
| Radius | b | Cage A Wire a | C |
| Axial Impedance Loading | $\tilde{Z}'_w(s)$ | $\tilde{Z}'_w(c)(s)$ | $\tilde{Z}'(s)$ |
| Number of Wires | 1 | N | ∞ |

Table IIA

| | 1 | 2 | 3 |
|-------------------------------------|--|--|--|
| Far Fields | Infinitely Long Loaded Thin Wire | Infinitely Long Loaded Wire Cage | Infinitely Long Loaded Hollow Circular Cylinder |
| $\tilde{E}_Z(r, \alpha, s) \sim$ | $-\frac{\tilde{V}}{2} \frac{\cos \alpha}{\tilde{L}_1(\gamma, \alpha)} \frac{e^{-\gamma r}}{r}$ | $-\frac{\tilde{V}}{2} \frac{\cos \alpha}{\tilde{L}_2(\gamma, \alpha)} \frac{e^{-\gamma r}}{r} \tilde{C}_f$ | $-\frac{\tilde{V}}{2} \frac{\cos \alpha}{\tilde{L}_3(\gamma, \alpha)} \frac{e^{-\gamma r}}{r} \tilde{p}_f$ |
| $\tilde{E}_\Psi(r, \alpha, s) \sim$ | $-\frac{\tilde{V}}{2} \frac{\sin \alpha}{\tilde{L}_1(\gamma, \alpha)} \frac{e^{-\gamma r}}{r}$ | $-\frac{\tilde{V}}{2} \frac{\sin \alpha}{\tilde{L}_2(\gamma, \alpha)} \frac{e^{-\gamma r}}{r} \tilde{C}_f$ | $-\frac{\tilde{V}}{2} \frac{\sin \alpha}{\tilde{L}_3(\gamma, \alpha)} \frac{e^{-\gamma r}}{r} \tilde{p}_f$ |
| $\tilde{H}_\phi(r, \alpha, s) \sim$ | $\frac{\tilde{V}}{2Z_0} \frac{1}{\tilde{L}_1(\gamma, \alpha)} \frac{e^{-\gamma r}}{r}$ | $\frac{\tilde{V}}{2Z_0} \frac{1}{\tilde{L}_2(\gamma, \alpha)} \frac{e^{-\gamma r}}{r} \tilde{C}_f$ | $\frac{\tilde{V}}{2Z_0} \frac{1}{\tilde{L}_3(\gamma, \alpha)} \frac{e^{-\gamma r}}{r} \tilde{p}_f$ |

Table IIB

| | 1 | 2 | 3 |
|---------------------------------------|--|---|---|
| | Infinitely Long Loaded Thin Wire | Infinitely Long Loaded Wire Cage | Infinitely Long Loaded Hollow Circular Cylinder |
| $\tilde{L}_n(\gamma, \alpha)$ | $\tilde{L}_1(\gamma, \alpha) =$ $\cos \alpha K_0(\gamma b \cos \alpha)$ $+ \tilde{h}_1(s) K_1(\gamma b \cos \alpha)$ | $\tilde{L}_2(\gamma, \alpha) =$ $\cos \alpha \sum_{n=1}^N K_0(\gamma A_{1,n} \cos \alpha)$ $+ \tilde{h}_2(s) K_1(\gamma a \cos \alpha)$ | $\tilde{L}_3(\gamma, \alpha) =$ $\cos \alpha I_0(\gamma C \cos \alpha) \cdot$ $K_0(\gamma C \cos \alpha)$ $+ \tilde{h}_3(s) \frac{1}{(\gamma C \cos \alpha)}$ |
| Loading Factor $\tilde{h}_n(s)$ | $\tilde{h}_1(s) = 2\pi b \frac{\tilde{Z}'_w(s)}{Z_0}$ | $\tilde{h}_2(s) = 2\pi a \frac{\tilde{Z}'_w(c)(s)}{Z_0}$ | $\tilde{h}_3(s) = 2\pi C \frac{\tilde{Z}'(s)}{Z_0}$ |
| Geometric Factor | 1 | $\tilde{C}_f = NI_0(\gamma A \cos \alpha)$ | $\tilde{P}_f = I_0(\gamma C \cos \alpha)$ |

294

$$\frac{\tilde{C}_f}{\tilde{L}_2(\gamma, \alpha)} = \frac{\tilde{P}_f}{\tilde{L}_3(\gamma, \alpha)} \left| \begin{array}{l} C = \Psi_{eq} \\ \tilde{Z}' = \tilde{Z}'_{eq} \end{array} \right. \quad (4.1)$$

where

Ψ_{eq} = equivalent radius

\tilde{Z}'_{eq} = equivalent impedance loading

From the expressions (2.34) and (3.11), the expression (4.1) takes the form,

$$\frac{NI_0(\gamma A \cos \alpha)}{\cos \alpha \sum_{n=1}^N K_0(\gamma A_{1,n} \cos \alpha) + \tilde{h}_2(s) K_1(\gamma A \cos \alpha)} = \frac{I_0(\gamma C \cos \alpha)}{\cos \alpha I_0(\gamma C \cos \alpha) K_0(\gamma C \cos \alpha) + \tilde{h}_3(s) \left[\frac{1}{\gamma C \cos \alpha} \right]} \left| \begin{array}{l} C = \Psi_{eq} \\ \tilde{Z}' = \tilde{Z}'_{eq} \end{array} \right. \quad (4.2)$$

The expression (4.1) depicts equivalence condition for the loaded cage wire model and the hollow cylinder model, and is a function of the frequency γ and the angle of observation α . Practically it is impossible to extract both the equivalent radius Ψ_{eq} and equivalent impedance $\tilde{Z}'_{eq}(s)$ from one equation unless one makes certain choices or forces one more realizable constraint. Some of the alternatives available are discussed in the following.

CASE I: Equivalence of perfectly conducting wire cage and perfectly conducting hollow cylinder

For this we have the impedance loading functions

$$\tilde{Z}'_w(c)'(s) = 0 \quad (4.3a)$$

and

$$\tilde{Z}'(s) = 0 \quad (4.3b)$$

the expression (4.2) yields the equivalence condition

$$\sum_{n=1}^N K_0(\gamma A_{1,n} \cos \alpha) - N I_0(\gamma A \cos \alpha) K_0(\gamma \psi_{eq}^{(c)} \cos \alpha) = 0 \quad (4.4)$$

We note $\psi_{eq}^{(c)}$ is to be determined as the solution to the equation (4.4) and it appears implicitly in the argument of the modified Bessel function. Further

$$\psi_{eq}^{(c)} = \psi_{eq}^{(c)}(\gamma, \cos(\alpha)) \quad (4.5)$$

In the quasi-static case $|\gamma A| \ll 1$, the modified Bessel functions can be replaced by their small argument approximations,¹⁵

$$K_0(z) = -\ln\left(\frac{\Gamma z}{2}\right) \quad (4.6a)$$

$$I_0(z) = 1.0 \quad (4.6b)$$

On substituting the above small argument approximations, the equivalence condition (4.4) simplifies to

$$\psi_{eq_0}^{(c)} = [aA_{1,2}A_{1,3}\dots A_{1,N}]^{1/N} \quad (4.7)$$

where the inter-chord distances $A_{1,n}$, $n = 2, 3, \dots, N$ are defined in (2.30). It is interesting to note the equivalent radius $\psi_{eq_0}^{(c)}$ is independent of the variables γ and $\cos(\alpha)$ in the quasi-static case. The equivalence condition (4.4) yields the same result (4.7) even for the limiting case as $\alpha \rightarrow \pi/2$ and $|\gamma \cos \alpha| \ll 1$. The equivalent radius result (4.7) checks with King's equivalent radius² obtained for a perfectly conducting finite circular cage antenna. In fact, $\psi_{eq_0}^{(c)}$ can be shown also to be identical to the equivalent radius obtained by Baum,³

$$\frac{\psi_{eq_0}^{(c)}}{A} = \left[\frac{aN}{A}\right]^{1/N} \quad (4.8)$$

which is based on conformal transformation; an equivalence between a single charged conductor and number of equally spaced concentric charged conductors. Appendix C discusses the two results (4.7) and (4.8) as one and the same.

In figure 4.1 is shown the variation of the normalized equivalent radius $\psi_{eq}^{(c)}/A$ as a function of A and similarly in figure 4.2 as a function of a/A ,³ for different values of number of cage wire N .

As stated earlier $\psi_{eq}^{(c)}$ is independent of the complex frequency γ and of the variable $\cos(\alpha)$, figure B-2, in the quasi-static limit. The first order effect of the complex frequency γ on the equivalent radius $\psi_{eq}^{(c)}$ can be obtained if higher order terms are included in the series expansion of the modified Bessel functions, and can be written as,¹⁵

$$K_0(z) = \left[-\ln\left(\frac{\Gamma z}{2}\right) \right] I_0(z) + \frac{\frac{1}{4} z^2}{1!} + \left(1 + \frac{1}{2}\right) \frac{\left(\frac{1}{4} z^2\right)^2}{2!} + \dots \quad (4.9a)$$

$$I_0(z) = 1 + \frac{\frac{1}{4} z^2}{1!} + \frac{\left(\frac{1}{4} z^2\right)^2}{2!} + \dots \quad (4.9b)$$

Picking the first two terms in the above series expansion (4.9) and substituting into the equivalence condition (4.4), it reduces to the following transcendental equation,

$$\left[\frac{\psi_{eq}^{(c)}}{A} \right]^2 - B_1 \ln \left[\frac{\psi_{eq}^{(c)}}{A} \right] - B_2 \approx 0 \quad (4.10a)$$

$$B_1 = \frac{4N}{(\gamma'A)^2} \quad (4.10b)$$

$$B_2 = \left[\frac{a^2}{A^2} + 2N \right] - \frac{4}{(\gamma'A)^2} \ln \left(\frac{aN}{A} \right) \quad (4.10c)$$

$$\gamma' = \gamma \cos(\alpha) \quad (4.10d)$$

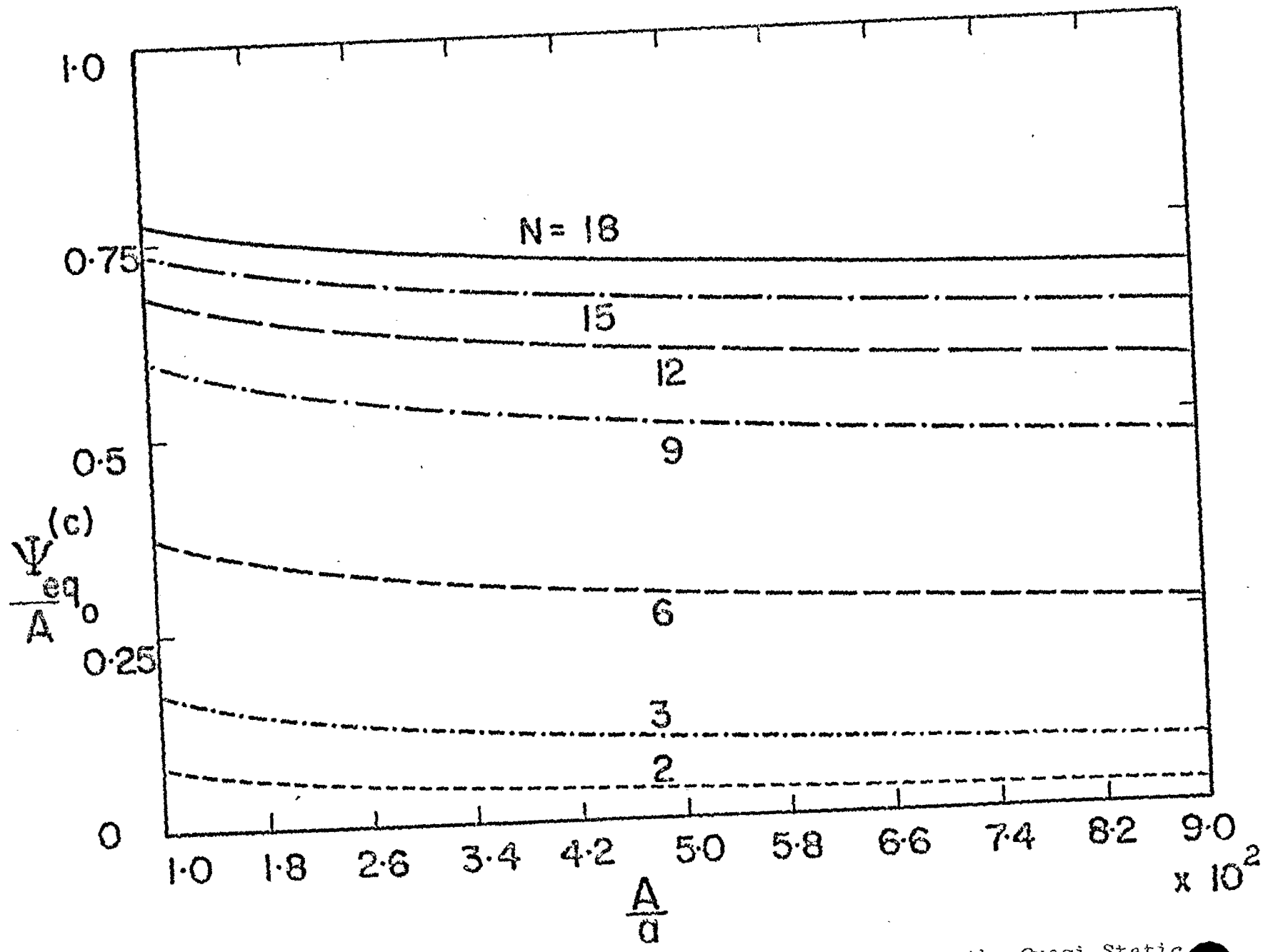


Figure 4.1. Equivalent Radius of a Conductive Circular Wire Cage in the Quasi-Static Range, $a = 0.01$

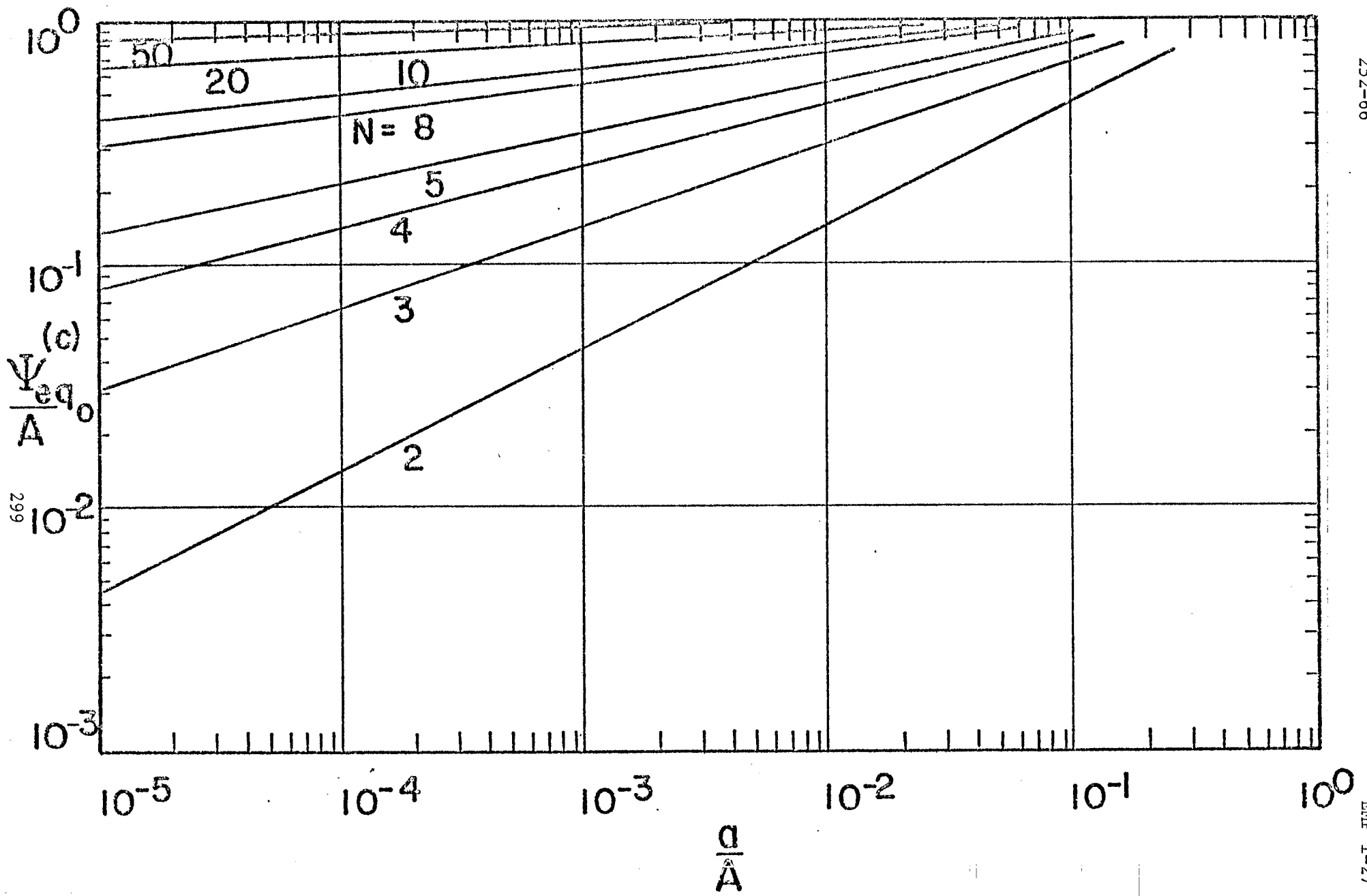


Figure 4.2. Equivalent Radius of a Conducting Circular Wire Cage for Various N

Further, the equation (4.10a) yields the first order solution,

$$\left(\frac{\psi_{eq}^{(c)}}{A}\right) \approx \left(\frac{\psi_{eq_0}^{(c)}}{A}\right) \left[1 - \frac{1}{N} \left(\frac{a^2}{A^2} + 2N\right) \left(\frac{\gamma'A}{2}\right)^2\right], \quad |\gamma'A| < 1 \quad (4.11)$$

The expression (4.4) is also solved numerically¹⁹ to determine the more exact quasi-static frequency range up to which the results of figure 4.1 are valid. Table III gives the lowest first zero solution to the implicit equation (4.4) for a particular set of wire cage parameters. As the frequency approaches large values, the equivalent radius result (4.7) is no longer valid, and $\psi_{eq}^{(c)}$ should be obtained from the solution to equation (4.4) or equation (4.11) for a given complex frequency γ and observation angle α . Figure 4.3 indicates the variation of the equivalent radius $\psi_{eq}^{(c)}$ as a function of $K'A$. For very large values of $|\gamma A \cos(\alpha)|$, one may substitute asymptotic forms of the modified Bessel function in the expression (4.4) and solve for the equivalent radius $\psi_{eq}^{(c)}$.

CASE II: Equivalence of loaded wire cage and loaded hollow cylinder

For this general case the equivalence condition (4.2) should be considered leading to the difficulty of one equation and two unknown parameters ψ_{eq} and $\tilde{Z}'_{eq}(s)$ to be determined. We can conveniently make a choice of one of the unknown parameters. Suppose the equivalent radius is chosen to be the same as the frequency-dependent equivalent radius $\psi_{eq}^{(c)}$ (as obtained from (4.4) or approximately from (4.11)) for the perfectly conducting case (case I), we obtain for the equivalent impedance loading function $\tilde{Z}'_{eq}(s)$,

$$\psi_{eq} \equiv \psi_{eq}^{(c)} \quad (4.12a)$$

$$\tilde{Z}'_{eq}(s) = \left(\frac{\tilde{Z}'_w(s)}{N}\right) \gamma a \cos \alpha K_1(\gamma a \cos \alpha) \frac{I_0(\gamma \psi_{eq}^{(c)} \cos(\alpha))}{I_0(\gamma A \cos(\alpha))} \quad (4.12b)$$

As pointed out earlier, the equivalent impedance-per-unit-length function $\tilde{Z}'_{eq}(s)$ is a function of γ and $\cos(\alpha)$. In the quasi-static

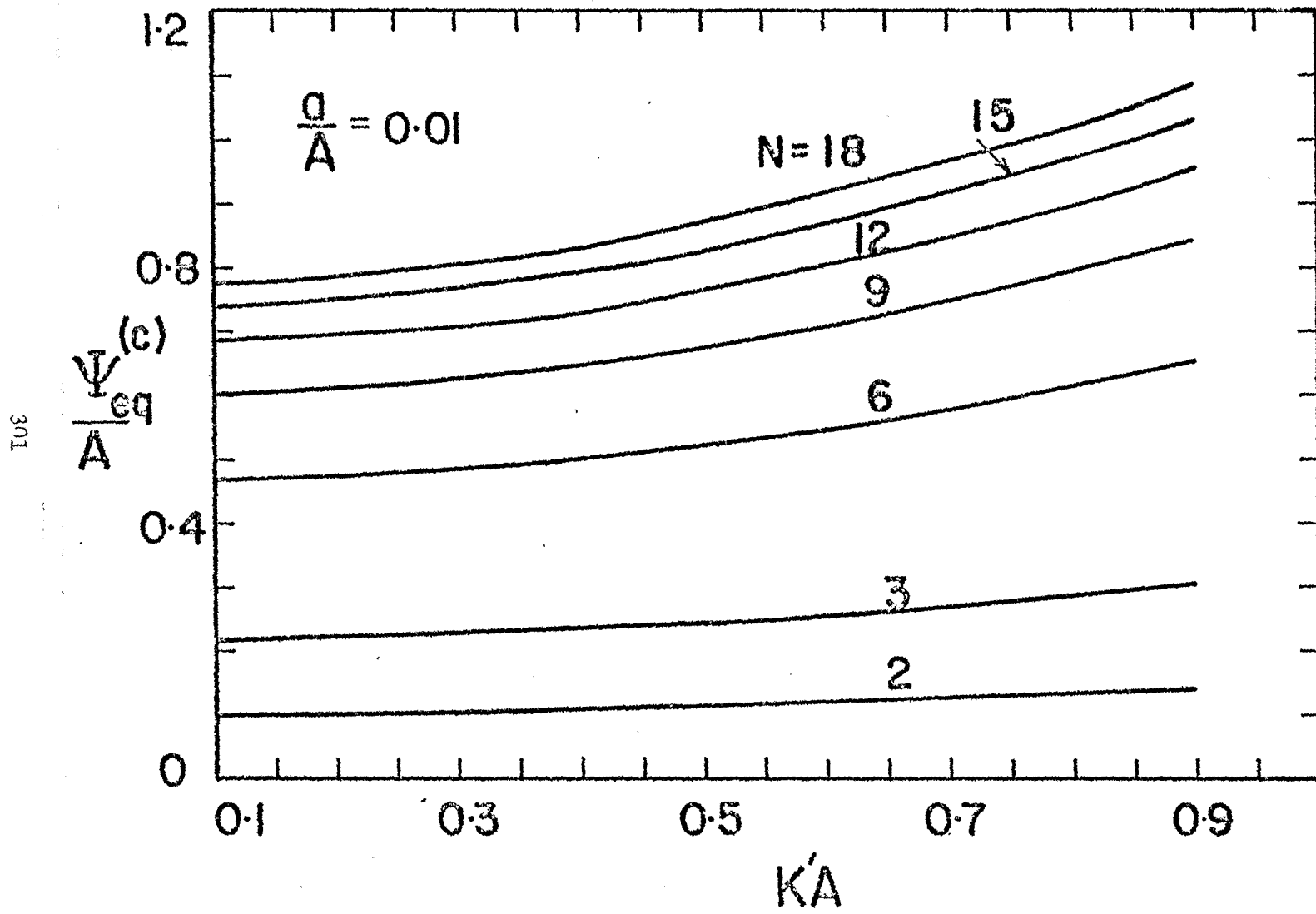


Figure 4.3. Equivalent Radius of a Conducting Circular Wire Cage as a Function of $K'A$, $\gamma = jK$

Table III

| KA cos(α) | | $K\psi_{eq}^{(c)}$ cos(α) | | $\frac{\psi_{eq}^{(c)}}{A}$ | |
|--------------------|-------|------------------------------------|----------|-----------------------------|----------|
| .1 | j 0.0 | .08395 | j-.00010 | .83953 | j-.00096 |
| .2 | 0.0 | .16844 | -.00074 | .84221 | -.00370 |
| .3 | 0.0 | .25353 | -.00239 | .84511 | -.00795 |
| .4 | 0.0 | .33913 | -.00538 | .84783 | -.01345 |
| .5 | 0.0 | .42508 | -.00999 | .85015 | -.01999 |
| .6 | 0.0 | .51121 | -.01647 | .85201 | -.02746 |
| .7 | 0.0 | .59736 | -.02506 | .85337 | -.03581 |
| .8 | 0.0 | .68338 | -.03605 | .85422 | -.04507 |
| .9 | 0.0 | .76909 | -.04981 | .85454 | -.05534 |
| 1.0 | 0.0 | .85430 | -.06681 | .85430 | -.06681 |
| 1.1 | 0.0 | .93877 | -.08772 | .85343 | -.07974 |
| 1.2 | 0.0 | 1.02218 | -.11346 | .85182 | -.09455 |
| 1.3 | 0.0 | 1.10405 | -.14535 | .84927 | -.11180 |
| 1.4 | 0.0 | 1.18360 | -.18534 | .84543 | -.13239 |
| 1.5 | 0.0 | 1.25953 | -.23643 | .88969 | -.15762 |
| 1.6 | 0.0 | 1.32939 | -.30342 | .83087 | -.18964 |
| 1.7 | 0.0 | 1.38810 | -.39446 | .81653 | -.23204 |
| 1.8 | 0.0 | 1.42353 | -.52418 | .79085 | -.29121 |
| 1.9 | 0.0 | 1.40057 | -.71896 | .73714 | -.37840 |
| 2.0 | 0.0 | 1.19554 | -.99934 | .59777 | -.49967 |

$$\frac{a}{A} = 0.01$$

$$N = 12$$

frequency range $|\gamma A| \ll 1$, the above expression (4.12b) simplifies to

$$\tilde{Z}'_{eq}(s) = \frac{\tilde{Z}_w^{(c)'}(s)}{N} \quad (4.12c)$$

which is exactly the equivalent parallel impedance of the N cage wires. The first order effect of the complex frequency γ on the equivalent sheet impedance per unit length $\tilde{Z}'_{eq}(s)$ can be obtained by substituting higher order terms for the modified Bessel functions in the expression (4.12b), hence we have

$$\begin{aligned} \tilde{Z}'_{eq}(s) &= \left[1 + \frac{1}{2}(\gamma'a)^2 \right] \left[\frac{4 + (\gamma'\psi_{eq}^{(c)})^2}{4 + (\gamma'A)^2} \right] \frac{\tilde{Z}_w^{(c)'}(s)}{N} \quad (4.13a) \\ &\approx \left(\frac{\psi_{eq}^{(c)}}{A} \right)^2 \left[1 + \left(\frac{2}{\gamma'\psi_{eq}^{(c)}} \right)^2 - \left(\frac{2}{\gamma'A} \right)^2 - \left(\frac{4}{\gamma'\psi_{eq}^{(c)}\gamma'A} \right)^2 \right] \frac{\tilde{Z}_w^{(c)'}(s)}{N} \end{aligned}$$

$$\text{for} \quad \left| \left(\frac{2}{\gamma'A} \right)^4 \right| < 1 \quad (4.13b)$$

CASE III:

In the above case II, we made a choice for the equivalent radius to be the same as the perfectly conducting case. We can make another practical choice of choosing the equivalent radius $\psi_{eq}^{(c)} = A$, the radius of the wire cage, and work out the corresponding appropriate equivalent loading function so that far-field equivalence holds good.

Hence substituting $\psi_{eq}^{(c)} = A$ in the expression (4.2) yields an expression for the equivalent loading function $\tilde{Z}'_{eq}(s)$. In the quasi-static limit as $|\gamma A| \ll 1$, we obtain

$$\tilde{Z}'_{eq}(s) = \frac{\tilde{Z}_w^{(c)'}(s)}{N} - \frac{\gamma \cos^2(\alpha) Z_o}{2\pi} \ln \left(\frac{\psi_{eq}^{(c)}}{A} \right) \quad (4.14)$$

which shows an angle dependent (α) positive inductance per-unit-length term as

$$\tilde{Z}'_{eq}(s) = \frac{\tilde{Z}'_w(c)(s)}{N} + sL' \quad (4.15)$$

$$L' \equiv \frac{\mu}{2\pi} \cos^2(\alpha) \ln\left(\frac{A}{\psi'_{eq}(c)}\right) > 0$$

Note that as $s \rightarrow 0$ the inductive term is negligible giving the wire loading as the dominant term as one would expect. For higher frequencies, however, the property of having an angle (α) dependent impedance per unit length is an undesirable feature because there is then no unique equivalent impedance per unit length; it depends where one looks.

V. CONCLUSIONS

A preliminary analysis is carried out to aim at suitably modeling hybrid EMP simulators made up of thin wire structures and wire meshes. Canonical infinitely long loaded wire geometries in the form of a thin wire, a circular wire cage and hollow cylindrical structures are analyzed systematically by treating them as boundary value antenna problems. Results of the induced current distribution and the corresponding radiated fields are obtained for each of the canonical geometries.

The radiated fields of the loaded concentric wire cage are compared with the radiated fields of the loaded hollow cylinder to arrive at an electromagnetic equivalence condition. Based on this equivalence, the equivalent radius of the wire cage and the corresponding equivalent sheet impedance per-unit-length loading function are obtained so that both the compared structures radiate the same far fields. In fact the results obtained are a function of the complex frequency. In the low frequency ranges an explicit expression for the equivalent radius of the cage is obtained; one has to solve implicit equations for higher frequencies.

The theory and the concept of the electromagnetic equivalence applied to wire structures, discussed in this note is used in the future work as a foundation to effectively model hybrid simulators including their complex feeding generators.

APPENDIX A

LONGITUDINAL ϕ -INDEPENDENT IMPEDANCE CHARACTERISTICS
OF CIRCULAR CYLINDRICAL STRUCTURES

The impedance characteristics of infinitely long circular-cross-section structures are discussed in detail in reference 20. A summary of the expressions utilized in the previous sections is given below.

1. Thin Solid Cylindrical Wire

In figure A-1 is shown the geometry of an infinitely long solid circular thin wire of radius b . The material of the wire has homogeneous characteristics of permeability μ_w , permittivity ϵ_w , and conductivity σ_w . The structure is oriented along z -axis in an isotropic homogeneous medium. Only axial electric current $\tilde{I}(\zeta, s)$ is assumed to exist and hence only the TM (transverse magnetic to z) electromagnetic field components $\tilde{E}_\psi(\zeta, s)$, $\tilde{E}_z(\zeta, s)$ and $\tilde{H}_\phi(\phi, s)$ are present and are symmetric with respect to ϕ -angular variations.

In the region $\psi < b$, the magnetic vector potential is

$$\tilde{A}_z(\psi, \zeta, s) = \tilde{C}(\zeta, s) I_0(u_w \psi) \quad (\text{A.1})$$

where

$$u_w = [\gamma_w^2 - \zeta^2]^{\frac{1}{2}} \quad (\text{A.2})$$

$$\gamma_w = [\mu_w s(\sigma_w + \epsilon_w s)]^{\frac{1}{2}} \quad (\text{A.3})$$

In the expression (A.1), $\tilde{C}(\zeta, s)$ is a constant which determines the potential distribution. If displacement currents are neglected $\gamma_w = [\mu_w \sigma_w s]^{\frac{1}{2}}$. The series axial impedance per unit length of the solid infinitely long wire is given by

$$\tilde{Z}'_w(\zeta, s) = \frac{\tilde{E}_z(\psi, \zeta, s)}{2\pi b \tilde{H}_\phi(\psi, \zeta, s)} \Big|_{\psi=b} \quad (\text{A.4})$$

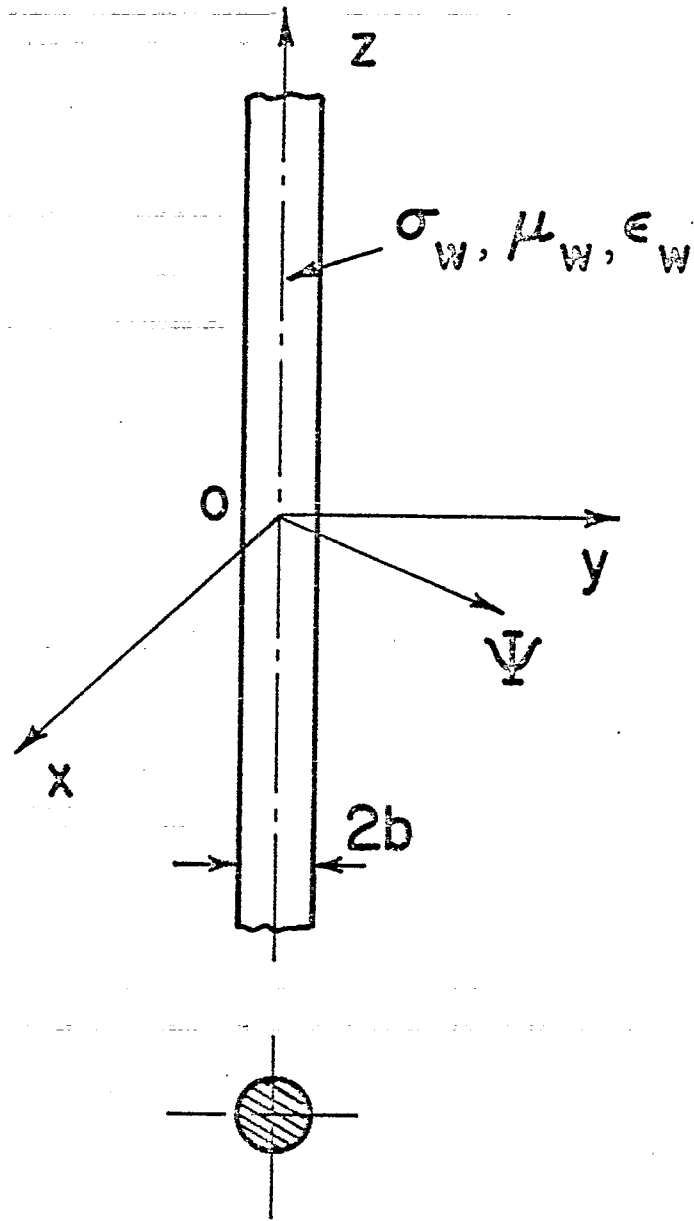


Figure A-1. Thin Solid Cylindrical Wire

which is the ratio of the axial electric field to the total axial current. Using the expressions (2.4a and b)

$$\tilde{Z}'_w(\zeta, s) = \frac{u_w I_0(u_w b)}{2\pi b(\sigma_w + s\epsilon_w) I_1(u_w b)} \quad (\text{A.5})$$

I_0 and I_1 are the modified Bessel functions of first kind, zero and first orders, respectively. In the quasi-static range $|\gamma_w|^2 \gg \zeta^2$, and the axial impedance per unit length reduces to

$$\tilde{Z}'_w(s) = \frac{\gamma_w I_0(\gamma_w b)}{2\pi b(\sigma_w + s\epsilon_w) I_1(\gamma_w b)} \quad (\text{A.6})$$

For the limiting case of static conditions, $s \rightarrow 0$,

$$I_0(\gamma_w b) \approx 1 \quad (\text{A.7})$$

$$I_1(\gamma_w b) \approx \frac{\gamma_w b}{2} \quad (\text{A.8})$$

$$Z'_w \approx \frac{1}{\pi b^2 \sigma_w} \quad (\text{A.9})$$

The infinitely long thin cable wire characteristics for a typical copper conductor $\sigma_w = 5.65 \times 10^7$ mho/meter are shown in figures A-2 and A-3, as a function of frequency in the quasi-static range for different radii of the wire. Figure A-1 gives $\tilde{R}'_w = \text{real}(\tilde{Z}'_w)$, resistance of the cable wire/meter length and figure A-2 gives $\tilde{X}'_w = \text{imag.}(\tilde{Z}'_w)$, self reactance of the cable wire/meter length. As the frequency is increased both \tilde{R}'_w and \tilde{X}'_w increase linearly on the logarithmic scale. At very low frequencies \tilde{X}'_w approaches zero, while \tilde{R}'_w approaches its static value.

Even if the structure is loaded with extra lumped impedances, it can be included into $\tilde{Z}'_w(s)$ of (A.6) and characterized as certain uniform impedance per unit length as a function frequency. Whenever external loadings are built into the structure, the

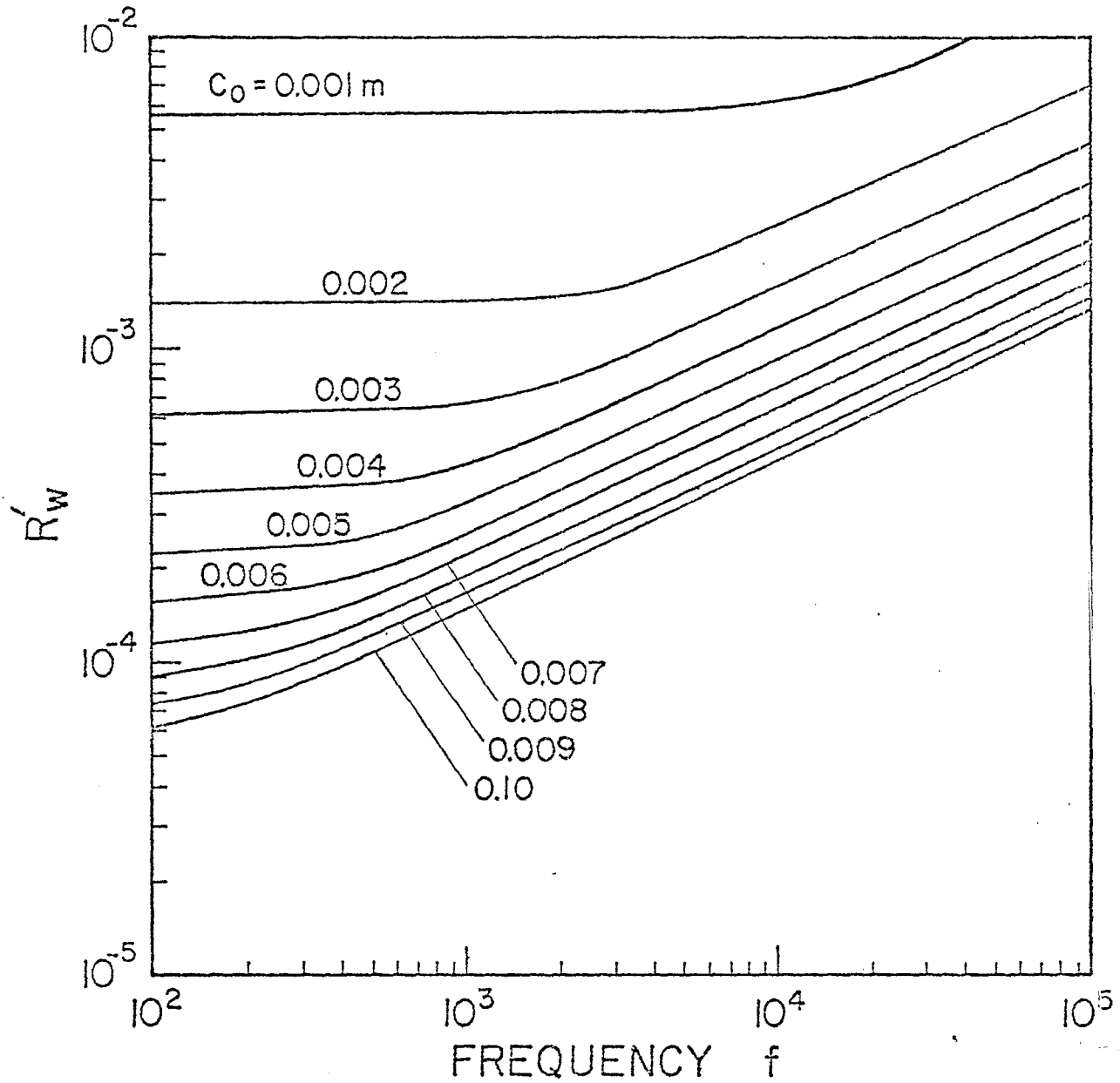


Figure A-2. Resistance per Unit Length for Copper Conductor

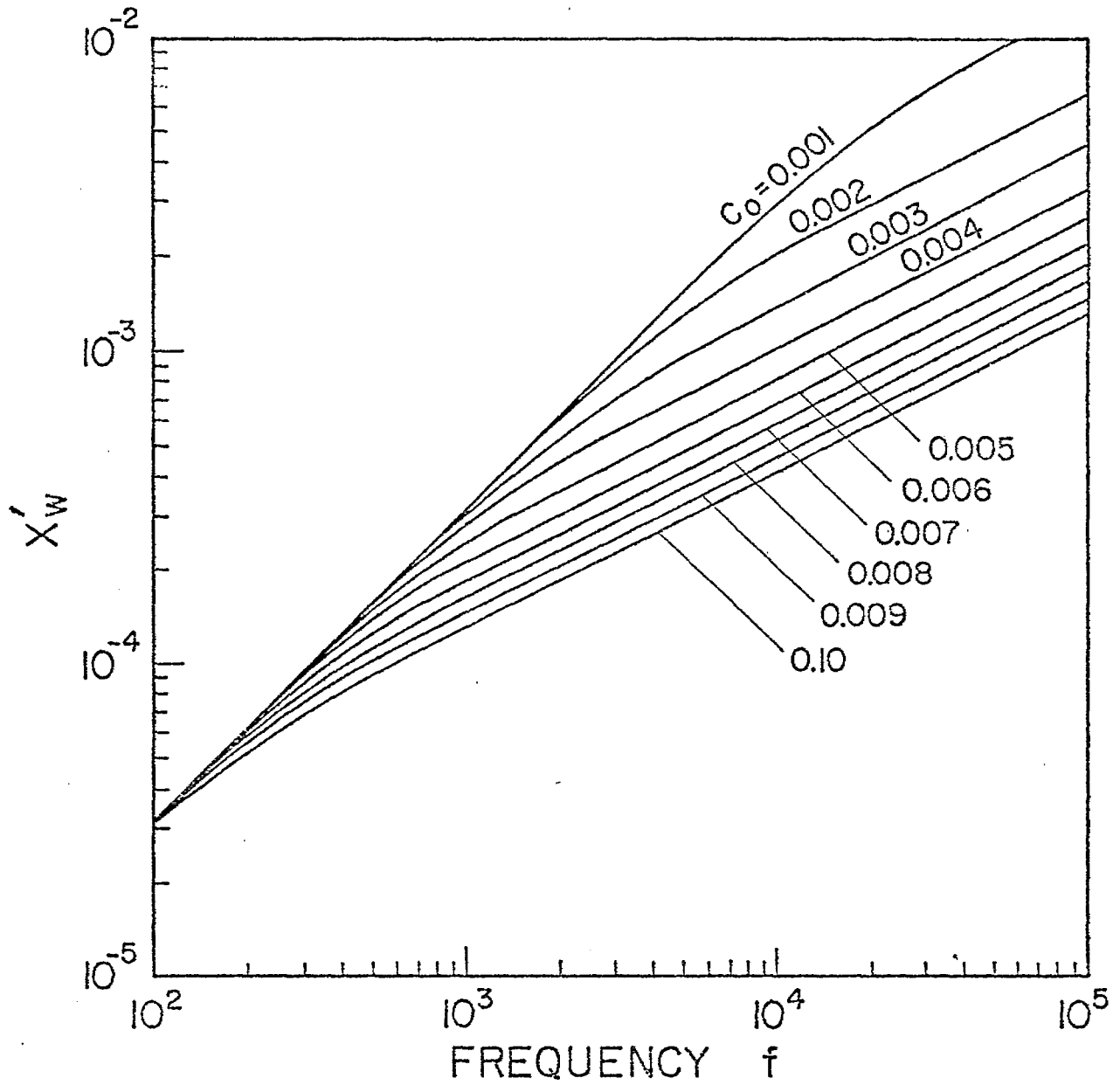


Figure A-3. Reactance per Unit Length for Copper Conductor

impedance loading due to the material characteristics of the wire is a very small percentage of the total loading and hence can be neglected. The concept of the impedance definition is based on the surface impedance in contrast to the sheet impedance definition discussed in the next section.

2. Hollow Circular Cylinder

The geometry of the hollow cylindrical tube, having a radius equal to C , is shown in figure A-4. The thickness of the wall is neglected and the material of the tube has permeability μ_c , permittivity ϵ_c and conductivity σ_c . The tubular structure is oriented along z axis in an isotropic, homogeneous medium. Again, only the axial currents are assumed to exist on the outer and inner surface of the hollow cylinder. Similar to the definition (A.4), the impedance per unit length of the hollow circular cylinder is given by the ratio of the axial electric field $\tilde{E}_z(\zeta, s)$ to the net total current in the axial direction which is obtained by the sum of the outer $\tilde{I}^{(2)}(\zeta, s)$ and the inner $\tilde{I}^{(1)}(\zeta, s)$ total currents,

$$\tilde{Z}'(\zeta, s) = \frac{\tilde{E}_z(\zeta, s)}{\tilde{I}^{(2)}(\zeta, s) + \tilde{I}^{(1)}(\zeta, s)} \quad (\text{A.10})$$

evaluated on the surface of the cylinder. According to the expressions (3.5) through (3.8) and (3.10), the expression (A.10) takes the form, after making use of the Wronskin relationship

$$\tilde{Z}'(\zeta) = \frac{Z_{oc}}{2\pi\gamma_c} u_c^2 K_0(u_c C) I_0(u_c C) \quad (\text{A.11})$$

where

$$u_c = [\gamma_c^2 - \zeta^2]^{\frac{1}{2}} \quad (\text{A.12})$$

$$\gamma_c = [u_c s(\sigma_c + \epsilon_c s)]^{\frac{1}{2}} \quad (\text{A.13})$$

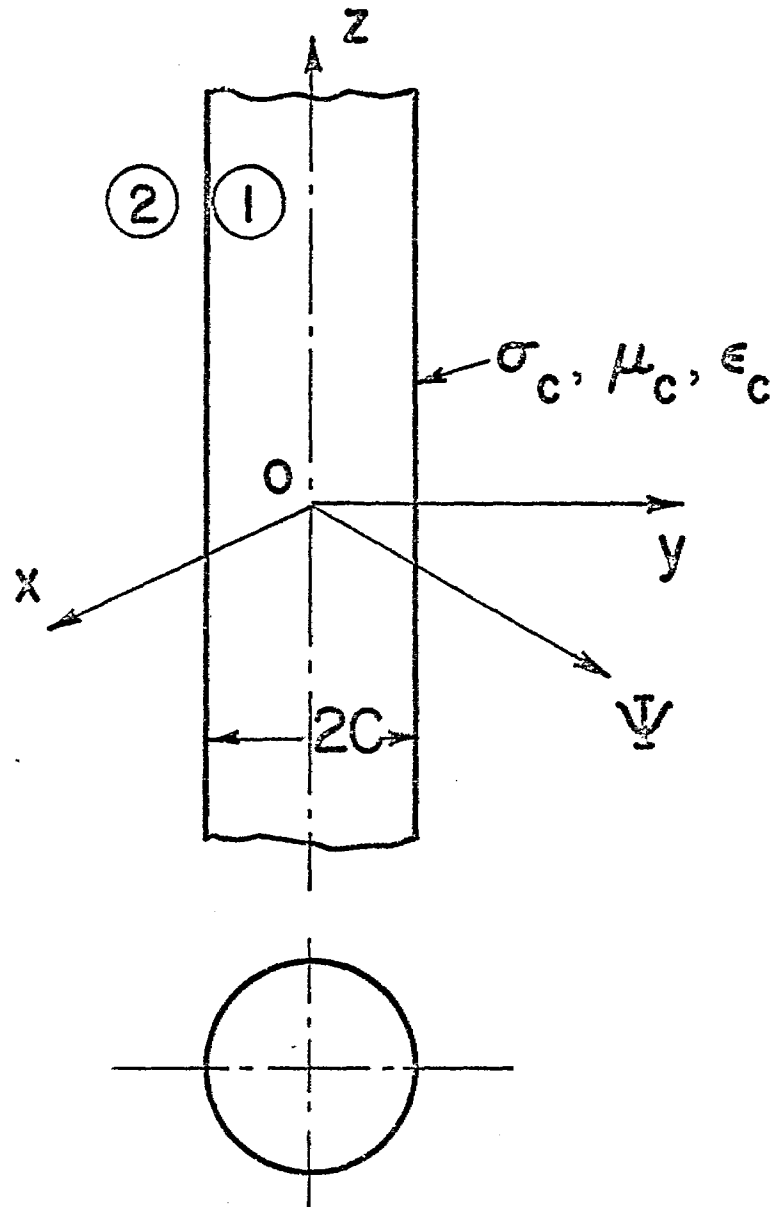


Figure A-4. Hollow Circular Cylinder

and in the quasi-static range $|\gamma_c^2| \gg \zeta^2$, the axial impedance $\tilde{Z}'(s)$ per unit length of the hollow circular cylinder becomes,

$$\tilde{Z}'(s) = \frac{Z_{oc}}{2\pi} \gamma_c K_0(\gamma_c C) I_0(\gamma_c C) \quad (A.14)$$

where

$$Z_{oc} = \left[\frac{\mu_c s}{\sigma_c + \epsilon_c s} \right]^{\frac{1}{2}} \quad (A.15)$$

Further, the sheet impedance of the cylinder is given by

$$\tilde{Z}_s(s) = 2\pi C \tilde{Z}'(s) \quad (A.16)$$

3. General Solid Cylindrical Wire

In section A-(1), the impedance characteristics of a thin solid cylindrical wire are discussed with the obvious assumption that the current on the surface of the wire is uniform with respect to ϕ -angular variation. Let us consider another case with current density $\tilde{J}_z(\phi, s)$ on the surface as a function of angle ϕ , but which is independent of the z -coordinate variable. Then in the region $\psi < b$, figure A-1, the electric field distribution is given by,

$$\tilde{E}_z(\psi, \phi, s) = \sum_{m=-\infty}^{\infty} \tilde{C}_m(b, m, s) I_m(\gamma_w \psi) e^{jm\phi} \quad (A.17)$$

where \tilde{C}_m is the m^{th} Fourier mode coefficient, so that the representation (A.1) is for the special case of the $m = 0$ mode.

According to the expression (2.4a) and (2.4b) the current density on the surface of the wire is obtained,

$$\begin{aligned} \tilde{J}_z(b, \phi, s) &= \tilde{H}_\phi(b, \phi, s) \\ &= \frac{1}{Z_{ow}} \sum_{m=-\infty}^{\infty} \tilde{C}_m(b, \phi, s) I'_m(\gamma_w b) e^{jm\phi} \end{aligned} \quad (A.18)$$

On the surface of the cylindrical wire, we have the surface impedance boundary relationship,

$$\tilde{E}_Z(b, \phi, s) = \tilde{Z}_{S_w}(s) \tilde{J}_Z(b, \phi, s) \quad (\text{A.19})$$

Substituting (A.17) and (A.18) into (A.19) and enforcing orthogonality of the modes

$$\tilde{Z}_{S_{w_m}}(s) = Z_{ow} \frac{I_m(\gamma_w b)}{I_m'(\gamma_w b)} \quad (\text{A.20})$$

Hence for any given mode excitation m on the wire, the mode surface impedance $\tilde{Z}_{S_{w_m}}(s)$ is associated.

4. General Hollow Circular Cylinder

The impedance characteristics of the general solid cylindrical wire can also be extended to the case of a hollow circular cylinder, figure A-2, with the current density $\tilde{J}_Z^{(t)}(C, \phi, s)$ on the surface as a function of angle ϕ , but is independent of z -coordinate variable. On the surface of the hollow cylinder, we have the sheet-impedance boundary relationship,

$$\tilde{E}_Z(C, \phi, s) = \tilde{Z}_S(s) \tilde{J}_Z^{(t)}(C, \phi, s) \quad (\text{A.21})$$

where the current density is obtained by the difference in the tangential magnetic field

$$\tilde{J}_Z^{(t)}(C, \phi, s) = \tilde{H}_\phi^{(2)}(C, \phi, s) - \tilde{H}_\phi^{(1)}(C, \phi, s) \quad (\text{A.22})$$

Hence for any given mode excitation m on the hollow cylinder, the associated mode sheet impedance $\tilde{Z}_{S_m}(s)$ is given by

$$\tilde{Z}_{S_m}(s) = \gamma_c C Z_{oc} I_m(\gamma_c C) K_m(\gamma_c C) \quad (\text{A.23})$$

APPENDIX B
FAR-FIELD EXPRESSION

The ϕ -component of the magnetic field radiated by the infinitely long thin solid wire is given by the expression (2.17a),

$$\tilde{H}_\phi(\Psi, z, s) = \frac{\tilde{V}\gamma}{j2\pi Z_0} \int_{C_\zeta} G(\zeta) \frac{K_1(u\Psi)}{\tilde{D}(\zeta, s)} e^{\zeta z} d\zeta \quad (\text{B.1})$$

In fact the expression (B.1) reduces to the (2.19) for the total axial current $\tilde{I}(z, s) = 2\pi b \tilde{H}_\phi(\Psi, z, s)$ evaluated on the surface of the infinitely long wire $\Psi = b$. In the expression (B.1), the integration is along a Bromwich contour in the ζ -plane, figure 2.2, and

$$u = [\gamma^2 - \zeta^2]^{\frac{1}{2}} \quad (\text{B.2})$$

$$\tilde{D}(\zeta, s) = uK_0(ub) + \tilde{h}_1(s) K_1(ub) \quad (\text{B.3})$$

$$\tilde{h}(s) = 2\pi b(\sigma + s\varepsilon) \tilde{Z}'_w(s) \quad (\text{B.4})$$

and $\tilde{Z}'_w(\zeta, s)$ as given by the expression (A.5) has the form,

$$\tilde{Z}'_w(\zeta, s) = \frac{(\gamma_w^2 - \zeta^2)^{\frac{1}{2}} I_0[b(\gamma_w^2 - \zeta^2)^{\frac{1}{2}}]}{2\pi b(\sigma_w + s\varepsilon_w) I_1[b(\gamma_w^2 - \zeta^2)^{\frac{1}{2}}]} \quad (\text{B.5})$$

and $\tilde{Z}_w(\zeta, s)$ would be independent of ζ , (A.6), in the quasi-static region. Assuming an ideal slice generator excitation, $d \rightarrow 0$ and $G(\zeta) \rightarrow 1$.

It is possible to obtain the general solution to the integral (B.1) by closing the contour, figure 2.2, in the left half of the ζ -plane for $z \rightarrow 0$, but this procedure involves some numerical work. However, as $\Psi \rightarrow \infty$, in the far-field region, an

explicit expression for $\tilde{H}_\phi(\Psi, z, s)$ can be obtained based on the saddle-point method of integration.^{13,14} With the substitution $\zeta = \zeta' + j\zeta''$, $\zeta' = 0$ and $\gamma = jp$, the integral (B.1) reduces to the form discussed in reference 14 and hence we have for $z > 0$,

$$\tilde{H}_\phi(\Psi, z, s) = \frac{\tilde{V}_\gamma}{2\pi Z_0} \int_{-\infty}^{\infty} \frac{K_1(u\Psi)}{\tilde{D}(\zeta'', s)} e^{-j\zeta''z} d\zeta'' \quad (\text{B.6})$$

and

$$u = jv = j[p^2 - \zeta''^2]^{\frac{1}{2}} \quad (\text{B.7})$$

In the far-field region as $\Psi \rightarrow \infty$,¹⁵

$$K_1(u\Psi) e^{-j\zeta''z} \sim \left(\frac{\pi}{2u\Psi}\right)^{\frac{1}{2}} e^{-j[v\Psi + \zeta''z]} , \quad |\arg(u\Psi)| < \frac{3\pi}{2} \quad (\text{B.8})$$

The saddle point ζ_0'' is obtained by solving the equation obtained from the exponent of (B.8),

$$\frac{d}{d\zeta''}[v\Psi + \zeta''z]_{\zeta''=\zeta_0''} = 0 \quad (\text{B.9})$$

The expression (B.9) yields $\zeta_0'' = p \sin(\alpha)$, with the proper substitution $\Psi = r \cos(\alpha)$, $z = r \sin(\alpha)$ and $\theta = 90 - \alpha$ where r and θ are the spherical coordinate variables and α is the angle measured from $z = 0$ plane, figure B-1. Calling the exponent term in (B.9) as

$$f(\zeta'') = -j(v\Psi + \zeta''z) \quad (\text{B.10})$$

and at $\zeta'' = \zeta_0''$

$$f(\zeta'') \Big|_{\zeta''=\zeta_0''} = -jp(\Psi \cos(\alpha) + z \sin(\alpha)) \quad (\text{B.11})$$

In the neighborhood of the saddle point $\zeta'' = \zeta_0''$, $f(\zeta'')$ can be expanded in a Taylor series,

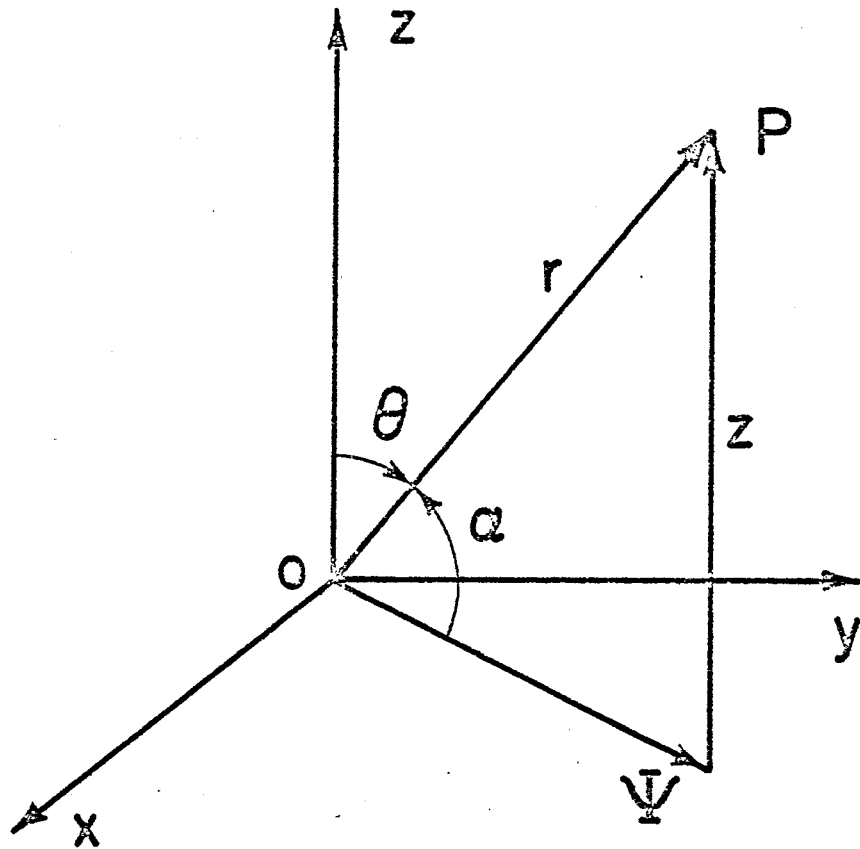


Figure B-1. Coordinates for Far-Field Calculation

$$f(\zeta) \approx -j \left[p(\Psi \cos(\alpha) + z \sin(\alpha)) - \frac{\Psi}{p \cos^3(\alpha)} (\zeta'' - \zeta_0'')^2 \right] \quad (B.12)$$

Hence, according to the expression (B.12) the path of the saddle point integration is obtained by forcing the imaginary part of (B.12) to be constant along the path. With the substitution $\zeta'' - \zeta_0'' = R e^{j\delta_1}$ and $p = |p| e^{j\delta_2}$, the path of the saddle point integration is given by the imaginary part (Im) as

$$\text{Im} \left[-jp \left\{ (\Psi \cos(\alpha) + z \sin(\alpha)) - \frac{\Psi}{|p| \cos^3(\alpha)} R^2 e^{j2(\delta_1 - \delta_2)} \right\} \right] = \text{constant} \quad (B.13)$$

and (B.13) is satisfied only when

$$\text{Re} \left[e^{j(\delta_1 - \delta_2)} \right] = 0 \quad (B.14)$$

The expression (B.14) yields $(\delta_1 - \delta_2) = \pm\pi/4$. Only the positive value of $(\delta_1 - \delta_2) = \pi/4$ represents the correct slope of the integration path through the saddle point $\zeta_0'' = p \sin(\alpha)$, which is also obvious from the further transformations used in reference 14. Changing the variable of integration ζ'' in the expression (B.1) to τ by the transformation $\zeta'' = p \sin\tau$, and $\tau = \alpha_1 + j\alpha_2$, the saddle point is located at $\alpha_1 = \alpha$ on the real axis of the complex τ -plane. The reader may refer to reference 21 for the complete details of the various transformations from ζ'' -plane to τ -plane and the paths of the integration. Hence the expression (B.8) can be written as

$$K_1(u\Psi) e^{-j\zeta''z} \sim \left(\frac{\pi}{j2p\Psi \cos(\tau)} \right)^{\frac{1}{2}} e^{-jr p \cos(\tau - \alpha)} \quad (B.15)$$

In the far-field region, the expression (B.1) for $\tilde{H}_\phi(\Psi, z, s)$ becomes,

$$\tilde{H}_\phi(\Psi, z, s) \sim \frac{\tilde{V}_\gamma}{2\pi Z_0} \int_{\alpha - \frac{\pi}{2} - j\infty}^{\alpha + \frac{\pi}{2} + j\infty} \left(\frac{\pi}{j2p\Psi \cos(\tau)} \right)^{\frac{1}{2}} \frac{e^{-jr p \cos(\tau - \alpha)}}{\tilde{L}_1(\gamma, \alpha)} p \cos(\tau) d\tau \quad (B.16)$$

Most of the contribution to the integral (B.16) comes from the vicinity of the saddle point $\tau = \alpha$, and with the approximation $\cos x \approx 1 - x^2/2$, and $\tau - \alpha = e^{j\pi/4}$, the expression (B.16) reduces to,

$$\tilde{H}_\phi(\Psi, z, s) \sim \frac{\tilde{V}\gamma}{2\pi Z_0} \left(\frac{\pi p}{2r}\right)^{\frac{1}{2}} \frac{e^{-\gamma r}}{\tilde{L}_1(\gamma, \alpha)} \int_{-\epsilon}^{\epsilon} e^{-\frac{1}{2}pr\eta^2} d\eta \quad (\text{B.17})$$

and the integral in (B.17) as $r \rightarrow \infty$, $\epsilon \rightarrow \infty$,¹⁵

$$\int_{-\infty}^{\infty} e^{-\frac{1}{2}pr\eta^2} d\eta = \left(\frac{2\pi}{pr}\right)^{\frac{1}{2}} \quad (\text{B.18})$$

Hence $\tilde{H}_\phi(r, \alpha, s)$ in the far-field region has the form

$$\tilde{H}_\phi(r, \alpha, s) \sim \frac{\tilde{V}\gamma}{2Z_0} \frac{1}{\tilde{L}(\gamma, \alpha)} \frac{e^{-\gamma r}}{r} \quad (\text{B.19})$$

where the denominator term is

$$\begin{aligned} \tilde{L}(\gamma, \alpha) &= \tilde{D}(\zeta'' = \zeta''_0) \\ &= \gamma \cos\alpha K_0(\gamma b \cos\alpha) + \tilde{h}(s) K_1(\gamma b \cos\alpha) \end{aligned} \quad (\text{B.20})$$

where $\tilde{h}(s)$ is defined in the expression (B.4).

We note that $\tilde{h}(s)$ in the expression (B.20) holds good only in the quasi-static frequency ranges, or when the wire is loaded uniformly by external impedances. For very large frequencies $\tilde{h}_1(s)$ in (B.20) should be replaced by $\tilde{h}(\zeta''_0, s)$ where

$$\begin{aligned} \tilde{h}(\zeta''_0, s) &= \tilde{h}(\zeta'', s) \Big|_{\zeta'' = \zeta''_0 = -j\gamma s \sin\alpha} \\ &= 2\pi b(\sigma + s\epsilon) \tilde{Z}'_w(\zeta''_0, s) \end{aligned} \quad (\text{B.21})$$

APPENDIX C

DIFFERENT FORMS OF THE EQUIVALENT-RADIUS EXPRESSIONS
IN THE QUASI-STATIC LIMIT

It is interesting to note the different forms of the equivalent radius¹⁻³ of a circular wire cage derived in quasi-static limit are one and the same, and check with the result obtained in section IV. In the earlier studies,

- (i) a cage consisting of conical wires equally spaced over surface of a cone is studied, and compared with respect to a solid cone of same characteristic impedance so that there is only a transmission line mode excited,^{1,10} expression (4.8)
- (ii) an equivalence between a single charged conductor and number of equally spaced concentric charged conductors is studied based on conformal transformation,³ expression (4.8)
- (iii) a wire cage antenna consisting of closely spaced parallel and identical conductors placed around a circle is compared to a single conductor antenna, so that the total axial assumed current distribution is approximately the same,² expression (4.7)
- (iv) far-field equivalence of the canonical infinitely long circular wire cage and hollow cylindrical antenna structure, section IV, expression (4.7).

In the following, the expression (4.7) for the circular wire cage equivalent radius

$$\psi_{eq}^{(c)} = [aA_{1,2}A_{1,3}\dots A_{1,N}]^{1/N} \quad (C.1)$$

is shown to be equivalent to the expression (4.8)

$$\frac{\psi_{eq_0}^{(c)}}{A} = \left(\frac{aN}{A}\right)^{1/N} \quad (C.2)$$

Normalizing (C.1) with respect to A,

$$\frac{\psi_{eq_0}^{(c)}}{A} = \left[\frac{aA_{1,2}A_{1,3}\cdots A_{1,N}}{A^N}\right]^{1/N} \quad (C.3)$$

$$= \left[\frac{aR}{A}\right]^{1/N} \quad (C.4)$$

where the mean inter-chord distance is

$$R = \frac{A_{1,2}A_{1,3}\cdots A_{1,N}}{A^{N-1}} \quad (C.5)$$

The various inter-chord distances $A_{1,n}$, $n = 2, 3, \dots, N$, are defined in (2.30). On substituting $A_{1,n}$ into (C.5)

$$\begin{aligned} R &= \frac{(2A \sin \frac{\pi}{N})(2A \sin \frac{2\pi}{N})\cdots(2A \sin \frac{(N-1)\pi}{N})}{A^{N-1}} \\ &= 2^{N-1} \prod_{n=1}^{N-1} \sin\left(\frac{n\pi}{N}\right) \end{aligned} \quad (C.6)$$

But we have the product expression,²²

$$\sin(Nx) = 2^{N-1} \prod_{n=1}^{N-1} \sin\left(x + \frac{n\pi}{N}\right) \quad (C.7)$$

Hence, from (C.6) and (C.7)

$$\begin{aligned} R &= \frac{\sin(Nx)}{\sin(x)} \Big|_{x \rightarrow 0} \\ &= \frac{N \cos(Nx)}{\cos(x)} \Big|_{x \rightarrow 0} \\ &= N \end{aligned} \quad (C.8)$$

REFERENCES

1. Schelkunoff, S. A., and H. T. Friis, Antennas Theory and Practice, John Wiley and Sons, NY, 1952.
2. King, R.W.P., The Theory of Linear Antennas, Harvard University Press, MA, 1956.
3. Baum, C. E., "Design of a Pulse Radiating Dipole Antenna as Related to High Frequency and Low Frequency Limits," Sensor and Simulation Notes, Note 69, January 1969.
4. Baum, C. E., "EMP Simulators for Various Types of Nuclear EMP Environments: An Interim Categorization," Sensor and Simulation Notes, Note 151, July 1972.
5. Kehrer, W. S., and C. E. Baum, "Summary of Characteristics," ATHAMAS Memos, Memo 1, November 1973.
6. Castillo, J. P., "Some Notes on the Design of ACHILLES II," ACHILLES Memos, Memo 1, August 1973.
7. Blackburn, R. F., and C. D. Taylor, "On the Electromagnetic Fields from a Hybrid Type of EMP Simulator," Sensor and Simulation Notes, Note 211, November 1975.
8. Casey, K. F., "Electromagnetic Shielding by Advanced Composite Materials," Interaction Notes, Note 341, June 1977.
9. Hill, D. A., and J. R. Wait, "Gap Excitation of an Axial Conductor in a Circular Tunnel," Journal of Applied Physics, Vol. 45, No. 11, November 1974.
10. Higgins, D. F., "The Effects of Constructing a Conical Antenna Above a Ground Plane Out of a Number of Thin Wires," Sensor and Simulation Notes, Note 142, January 1972.
11. Jones, D. S., The Theory of Electromagnetism, Pergamon Press, 1964.
12. Latham, R. W., and K.S.H. Lee, "Waveforms Near a Cylindrical Antenna," Sensor and Simulation Notes, Note 89, June 1969.
13. Mittra, R., and S. W. Lee, Analytical Techniques in the Theory of Guided Waves, MacMillan, 1971.
14. Papas, C. H., "On the Infinitely Long Cylindrical Antenna," Journal of Applied Physics, Vol. 20, pp. 437-440, May 1949.

15. Abramowitz, M., and I. A. Segun, Handbook of Mathematical Functions, Dover, NY, 1968.
16. Kunz, K. S., "Asymptotic Behavior of the Current on an Infinite Cylindrical Antenna," *Journal of Research of NBS*, Vol. 67D, No. 4, July-August 1963.
17. Shen, L. C., T. T. Wu, and R.W.P. King, "A Simple Formula of Current in Dipole Antennas," *IEEE Transactions on Antennas and Propagation*, Vol. 16, No. 5, September 1968.
18. Hill, D. A., and J. R. Wait, "Coupling between a Dipole Antenna and an Infinite-Cable over an Ideal Ground Plane," *Radio Science*, Vol. 12, No. 2, March-April 1977.
19. Conte, S. D., Elementary Numerical Analysis, McGraw Hill, NY, 1966.
20. King, R.W.P., Fundamental Electromagnetic Theory, Dover, NY, 1963.
21. Tyras, G., Radiation and Propagation of Electromagnetic Waves, Academic Press, NY, 1960.
22. Gradshteyn, I. S., and I. M., Ryzhik, Tables of Integrals, Series and Product, Academic Press, NY, 1965.